Summary for Policymakers

Drafting Authors: Lisa Alexander (Australia), Simon Allen (Switzerland/New Zealand), Nathaniel L. Bindoff (Australia), François-Marie Bréon (France), John Church (Australia), Ulrich Cubasch (Germany), Seita Emori (Japan), Piers Forster (UK), Pierre Friedlingstein (UK/Belgium), Nathan Gillett (Canada), Jonathan Gregory (UK), Dennis Hartmann (USA), Eystein Jansen (Norway), Ben Kirtman (USA), Reto Knutti (Switzerland), Krishna Kumar Kanikicharla (India), Peter Lemke (Germany), Jochem Marotzke (Germany), Valérie Masson-Delmotte (France), Gerald Meehl (USA), Igor Mokhov (Russia), Shilong Piao (China), Gian-Kasper Plattner (Switzerland), Qin Dahe (China), Venkatachalam Ramaswamy (USA), David Randall (USA), Monika Rhein (Germany), Maisa Rojas (Chile), Christopher Sabine (USA), Drew Shindell (USA), Thomas F. Stocker (Switzerland), Lynne Talley (USA), David Vaughan (UK), Shang-Ping Xie (USA)

Draft Contributing Authors: Myles Allen (UK), Olivier Boucher (France), Don Chambers (USA), Jens Hesselbjerg Christensen (Denmark), Philippe Ciais (France), Peter Clark (USA), Matthew Collins (UK), Josefino Comiso (USA), Viviane Vasconcellos de Menezes (Australia/Brazil), Richard Feely (USA), Thierry Fichefet (Belgium), Arlene Fiore (USA), Gregory Flato (Canada), Jan Fuglestvedt (Norway), Gabriele Hegerl (UK/Germany), Paul Hezel (Belgium/USA), Gregory Johnson (USA), Georg Kaser (Austria/Italy), Vladimir Kattsov (Russia), John Kennedy (UK), Albert Klein Tank (Netherlands), Corinne Le Quéré (UK/France), , Gunnar Myhre (Norway), Tim Osborn (UK), Antony Payne (UK), Judith Perlwitz (USA/Germany), Scott Power (Australia), Michael Prather (USA), Stephen Rintoul (Australia), Joeri Rogelj (Switzerland), Matilde Rusticucci (Argentina), Michael Schulz (Germany), Jan Sedláček (Switzerland), Peter Stott (UK), Rowan Sutton (UK), Peter Thorne (USA/Norway/UK), Donald Wuebbles (USA)

Working Group I Contribution to the IPCC Fifth Assessment Report
Climate Change 2013: The Physical Science Basis
Summary for Policymakers

A. Introduction

The Working Group I contribution to the IPCC's Fifth Assessment Report (AR5) considers new evidence of climate change based on many independent scientific analyses from observations of the climate system, paleoclimate archives, theoretical studies of climate processes and simulations using climate models. It builds upon the Working Group I contribution to the IPCC's Fourth Assessment Report (AR4), and incorporates subsequent new findings of research. As a component of the fifth assessment cycle, the IPCC Special Report on Managing the Risks of Extreme Events to Advance Climate Change Adaptation (SREX) is an important basis for information on changing weather and climate extremes.

This Summary for Policymakers (SPM) follows the structure of the Working Group I report. The narrative is supported by a series of overarching highlighted conclusions which, taken together, provide a concise summary. Main sections are introduced with a brief paragraph in italics which outlines the methodological basis of the assessment.

The degree of certainty in key findings in this assessment is based on the author teams' evaluations of underlying scientific understanding and is expressed as a qualitative level of confidence (from *very low* to *very high*) and, when possible, probabilistically with a quantified likelihood (from *exceptionally unlikely* to *virtually certain*). Confidence in the validity of a finding is based on the type, amount, quality, and consistency of evidence (e.g., data, mechanistic understanding, theory, models, expert judgment) and the degree of agreement[1]. Probabilistic estimates of quantified measures of uncertainty in a finding are based on statistical analysis of observations or model results, or both, and expert judgment[2]. Where appropriate, findings are also formulated as statements of fact without using uncertainty qualifiers. (See Chapter 1 and Box TS.1 for more details about the specific language the IPCC uses to communicate uncertainty)

The basis for substantive paragraphs in this Summary for Policymakers can be found in the chapter sections of the underlying report and in the Technical Summary. These references are given in curly brackets.

B. Observed Changes in the Climate System

Observations of the climate system are based on direct measurements and remote sensing from satellites and other platforms. Global-scale observations from the instrumental era began in the mid-19th century for temperature and other variables, with more comprehensive and diverse sets of observations available for the period 1950 onwards. Paleoclimate reconstructions extend some

[1] In this Summary for Policymakers, the following summary terms are used to describe the available evidence: limited, medium, or robust; and for the degree of agreement: low, medium, or high. A level of confidence is expressed using five qualifiers: very low, low, medium, high, and very high, and typeset in italics, e.g., *medium confidence*. For a given evidence and agreement statement, different confidence levels can be assigned, but increasing levels of evidence and degrees of agreement are correlated with increasing confidence (see Chapter 1 and Box TS.1 for more details).

[2] In this Summary for Policymakers, the following terms have been used to indicate the assessed likelihood of an outcome or a result: virtually certain 99–100% probability, very likely 90–100%, likely 66–100%, about as likely as not 33–66%, unlikely 0–33%, very unlikely 0–10%, exceptionally unlikely 0–1%. Additional terms (extremely likely: 95–100%, more likely than not >50–100%, and extremely unlikely 0–5%) may also be used when appropriate. Assessed likelihood is typeset in italics, e.g., *very likely* (see Chapter 1 and Box TS.1 for more details).

records back hundreds to millions of years. Together, they provide a comprehensive view of the variability and long-term changes in the atmosphere, the ocean, the cryosphere, and the land surface.

Warming of the climate system is unequivocal, and since the 1950s, many of the observed changes are unprecedented over decades to millennia. The atmosphere and ocean have warmed, the amounts of snow and ice have diminished, sea level has risen, and the concentrations of greenhouse gases have increased (see Figures SPM.1, SPM.2, SPM.3 and SPM.4). {2.2, 2.4, 3.2, 3.7, 4.2–4.7, 5.2, 5.3, 5.5–5.6, 6.2, 13.2}

B.1 Atmosphere

Each of the last three decades has been successively warmer at the Earth's surface than any preceding decade since 1850 (see Figure SPM.1). In the Northern Hemisphere, 1983–2012 was *likely* the warmest 30-year period of the last 1400 years (*medium confidence*). {2.4, 5.3}

[INSERT FIGURE SPM.1 HERE]

Figure SPM.1: (a) Observed global mean combined land and ocean surface temperature anomalies, from 1850 to 2012 from three data sets. Top panel: annual mean values, bottom panel: decadal mean values including the estimate of uncertainty for one dataset (black). Anomalies are relative to the mean of 1961−1990. (b) Map of the observed surface temperature change from 1901 to 2012 derived from temperature trends determined by linear regression from one dataset (orange line in panel a). Trends have been calculated where data availability permits a robust estimate (i.e., only for grid boxes with greater than 70% complete records and more than 20% data availability in the first and last 10% of the time period). Other areas are white. Grid boxes where the trend is significant at the 10% level are indicated by a + sign. For a listing of the datasets and further technical details see the Technical Summary Supplementary Material. {Figures 2.19–2.21; Figure TS.2}

- The globally averaged combined land and ocean surface temperature data as calculated by a linear trend, show a warming of 0.85 [0.65 to 1.06] °C [3], over the period 1880–2012, when multiple independently produced datasets exist. The total increase between the average of the 1850–1900 period and the 2003–2012 period is 0.78 [0.72 to 0.85] °C, based on the single longest dataset available[4]. (Figure SPM.1a) {2.4}

- For the longest period when calculation of regional trends is sufficiently complete (1901–2012), almost the entire globe has experienced surface warming. (Figure SPM.1b) {2.4}

- In addition to robust multi-decadal warming, global mean surface temperature exhibits substantial decadal and interannual variability (see Figure SPM.1). Due to natural variability, trends based on short records are very sensitive to the beginning and end dates and do not in general reflect long-term climate trends. As one example, the rate of warming over the past 15 years (1998–2012; 0.05 [–0.05 to +0.15] °C per decade), which begins with a strong El Niño, is smaller than the rate calculated since 1951 (1951–2012; 0.12 [0.08 to 0.14] °C per decade)[5]. {2.4}

[3] In the WGI contribution to the AR5, uncertainty is quantified using 90% uncertainty intervals unless otherwise stated. The 90% uncertainty interval, reported in square brackets, is expected to have a 90% likelihood of covering the value that is being estimated. Uncertainty intervals are not necessarily symmetric about the corresponding best estimate. A best estimate of that value is also given where available.

[4] Both methods presented in this bullet were also used in AR4. The first calculates the difference using a best fit linear trend of all points between 1880 and 2012. The second calculates the difference between averages for the two periods 1850 to 1900 and 2003 to 2012. Therefore, the resulting values and their 90% uncertainty intervals are not directly comparable (2.4).

[5] Trends for 15-year periods starting in 1995, 1996, and 1997 are 0.13 [0.02 to 0.24], 0.14 [0.03 to 0.24], 0.07 [–0.02 to 0.18] °C per decade, respectively.

- Continental-scale surface temperature reconstructions show, with *high confidence*, multi-decadal periods during the Medieval Climate Anomaly (year 950 to 1250) that were in some regions as warm as in the late 20th century. These regional warm periods did not occur as coherently across regions as the warming in the late 20th century (*high confidence*). {5.5}

- It is *virtually certain* that globally the troposphere has warmed since the mid-20th century. More complete observations allow greater confidence in estimates of tropospheric temperature changes in the extratropical Northern Hemisphere than elsewhere. There is *medium confidence* in the rate of warming and its vertical structure in the Northern Hemisphere extra-tropical troposphere and *low confidence* elsewhere. {2.4}

- *Confidence* in precipitation change averaged over global land areas since 1901 is *low* prior to 1951 and *medium* afterwards. Averaged over the mid-latitude land areas of the Northern Hemisphere, precipitation has increased since 1901 (*medium confidence* before and *high confidence* after 1951). For other latitudes area-averaged long-term positive or negative trends have *low confidence*. {Figure SPM.2, Figure TS.XX, 2.5}

[INSERT FIGURE SPM.2 HERE]
Figure SPM.2: Maps of observed precipitation change from 1901 to 2010 and from 1951 to 2010 (trends calculated using the same criteria as in Figure SPM.1b) from one data set. For further technical details see the Technical Summary Supplementary Material. {Figure TS.X; Figure 2.29} [FIGURE TO BE COPYEDITED AND MADE CONSISTENT WITH FIGURE SPM.1b]

- Changes in many extreme weather and climate events have been observed since about 1950 (see Table SPM.1 for details). It is *very likely* that the number of cold days and nights has decreased and the number of warm days and nights has increased on the global scale[6]. It is *likely* that the frequency of heat waves has increased in large parts of Europe, Asia and Australia. There are *likely* more land regions where the number of heavy precipitation events has increased than where it has decreased. The frequency or intensity of heavy precipitation events has *likely* increased in North America and Europe. In other continents, confidence in changes in heavy precipitation events is at most *medium.* {2.6}

[INSERT TABLE SPM.1 HERE]
Table SPM.1: Extreme weather and climate events: Global-scale assessment of recent observed changes, human contribution to the changes, and projected further changes for the early (2016–2035) and late (2081–2100) 21st century. Bold indicates where the AR5 (black) provides a revised* global-scale assessment from the SREX (blue) or AR4 (red). Projections for early 21st century were not provided in previous assessment reports. Projections in the AR5 are relative to the reference period of 1986–2005, and use the new Representative Concentration Pathway (RCP) scenarios (see Box SPM.1) unless otherwise specified. See the Glossary for definitions of extreme weather and climate events.

B.2 Ocean

Ocean warming dominates the increase in energy stored in the climate system, accounting for more than 90% of the energy accumulated between 1971 and 2010 (*high confidence*). It is *virtually certain* that the upper ocean (0−700 m) warmed from 1971 to 2010 (see Figure SPM.3), and it *likely* warmed between the 1870s and 1971. {3.2, Box 3.1}

- On a global scale, the ocean warming is largest near the surface, and the upper 75 m warmed by 0.11 [0.09 to 0.13] °C per decade over the period 1971–2010. Since AR4, instrumental biases in upper-ocean temperature records have been identified and reduced, enhancing confidence in the assessment of change. {3.2}

[6] See the Glossary for the definition of these terms: cold days / cold nights, warm days / warm nights, heat waves.

- It is *likely* that the ocean warmed between 700 and 2000 m from 1957 to 2009. Sufficient observations are available for the period 1992 to 2005 for a global assessment of temperature change below 2000 m. There were *likely* no significant observed temperature trends between 2000 and 3000 m for this period. It is *likely* that the ocean warmed from 3000 m to the bottom for this period, with the largest warming observed in the Southern Ocean. {3.2}

- More than 60% of the net energy increase in the climate system is stored in the upper ocean (0–700 m) during the relatively well-sampled 40-year period from 1971 to 2010, and about 30% is stored in the ocean below 700 m. The increase in upper ocean heat content during this time period estimated from a linear trend is *likely* 17 [15 to 19] $\times$ 10^{22} J [7] (Figure SPM.3). {3.2, Box 3.1}

- It is *about as likely as not* that ocean heat content from 0–700 m increased more slowly during 2003–2010 than during 1993–2002 (see Figure SPM.3). Ocean heat uptake from 700–2000 m, where interannual variability is smaller, *likely* continued unabated from 1993 to 2009. {3.2, Box 9.2}

- It is *very likely* that regions of high salinity where evaporation dominates have become more saline, while regions of low salinity where precipitation dominates have become fresher since the 1950s. These regional trends in ocean salinity provide indirect evidence that evaporation and precipitation over the oceans have changed (*medium confidence*). {2.5, 3.3, 3.5}

- There is no observational evidence of a trend in the Atlantic Meridional Overturning Circulation (AMOC), based on the decade-long record of the complete AMOC and longer records of individual AMOC components. {3.6}

B.3 Cryosphere

Over the last two decades, the Greenland and Antarctic ice sheets have been losing mass, glaciers have continued to shrink almost worldwide, and Arctic sea ice and Northern Hemisphere spring snow cover have continued to decrease in extent (*high confidence*) (see Figure SPM.3). {4.2–4.7}

- The average rate of ice loss[8] from glaciers around the world, excluding glaciers on the periphery of the ice sheets[9], was *very likely* 226 [91 to 361] Gt yr^{-1} over the period 1971−2009, and *very likely* 275 [140 to 410] Gt yr^{-1} over the period 1993−2009[10]. {4.3}

- The average rate of ice loss from the Greenland ice sheet has *very likely* substantially increased from 34 [–6 to 74] Gt yr^{-1} over the period 1992–2001 to 215 [157 to 274] Gt yr^{-1} over the period 2002–2011. {4.4}

- The average rate of ice loss from the Antarctic ice sheet has *likely* increased from 30 [–37 to 97] Gt yr^{-1} over the period 1992–2001 to 147 [72 to 221] Gt yr^{-1} over the period 2002–2011. There is *very high confidence* that these losses are mainly from the northern Antarctic Peninsula and the Amundsen Sea sector of West Antarctica. {4.4}

[INSERT FIGURE SPM.3 HERE]

[7] A constant supply of heat through the ocean surface at the rate of 1 W m^{-2} for 1 year would increase the ocean heat content by 1.1 $\times$ 10^{22} J.
[8] All references to 'ice loss' or 'mass loss' refer to net ice loss, accumulation minus melt and iceberg calving.
[9] For methodological reasons, this assessment of ice loss from the Antarctic and Greenland ice sheets includes change in the glaciers on the periphery. These peripheral glaciers are thus excluded from the values given for glaciers.
[10] 100 Gt yr^{-1} of ice loss is equivalent to about 0.28 mm yr^{-1} of global mean sea level rise.

Figure SPM.3: Multiple observed indicators of a changing global climate: (a) Extent of Northern Hemisphere March-April (spring) average snow cover, (b) Extent of Arctic July-August-September (summer) average sea ice, (c) change in global mean upper ocean (0–700 m) heat content aligned to 2006−2010, and relative to the mean of all datasets for 1971, (d) global mean sea level relative to the 1900–1905 mean of the longest running dataset, and with all datasets aligned to have the same value in 1993, the first year of satellite altimetry data. All time-series (coloured lines indicating different data sets) show annual values, and where assessed, uncertainties are indicated by coloured shading. See Technical Summary Supplementary Material for a listing of the datasets. {Figures 3.2, 3.13, 4.19, and 4.3; FAQ 2.1, Figure 2; Figure TS.1}

- The annual mean Arctic sea ice extent decreased over the period 1979–2012 with a rate that was *very likely* in the range 3.5 to 4.1% per decade (range of 0.45 to 0.51 million km^2 per decade), and *very likely* in the range 9.4 to 13.6% per decade (range of 0.73 to 1.07 million km^2 per decade) for the summer sea ice minimum (perennial sea ice). The average decrease in decadal mean extent of Arctic sea ice has been most rapid in summer (*high confidence*); the spatial extent has decreased in every season, and in every successive decade since 1979 (*high confidence*) (see Figure SPM.3). There is *medium confidence* from reconstructions that over the past three decades, Arctic summer sea ice retreat was unprecedented and sea surface temperatures were anomalously high in at least the last 1,450 years. {4.2, 5.5}

- It is *very likely* that the annual mean Antarctic sea ice extent increased at a rate in the range of 1.2 to 1.8% per decade (range of 0.13 to 0.20 million km^2 per decade) between 1979 and 2012. There is *high confidence* that there are strong regional differences in this annual rate, with extent increasing in some regions and decreasing in others. {4.2}

- There is *very high confidence* that the extent of Northern Hemisphere snow cover has decreased since the mid-20th century (see Figure SPM.3). Northern Hemisphere snow cover extent decreased 1.6 [0.8 to 2.4] % per decade for March and April, and 11.7 [8.8 to 14.6] % per decade for June, over the 1967–2012 period. During this period, snow cover extent in the Northern Hemisphere did not show a statistically significant increase in any month. {4.5}

- There is *high confidence* that permafrost temperatures have increased in most regions since the early 1980s. Observed warming was up to 3°C in parts of Northern Alaska (early 1980s to mid-2000s) and up to 2°C in parts of the Russian European North (1971–2010). In the latter region, a considerable reduction in permafrost thickness and areal extent has been observed over the period 1975–2005 (*medium confidence*). {4.7}

- Multiple lines of evidence support very substantial Arctic warming since the mid-20th century. {Box 5.1, 10.3}

B.4 Sea Level

The rate of sea level rise since the mid-19th century has been larger than the mean rate during the previous two millennia (*high confidence*). Over the period 1901–2010, global mean sea level rose by 0.19 [0.17 to 0.21] m (see Figure SPM.3). {3.7, 5.6, 13.2}

- Proxy and instrumental sea level data indicate a transition in the late 19th to the early 20th century from relatively low mean rates of rise over the previous two millennia to higher rates of rise (*high confidence*). It is *likely* that the rate of global mean sea level rise has continued to increase since the early 20th century. {3.7, 5.6, 13.2}

- It is *very likely* that the mean rate of global averaged sea level rise was 1.7 [1.5 to 1.9] mm yr^{-1} between 1901 and 2010, 2.0 [1.7 to 2.3] mm yr^{-1} between 1971 and 2010 and 3.2 [2.8 to 3.6] mm yr^{-1} between 1993 and 2010. Tide-gauge and satellite altimeter data are consistent regarding the higher rate of the latter period. It is *likely* that similarly high rates occurred between 1920 and 1950. {3.7}

- Since the early 1970s, glacier mass loss and ocean thermal expansion from warming together explain about 75% of the observed global mean sea level rise (*high confidence*). Over the period 1993–2010, global mean sea level rise is, with *high confidence*, consistent with the sum of the observed contributions from ocean thermal expansion due to warming (1.1 [0.8 to 1.4] mm yr^{-1}), from changes in glaciers (0.76 [0.39 to 1.13] mm yr^{-1}), Greenland ice sheet (0.33 [0.25 to 0.41] mm yr^{-1}), Antarctic ice sheet (0.27 [0.16 to 0.38] mm yr^{-1}), and land water storage (0.38 [0.26 to 0.49] mm yr^{-1}). The sum of these contributions is 2.8 [2.3 to 3.4] mm yr^{-1}. {13.3}

- There is *very high confidence* that maximum global mean sea level during the last interglacial period (129,000 to 116,000 years ago) was, for several thousand years, at least 5 m higher than present and *high confidence* that it did not exceed 10 m above present. During the last interglacial period, the Greenland ice sheet *very likely* contributed between 1.4 and 4.3 m to the higher global mean sea level, implying with *medium confidence* an additional contribution from the Antarctic ice sheet. This change in sea level occurred in the context of different orbital forcing and with high-latitude surface temperature, averaged over several thousand years, at least 2°C warmer than present (*high confidence)*. {5.3, 5.6}

B.5 Carbon and Other Biogeochemical Cycles

The atmospheric concentrations of carbon dioxide (CO_2), methane, and nitrous oxide have increased to levels unprecedented in at least the last 800,000 years. CO_2 concentrations have increased by 40% since pre-industrial times, primarily from fossil fuel emissions and secondarily from net land use change emissions. The ocean has absorbed about 30% of the emitted anthropogenic carbon dioxide, causing ocean acidification (see Figure SPM.4). {2.2, 3.8, 5.2, 6.2, 6.3}

- The atmospheric concentrations of the greenhouse gases carbon dioxide (CO_2), methane (CH_4), and nitrous oxide (N_2O) have all increased since 1750 due to human activity. In 2011 the concentrations of these greenhouse gases were 391 ppm[11], 1803 ppb, 324 ppb and exceeded the pre-industrial levels by about 40%, 150%, and 20%, respectively. {2.2, 5.2, 6.1, 6.2}

- Concentrations of CO_2, CH_4, and N_2O now substantially exceed the highest concentrations recorded in ice cores during the past 800,000 years. The mean rates of increase in atmospheric concentrations over the past century are, with *very high confidence*, unprecedented in the last 22,000 years. {5.2, 6.1, 6.2}

- Annual CO_2 emissions from fossil fuel combustion and cement production were 8.3 [7.6 to 9.0] GtC[12] yr^{-1} averaged over 2002–2011 (*high confidence*) and were 9.5 [8.7 to 10.3] GtC yr^{-1} in 2011, 54% above the 1990 level. Annual net CO_2 emissions from anthropogenic land use change were 0.9 [0.1 to 1.7] GtC yr^{-1} on average during 2002 to 2011 (*medium confidence*). {6.3}

- From 1750 to 2011, CO_2 emissions from fossil fuel combustion and cement production have released 365 [335 to 395] GtC to the atmosphere, while deforestation and other land use change are estimated to have released 180 [100 to 260] GtC. This results in cumulative anthropogenic emissions of 545 [460 to 630] GtC. {6.3}

[11] ppm (parts per million) or ppb (parts per billion, 1 billion = 1,000 million) is the ratio of the number of gas molecules to the total number of molecules of dry air. For example, 300 ppm means 300 molecules of a gas per million molecules of dry air.

[12] 1 Gigatonne of carbon = 1 GtC = 10^{15} grams of carbon = 1 Petagram of carbon = 1 PgC. This corresponds to 3.67 $GtCO_2$.

- Of these cumulative anthropogenic CO_2 emissions, 240 [230 to 250] GtC have accumulated in the atmosphere, 155 [125 to 185] GtC have been taken up by the ocean and 150 [60 to 240] GtC have accumulated in natural terrestrial ecosystems (cf. cumulative residual land sink). {Figure TS.4, 3.8, 6.3}

- Ocean acidification is quantified by decreases in pH[13]. The pH of ocean surface water has decreased by 0.1 since the beginning of the industrial era (*high confidence*), corresponding to a 26% increase in hydrogen ion concentration (see Figure SPM.4). {3.8., Box 3.2}

[INSERT FIGURE SPM.4 HERE]
Figure SPM.4: Multiple observed indicators of a changing global carbon cycle: (a) atmospheric concentrations of carbon dioxide (CO_2) from Mauna Loa (19°32′N, 155°34′W – red) and South Pole (89°59′S, 24°48′W – black) since 1958; (b) partial pressure of dissolved CO_2 at the ocean surface (blue curves) and *in situ* pH (green curves), a measure of the acidity of ocean water. Measurements are from three stations from the Atlantic (29°10′N, 15°30′W – dark blue/dark green; 31°40′N, 64°10′W – blue/green) and the Pacific Oceans (22°45′N, 158°00′W − light blue/light green). Full details of the datasets shown here are provided in the underlying report and the Technical Summary Supplementary Material. {Figures 2.1 and 3.18; Figure TS.5}

C. Drivers of Climate Change

Natural and anthropogenic substances and processes that alter the Earth's energy budget are drivers of climate change. Radiative forcing[14] (RF) quantifies the change in energy fluxes caused by changes in these drivers for 2011 relative to 1750, unless otherwise indicated. Positive RF leads to surface warming, negative RF leads to surface cooling. RF is estimated based on in-situ and remote observations, properties of greenhouse gases and aerosols, and calculations using numerical models representing observed processes. Some emitted compounds affect the atmospheric concentration of other substances. The RF can be reported based on the concentration changes of each substance[15]. Alternatively, the emission-based RF of a compound can be reported, which provides a more direct link to human activities. It includes contributions from all substances affected by that emission. The total anthropogenic RF of the two approaches are identical when considering all drivers. Though both approaches are used in this Summary, emission-based RFs are emphasized.

Total radiative forcing is positive, and has led to an uptake of energy by the climate system. The largest contribution to total radiative forcing is caused by the increase in the atmospheric concentration of CO_2 since 1750 (see Figure SPM.5). {3.2, Box 3.1, 8.3, 8.5}

[INSERT FIGURE SPM.5 HERE]
Figure SPM.5: Radiative forcing estimates in 2011 relative to 1750 and aggregated uncertainties for the main drivers of climate change. Values are global average radiative forcing (RF[15]) partitioned according to the emitted compounds or processes that result in a combination of drivers. The best estimates of the net radiative forcing are shown as black diamonds with corresponding uncertainty intervals; the numerical values

[13] pH is a measure of acidity using a logarithmic scale: a pH decrease of 1 unit corresponds to a 10-fold increase in hydrogen ion concentration, or acidity.
[14] The strength of drivers is quantified as *Radiative Forcing* (RF) in units watts per square metre (W m^{-2}) as in previous IPCC assessments. RF is the change in energy flux caused by a driver, and is calculated at the tropopause or at the top of the atmosphere. In the traditional RF concept employed in previous IPCC reports all surface and tropospheric conditions are kept fixed. In calculations of RF for well-mixed greenhouse gases and aerosols in this report, physical variables, except for the ocean and sea ice, are allowed to respond to perturbations with rapid adjustments. The resulting forcing is called Effective Radiative Forcing (ERF) in the underlying report. This change reflects the scientific progress from previous assessments and results in a better indication of the eventual temperature response for these drivers. For all drivers other than well-mixed greenhouse gases and aerosols, rapid adjustments are less well characterized and assumed to be small, and thus the traditional RF is used. {8.1}
[15] This approach was used to report RF in the AR4 SPM.

are provided on the right of the figure, together with the confidence level in the net forcing (VH – *very high*, H – *high*, M – *medium*, L – *low*, VL – *very low*). Albedo forcing due to black carbon on snow and ice is included in the black carbon aerosol bar. Small forcings due to contrails (0.05 W m^{-2}, including contrail induced cirrus), and HFCs, PFCs and SF_6 (total 0.03 W m^{-2}) are not shown. Concentration-based RFs for gases can be obtained by summing the like-coloured bars. Volcanic forcing is not included as its episodic nature makes is difficult to compare to other forcing mechanisms. Total anthropogenic radiative forcing is provided for three different years relative to 1750. For further technical details, including uncertainty ranges associated with individual components and processes, see the Technical Summary Supplementary Material. {8.5; Figures 8.14–8.18; Figures TS.6 and TS.7}

- The total anthropogenic RF for 2011 relative to 1750 is 2.29 [1.13 to 3.33] W m^{-2} (see Figure SPM.5), and it has increased more rapidly since 1970 than during prior decades. The total anthropogenic RF best estimate for 2011 is 43% higher than that reported in AR4 for the year 2005. This is caused by a combination of continued growth in most greenhouse gas concentrations and improved estimates of RF by aerosols indicating a weaker net cooling effect (negative RF). {8.5}

- The RF from emissions of well-mixed greenhouse gases (CO_2, CH_4, N_2O, and Halocarbons) for 2011 relative to 1750 is 3.00 [2.22 to 3.78] W m^{-2} (see Figure SPM.5). The RF from changes in concentrations in these gases is 2.83 [2.26 to 3.40] W m^{-2}. {8.5}

- Emissions of CO_2 alone have caused an RF of 1.68 [1.33 to 2.03] W m^{-2} (see Figure SPM.5). Including emissions of other carbon-containing gases, which also contributed to the increase in CO_2 concentrations, the RF of CO_2 is 1.82 [1.46 to 2.18] W m^{-2}. {8.3, 8.5}

- Emissions of CH_4 alone have caused an RF of 0.97 [0.74 to 1.20] W m^{-2} (see Figure SPM.5). This is much larger than the concentration-based estimate of 0.48 [0.38 to 0.58] Wm^{-2} (unchanged from AR4). This difference in estimates is caused by concentration changes in ozone and stratospheric water vapour due to CH_4 emissions and other emissions indirectly affecting CH_4. {8.3, 8.5}

- Emissions of stratospheric ozone-depleting halocarbons have caused a net positive RF of 0.18 [0.01 to 0.35] W m^{-2} (see Figure SPM.5). Their own positive RF has outweighed the negative RF from the ozone depletion that they have induced. The positive RF from all halocarbons is similar to the value in AR4, with a reduced RF from CFCs but increases from many of their substitutes. {8.3, 8.5}

- Emissions of short-lived gases contribute to the total anthropogenic RF. Emissions of carbon monoxide are *virtually certain* to have induced a positive RF, while emissions of nitrogen oxides (NO_x) are *likely* to have induced a net negative RF (see Figure SPM.5). {8.3, 8.5}

- The RF of the total aerosol effect in the atmosphere, which includes cloud adjustments due to aerosols, is –0.9 [–1.9 to −0.1] W m^{-2} (*medium confidence*), and results from a negative forcing from most aerosols and a positive contribution from black carbon absorption of solar radiation. There is *high confidence* that aerosols and their interactions with clouds have offset a substantial portion of global mean forcing from well-mixed greenhouse gases. They continue to contribute the largest uncertainty to the total RF estimate. {7.5, 8.3, 8.5}

- The forcing from stratospheric volcanic aerosols can have a large impact on the climate for some years after volcanic eruptions. Several small eruptions have caused a RF of –0.11 [–0.15 to –0.08] W m^{-2} for the years 2008–2011, which is approximately twice as strong as during the years 1999–2002. {8.4}

- The RF due to changes in solar irradiance is estimated as 0.05 [0.00 to 0.10] W m^{-2}. Satellite observations of total solar irradiance changes from 1978 to 2011 indicate that the last solar minimum was lower than the previous two. This results in a RF of –0.04 [–0.08 to 0.00] W m^{-2} between the most recent minimum in 2008 and the 1986 minimum. {8.4}

- The total natural RF from solar irradiance changes and stratospheric volcanic aerosols made only a small contribution to the net radiative forcing throughout the last century, except for brief periods after large volcanic eruptions. {8.5}

D. Understanding the Climate System and its Recent Changes

Understanding recent changes in the climate system results from combining observations, studies of feedback processes, and model simulations. Evaluation of the ability of climate models to simulate recent changes requires consideration of the state of all modelled climate system components at the start of the simulation and the natural and anthropogenic forcing used to drive the models. Compared to AR4, more detailed and longer observations and improved climate models now enable the attribution of a human contribution to detected changes in more climate system components.

Human influence on the climate system is clear. This is evident from the increasing greenhouse gas concentrations in the atmosphere, positive radiative forcing, observed warming, and understanding of the climate system. {2–14}

D.1 Evaluation of Climate Models

Climate models have improved since the AR4. Models reproduce observed continental-scale surface temperature patterns and trends over many decades, including the more rapid warming since the mid-20th century and the cooling immediately following large volcanic eruptions (*very high confidence*). {9.4, 9.6, 9.8}

- The long-term climate model simulations show a trend in global-mean surface temperature from 1951 to 2012 that agrees with the observed trend (*very high confidence*). There are, however, differences between simulated and observed trends over periods as short as 10 to 15 years (e.g., 1998 to 2012). {9.4, Box 9.2}

- The observed reduction in surface warming trend over the period 1998–2012 as compared to the period 1951–2012, is due in roughly equal measure to a reduced trend in radiative forcing and a cooling contribution from internal variability, which includes a possible redistribution of heat within the ocean (*medium confidence*). The reduced trend in radiative forcing is primarily due to volcanic eruptions and the timing of the downward phase of the 11-year solar cycle. However, there is *low confidence* in quantifying the role of changes in radiative forcing in causing the reduced warming trend. There is *medium confidence* that internal decadal variability causes to a substantial degree the difference between observations and the simulations; the latter are not expected to reproduce the timing of internal variability. There may also be a contribution from forcing inadequacies and, in some models, an overestimate of the response to increasing greenhouse gas and other anthropogenic forcing (dominated by the effects of aerosols). {9.4, Box 9.2, 10.3, Box 10.2, 11.3}

- On regional scales, the confidence in model capability to simulate surface temperature is less than for the larger scales. However, there is *high confidence* that regional-scale surface temperature is better simulated than at the time of the AR4. {9.4, 9.6}

- There has been substantial progress in the assessment of extreme weather and climate events since AR4. Simulated global-mean trends in the frequency of extreme warm and cold days and nights over the second half of the 20th century are generally consistent with observations. {9.5}

- There has been some improvement in the simulation of continental-scale patterns of precipitation since the AR4. At regional scales, precipitation is not simulated as well, and the assessment is hampered by observational uncertainties. {9.4, 9.6}

- Some important climate phenomena are now better reproduced by models. There is *high confidence* that the statistics of monsoon and El Niño-Southern Oscillation (ENSO) based on multi-model simulations have improved since AR4. {9.5}

- Climate models now include more cloud and aerosol processes, and their interactions, than at the time of the AR4, but there remains *low confidence* in the representation and quantification of these processes in models. {7.3, 7.6, 9.4, 9.7}

- There is robust evidence that the downward trend in Arctic summer sea ice extent since 1979 is now reproduced by more models than at the time of the AR4, with about one-quarter of the models showing a trend as large as, or larger than, the trend in the observations. Most models simulate a small downward trend in Antarctic sea ice extent, albeit with large inter-model spread, in contrast to the small upward trend in observations. {9.4}

- Many models reproduce the observed changes in upper-ocean heat content (0–700 m) from 1961 to 2005 (*high confidence*), with the multi-model mean time series falling within the range of the available observational estimates for most of the period. {9.4}

- Climate models that include the carbon cycle (Earth System Models) simulate the global pattern of ocean-atmosphere CO_2 fluxes, with outgassing in the tropics and uptake in the mid and high latitudes. In the majority of these models the sizes of the simulated global land and ocean carbon sinks over the latter part of the 20th century are within the range of observational estimates. {9.4}

D.2 Quantification of Climate System Responses

Observational and model studies of temperature change, climate feedbacks and changes in the Earth's energy budget together provide confidence in the magnitude of global warming in response to past and future forcing. {Box 12.2, Box 13.1}

- The net feedback from the combined effect of changes in water vapour, and differences between atmospheric and surface warming is *extremely likely* positive and therefore amplifies changes in climate. The net radiative feedback due to all cloud types combined is *likely* positive. Uncertainty in the sign and magnitude of the cloud feedback is due primarily to continuing uncertainty in the impact of warming on low clouds. {7.2}

- The equilibrium climate sensitivity quantifies the response of the climate system to constant radiative forcing on multi-century time scales. It is defined as the change in global mean surface temperature at equilibrium that is caused by a doubling of the atmospheric CO_2 concentration. Equilibrium climate sensitivity is *likely* in the range 1.5°C to 4.5°C (*high confidence*), *extremely unlikely* less than 1°C (*high confidence*), and *very unlikely* greater than 6°C (*medium confidence*)[16]. The lower temperature limit of the assessed *likely* range is thus less than the 2°C in the AR4, but the upper limit is the same. This assessment reflects improved understanding, the extended temperature record in the atmosphere and ocean, and new estimates of radiative forcing. {TFE6.1, Figure 1; Box 12.2}

- The rate and magnitude of global climate change is determined by radiative forcing, climate feedbacks and the storage of energy by the climate system. Estimates of these quantities for recent decades are consistent with the assessed *likely* range of the equilibrium climate

[16] No best estimate for equilibrium climate sensitivity can now be given because of a lack of agreement on values across assessed lines of evidence and studies.

sensitivity to within assessed uncertainties, providing strong evidence for our understanding of anthropogenic climate change. {Box 12.2, Box 13.1}

- The transient climate response quantifies the response of the climate system to an increasing radiative forcing on a decadal to century timescale. It is defined as the change in global mean surface temperature at the time when the atmospheric CO_2 concentration has doubled in a scenario of concentration increasing at 1% per year. The transient climate response is *likely* in the range of 1.0°C to 2.5°C (*high confidence*) and *extremely unlikely* greater than 3°C. {Box 12.2}

- A related quantity is the transient climate response to cumulative carbon emissions (TCRE). It quantifies the transient response of the climate system to cumulative carbon emissions (see Section E.8). TCRE is defined as the global mean surface temperature change per 1000 GtC emitted to the atmosphere. TCRE is *likely* in the range of 0.8°C to 2.5°C per 1000 GtC and applies for cumulative emissions up to about 2000 GtC until the time temperatures peak (see Figure SPM.9). {12.5, Box 12.2}

- Various metrics can be used to compare the contributions to climate change of emissions of different substances. The most appropriate metric and time horizon will depend on which aspects of climate change are considered most important to a particular application. No single metric can accurately compare all consequences of different emissions, and all have limitations and uncertainties. Global Warming Potential is based on the cumulative radiative forcing over a particular time horizon, and the Global Temperature change Potential is based on the change in global mean surface temperature at a chosen point in time. Updated values are provided in this Report. {8.7}

D.3 Detection and Attribution of Climate Change

Human influence has been detected in warming of the atmosphere and the ocean, in changes in the global water cycle, in reductions in snow and ice, in global mean sea level rise, and in changes in some climate extremes (Figure SPM.6 and Table SPM.1). This evidence for human influence has grown since AR4. It is *extremely likely* that human influence has been the dominant cause of the observed warming since the mid-20th century. {10.3–10.6, 10.9}

[INSERT FIGURE SPM.6 HERE]

Figure SPM.6: Comparison of observed and simulated climate change based on three large-scale indicators in the atmosphere, the cryosphere and the ocean: change in continental land surface air temperatures (yellow panels), Arctic and Antarctic September sea ice extent (white panels), and upper ocean heat content in the major ocean basins (blue panels). Global average changes are also given. Anomalies are given relative to 1880–1919 for surface temperatures, 1960–1980 for ocean heat content and 1979–1999 for sea ice. All time-series are decadal averages, plotted at the centre of the decade. For temperature panels, observations are dashed lines if the spatial coverage of areas being examined is below 50%. For ocean heat content and sea ice panels the solid line is where the coverage of data is good and higher in quality, and the dashed line is where the data coverage is only adequate, and thus, uncertainty is larger. Model results shown are Coupled Model Intercomparison Project Phase 5 (CMIP5) multi-model ensemble ranges, with shaded bands indicating the 5 to 95% confidence intervals. For further technical details, including region definitions see the Technical Summary Supplementary Material. {Figure 10.21; Figure TS.12}

- It is *extremely likely* that more than half of the observed increase in global average surface temperature from 1951 to 2010 was caused by the anthropogenic increase in greenhouse gas concentrations and other anthropogenic forcings together. The best estimate of the human-induced contribution to warming is similar to the observed warming over this period. {10.3}

- Greenhouse gases contributed a global mean surface warming *likely* to be in the range of 0.5°C to 1.3°C over the period 1951−2010, with the contributions from other anthropogenic forcings, including the cooling effect of aerosols, *likely* to be in the range of −0.6°C to 0.1°C. The contribution from natural forcings is *likely* to be in the range of −0.1°C to 0.1°C, and from

internal variability is *likely* to be in the range of −0.1°C to 0.1°C. Together these assessed contributions are consistent with the observed warming of approximately 0.6°C to 0.7°C over this period. {10.3}

- Over every continental region except Antarctica, anthropogenic forcings have *likely* made a substantial contribution to surface temperature increases since the mid-20th century (see Figure SPM.6). For Antarctica, large observational uncertainties result in *low confidence* that anthropogenic forcings have contributed to the observed warming averaged over available stations. It is *likely* that there has been an anthropogenic contribution to the very substantial Arctic warming since the mid-20th century. {2.4, 10.3}

- It is *very likely* that anthropogenic influence, particularly greenhouse gases and stratospheric ozone depletion, has led to a detectable observed pattern of tropospheric warming and a corresponding cooling in the lower stratosphere since 1961. {2.4, 9.4, 10.3}

- It is *very likely* that anthropogenic forcings have made a substantial contribution to increases in global upper ocean heat content (0–700 m) observed since the 1970s (see Figure SPM.6). There is evidence for human influence in some individual ocean basins. {3.2, 10.4}

- It is *likely* that anthropogenic influences have affected the global water cycle since 1960. Anthropogenic influences have contributed to observed increases in atmospheric moisture content in the atmosphere (*medium confidence*), to global-scale changes in precipitation patterns over land (*medium confidence)*, to intensification of heavy precipitation over land regions where data are sufficient (*medium confidence*), and to changes in surface and sub-surface ocean salinity (*very likely*). {2.5, 2.6, 3.3, 7.6, 10.3, 10.4}

- There has been further strengthening of the evidence for human influence on temperature extremes since the SREX. It is now *very likely* that human influence has contributed to observed global scale changes in the frequency and intensity of daily temperature extremes since the mid-20th century, and *likely* that human influence has more than doubled the probability of occurrence of heat waves in some locations (see Table SPM.1). {10.6}

- Anthropogenic influences have *very likely* contributed to Arctic sea ice loss since 1979. There is *low confidence* in the scientific understanding of the small observed increase in Antarctic sea ice extent due to the incomplete and competing scientific explanations for the causes of change and *low confidence* in estimates of internal variability in that region (see Figure SPM.6). {10.5}

- Anthropogenic influences *likely* contributed to the retreat of glaciers since the 1960s and to the increased surface mass loss of the Greenland ice sheet since 1993. Due to a low level of scientific understanding there is *low confidence* in attributing the causes of the observed loss of mass from the Antarctic ice sheet over the past two decades. {4.3, 10.5}

- It is *likely* that there has been an anthropogenic contribution to observed reductions in Northern Hemisphere spring snow cover since 1970. {10.5}

- It is *very likely* that there is a substantial anthropogenic contribution to the global mean sea level rise since the 1970s. This is based on the *high confidence* in an anthropogenic influence on the two largest contributions to sea level rise, that is thermal expansion and glacier mass loss. {10.4, 10.5, 13.3}

- There is *high confidence* that changes in total solar irradiance have not contributed to the increase in global mean surface temperature over the period 1986 to 2008, based on direct satellite measurements of total solar irradiance. There is *medium confidence* that the 11-year cycle of solar variability influences decadal climate fluctuations in some regions. No robust

Figure SPM.1 [FIGURE SUBJECT TO FINAL COPYEDIT]

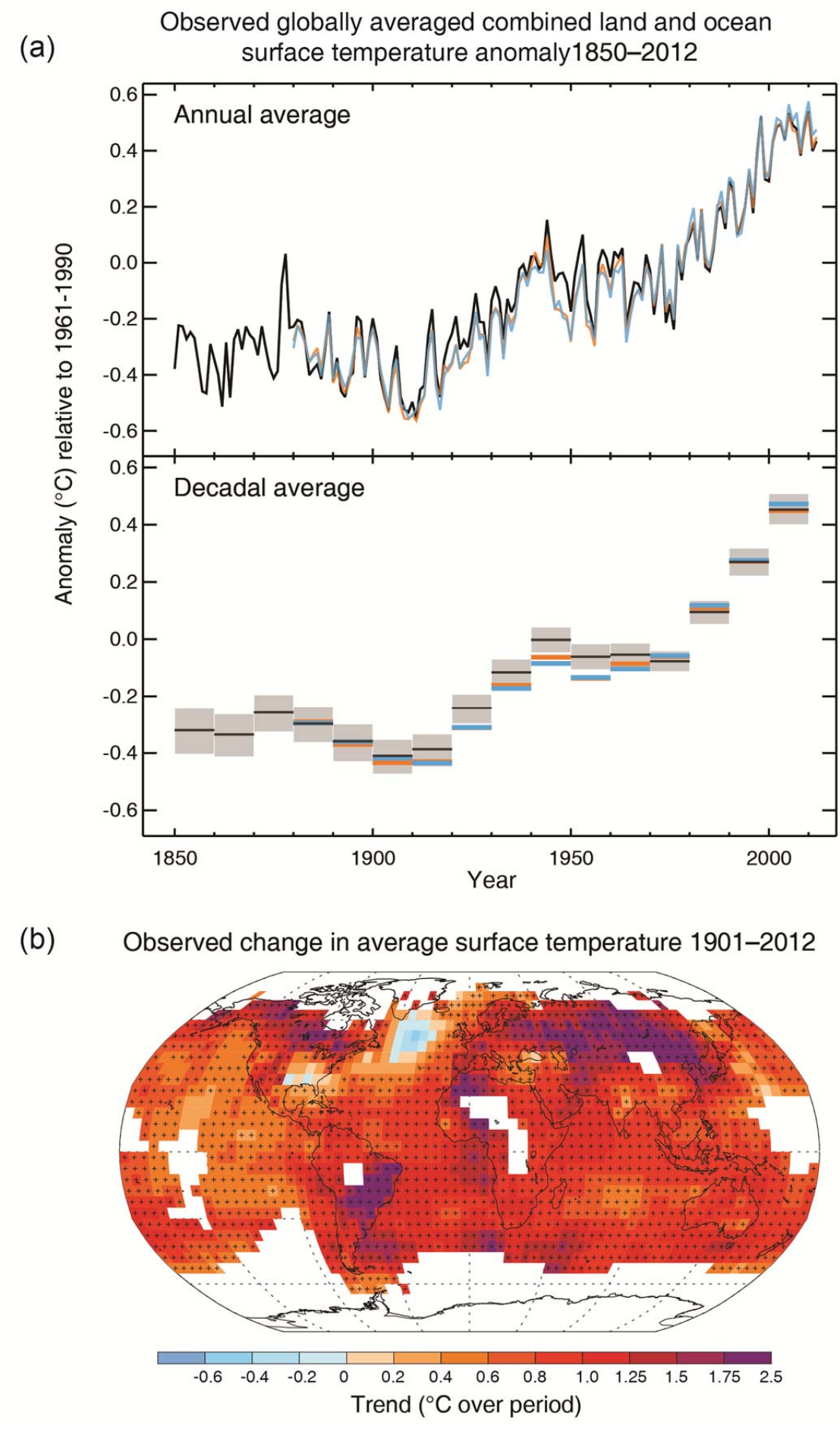

Figure SPM.2 [FIGURE SUBJECT TO FINAL COPYEDIT]

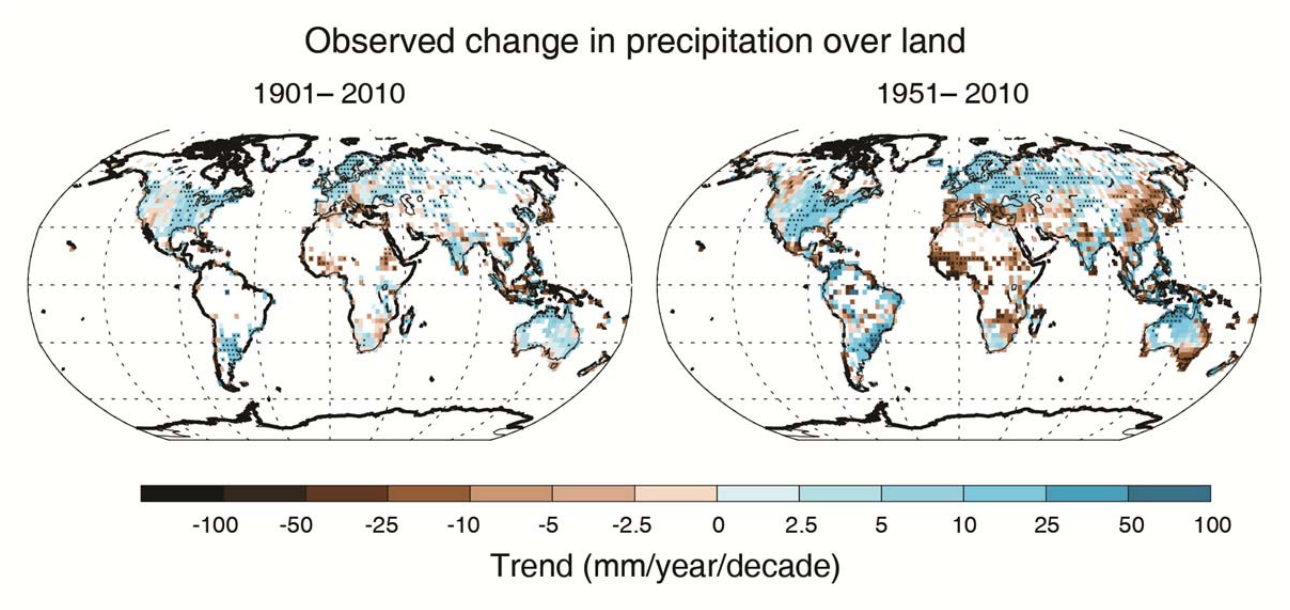

Figure SPM.3 [FIGURE SUBJECT TO FINAL COPYEDIT]

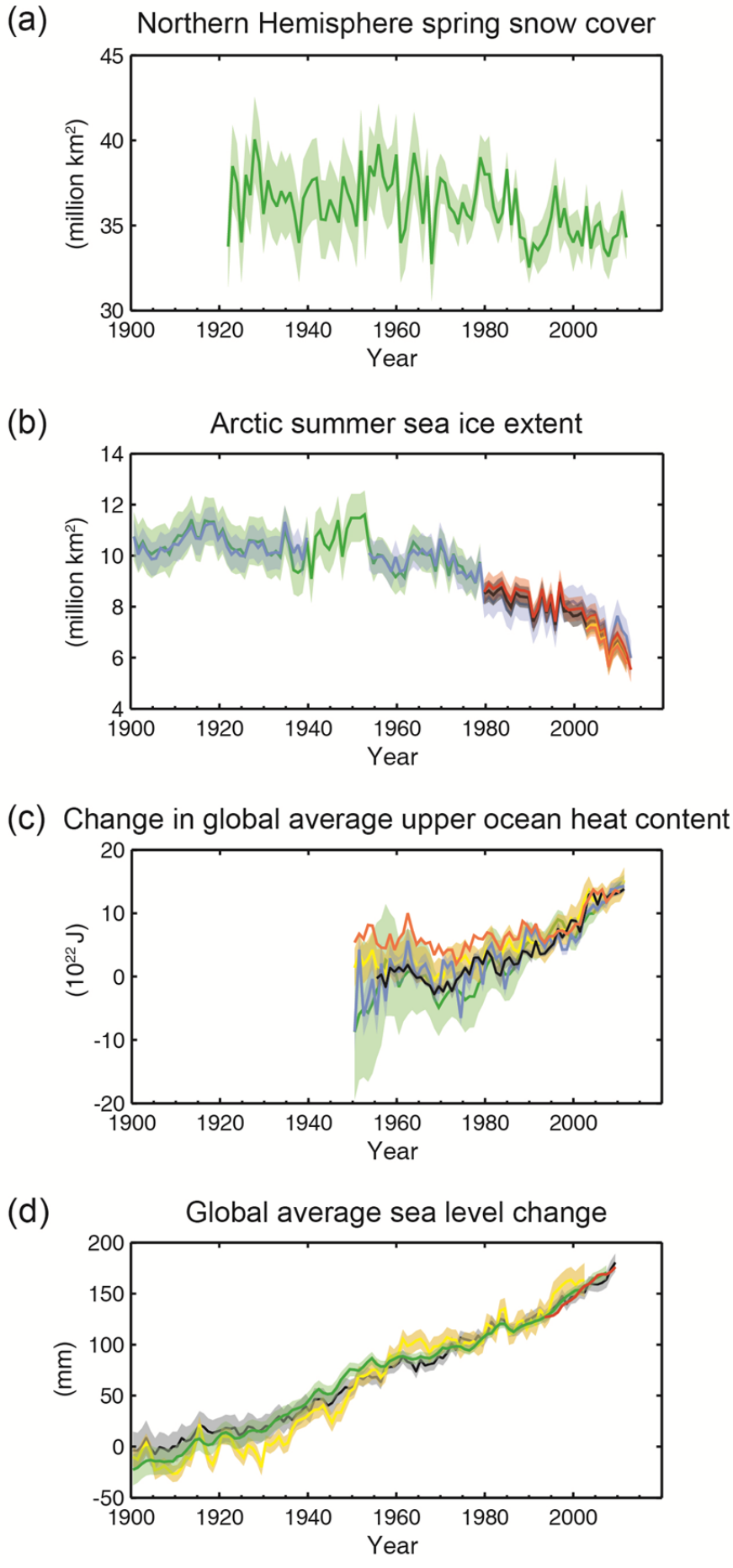

Figure SPM.4 [FIGURE SUBJECT TO FINAL COPYEDIT]

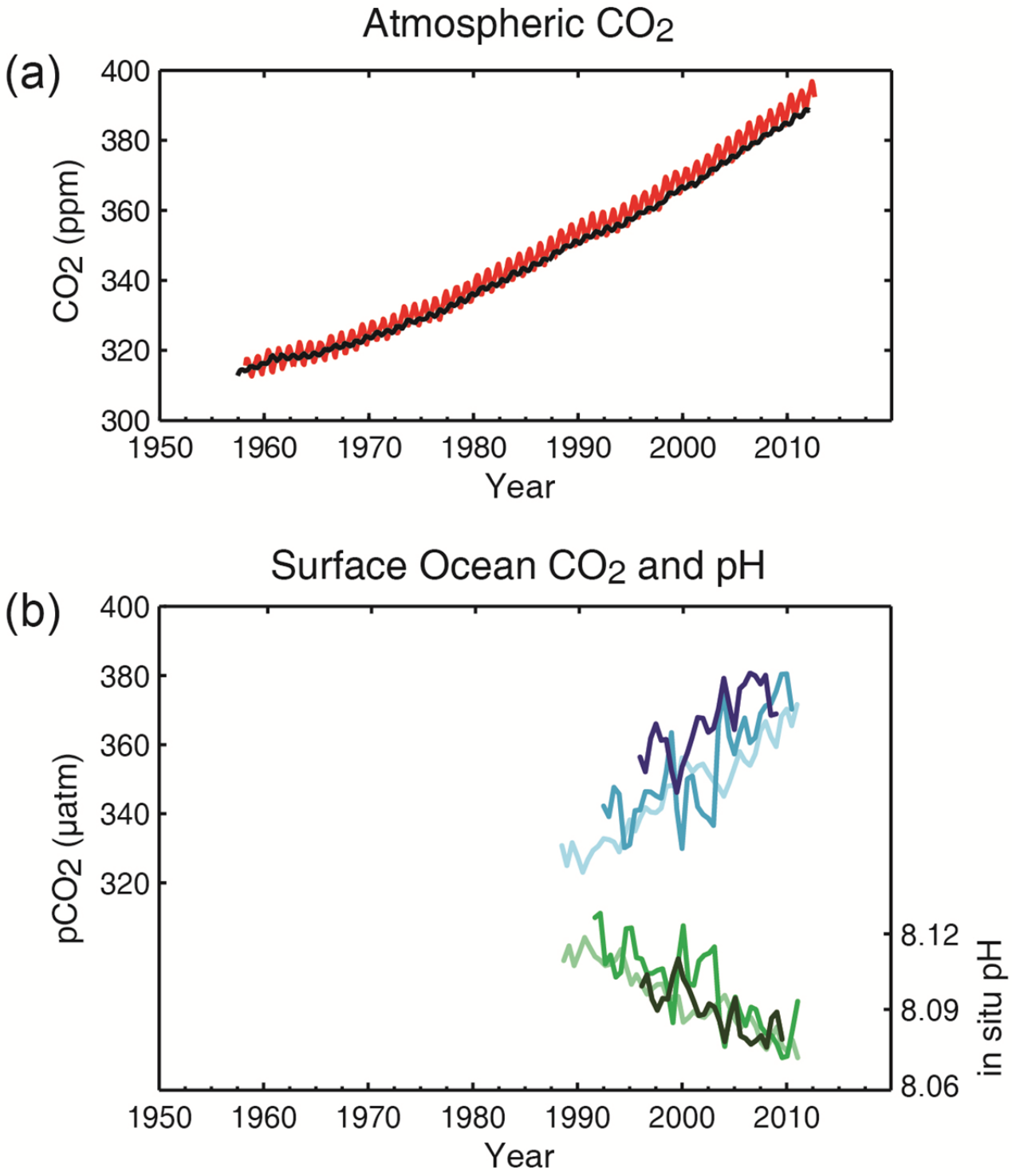

Figure SPM.5 [FIGURE SUBJECT TO FINAL COPYEDIT]

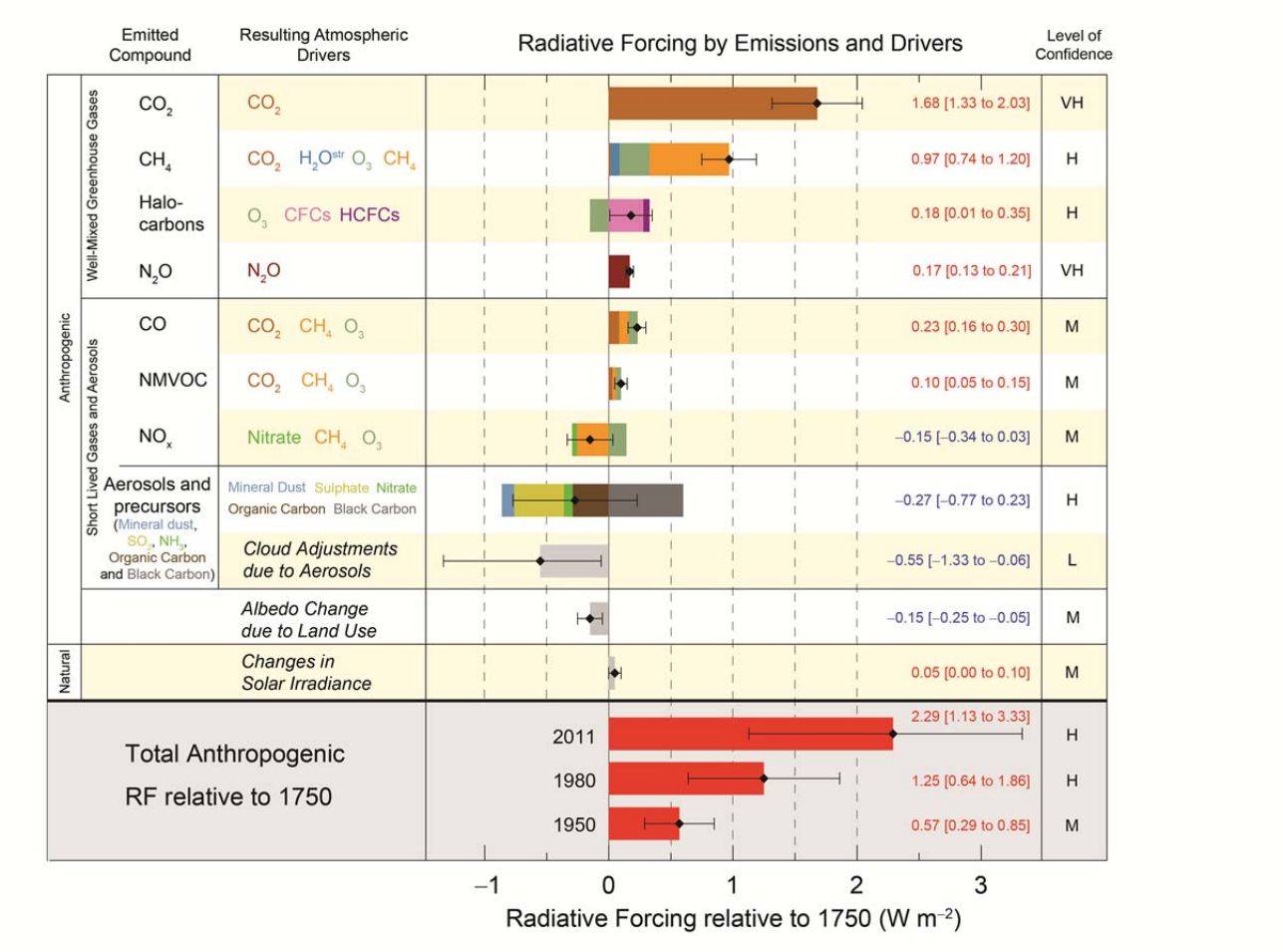

Figure SPM.6 [FIGURE SUBJECT TO FINAL COPYEDIT]

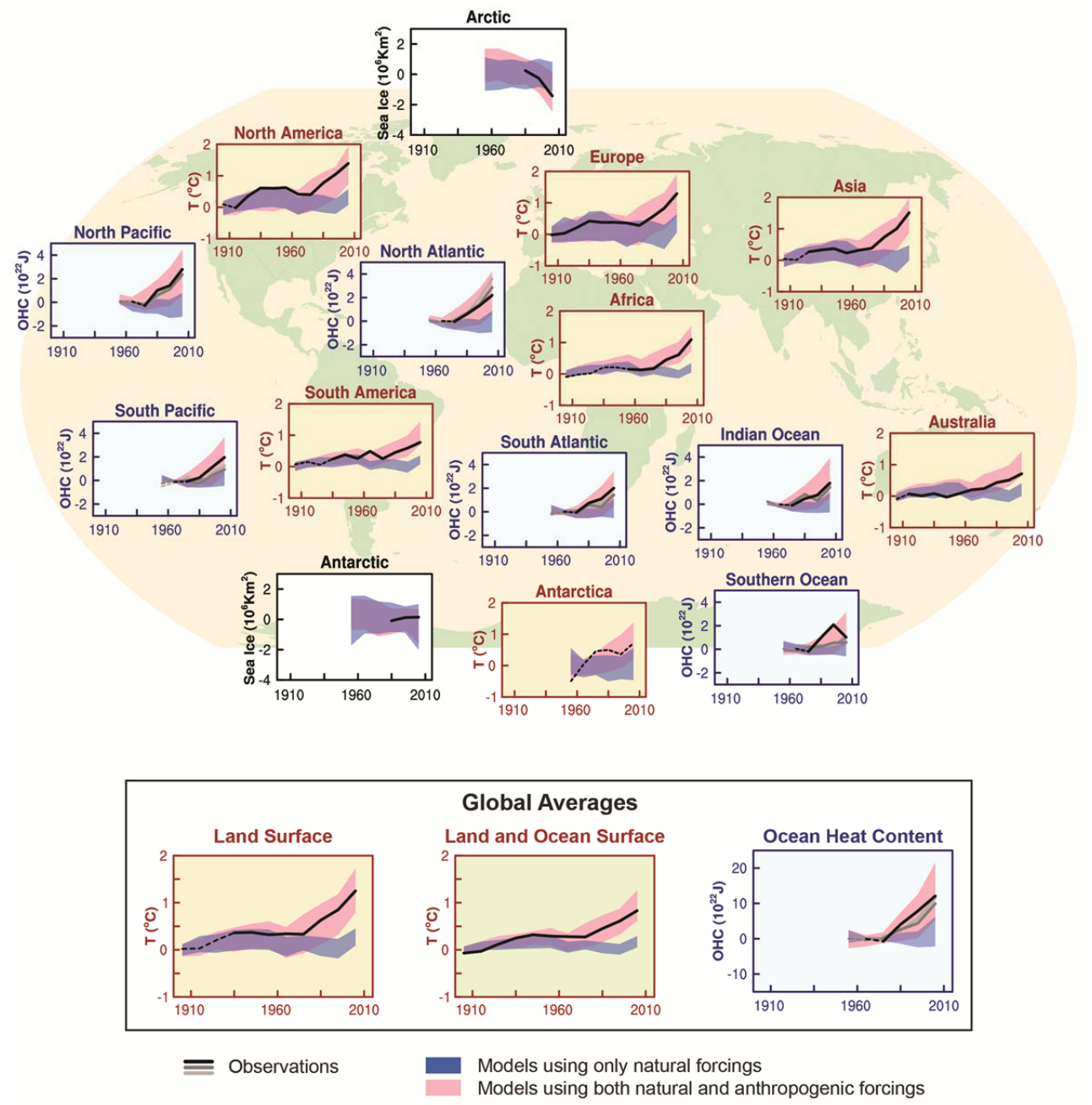

for projections of future climate change over the 21st century and beyond from regional to global scale. Section TS.6 combines and lists key uncertainties from the WGI assessment from Sections TS.2–TS.5. The overall nine Thematic Focus Elements (TFEs), cutting across the various components of the WGI AR5, are dispersed throughout the four main TS sections, are visually distinct from the main text, and should allow stand-alone reading.

The basis for substantive paragraphs in this Technical Summary can be found in the chapter sections of the underlying report. These references are given in curly brackets.

TS.2 Observation of Changes in the Climate System

TS.2.1 Introduction

Observations of the climate system are based on direct physical and biogeochemical measurements, remote sensing from ground stations and satellites; information derived from paleoclimate archives provides a long-term context. Global-scale observations from the instrumental era began in the mid-19th century, and paleoclimate reconstructions extend the record of some quantities back hundreds to millions of years. Together, they provide a comprehensive view of the variability and long-term changes in the atmosphere, the ocean, the cryosphere, and the land surface.

The assessment of observational evidence for climate change is summarized in this section. Substantial advancements in the availability, acquisition, quality and analysis of observational data sets in atmosphere, land surface, ocean, and cryosphere have occurred since the AR4. Many aspects of the climate system are showing evidence of a changing climate.

TS.2.2 Changes in Temperature

TS.2.2.1 Surface

It is certain that Global Mean Surface Temperature (GMST) has increased since the late 19th century (Figure TS.1). Each of the past three decades has been warmer than all the previous decades in the instrumental record, and the decade of the 2000's has been the warmest. The global combined land and ocean temperature data show an increase of about 0.89°C [0.69–1.08][5] over the period 1901–2012 and about 0.72°C [0.49-0.89] over the period 1951–2012 when described by a linear trend[6]. The warming from 1850–1900 (early-industrial) to 1986–2005 (reference period for the modelling chapters and the Atlas in Annex 1) is 0.61°C [0.55 to 0.67], when calculated using HadCRUT4 and its uncertainty estimates. It is also *virtually certain* that maximum and minimum temperatures over land have increased on a global scale since 1950. {2.4.1, 2.4.3, Supplementary Material 2.SM.3}

Despite the robust multi-decadal timescale warming, there exists substantial interannual to decadal variability in the rate of warming, with several periods exhibiting weaker trends (including the warming hiatus since 1998) (Figure TS.1). Although the trend uncertainty is large for short records, the rate of warming over the past 15 years (1998–2012; 0.05°C per decade [–0.05 to +0.15]) is smaller than the trend since 1951 (1951–2012; 0.12°C per decade [0.08 to 0.14])[6]. Several independently analysed data records of global and regional land surface air temperature obtained from station observations are in broad agreement that land surface air temperature s have increased. Sea surface temperatures have also increased. Intercomparisons of new sea surface temperature data records obtained by different measurement methods, including satellite data, have resulted in better understanding of errors and biases in the records. {2.4.1, 2.4.2, 2.4.3; Box 9.2}

[5] In the WGI contribution to the AR5, uncertainty is quantified using 90% uncertainty intervals unless otherwise stated. The 90% uncertainty interval, reported in square brackets, is expected to have a 90% likelihood of covering the value that is being estimated. The upper endpoint of the uncertainty interval has a 95% likelihood of exceeding the value that is being estimated and the lower endpoint has a 95% likelihood of being less than that value. A best estimate of that value is also given where available. Uncertainty intervals are not necessarily symmetric about the corresponding best estimate.

[6] The warming is reported as an unweighted average based upon linear trend estimates calculated from HadCRUT4, MLOST and GISS datasets (see Figure TS.2; Section 2.4.3)

[INSERT FIGURE TS.1 HERE]
Figure TS.1: Multiple complementary indicators of a changing global climate. Each line represents an independently-derived estimate of change in the climate element. The times series presented are assessed in chapters 2, 3, and 4. In each panel all datasets have been normalized to a common period of record. A full detailing of which source datasets go into which panel is given in Chapter 2, Supplementary Material 2.SM.5 and in the respective chapters (See also FAQ 2.1, Figure 1). {2.4, 2.5, 3.2, 3.7, 4.5.2, 4.5.3}

[INSERT FIGURE TS.2 HERE]
Figure TS.2: Change in surface temperature over 1901-2012 as determined by linear trend for three data sets. White areas indicate incomplete or missing data. Trends have been calculated only for those grid boxes with greater than 70% complete records and more than 20% data availability in the first and last 10% of the time period. Black plus signs (+) indicate grid boxes where trends are significant (i.e., a trend of zero lies outside the 90% confidence interval). Differences in coverage primarily reflect the degree of interpolation to account for data void regions undertaken by the dataset providers ranging from none beyond grid box averaging (HadCRUT4) to substantial (GISS). {Figure 2.21}

It is *unlikely* that any uncorrected urban heat-island effects and land use change effects have raised the estimated centennial globally averaged land surface air temperature trends by more than 10% of the reported trend. This is an average value; in some regions that have rapidly developed urban heat island and land use change impacts on regional trends may be substantially larger. {2.4.1}

There is *high confidence* that annual mean surface warming since the 20th century has reversed long-term cooling trends of the past 5,000 years in mid-to-high latitudes of the Northern Hemisphere. For average annual Northern Hemisphere temperatures, the period 1983–2012 was *very likely* the warmest 30-year period of the last 800 years (*high confidence*) and *likely* the warmest 30-year period of the last 1400 years (*medium confidence*). This is supported by comparison of instrumental temperatures with multiple reconstructions from a variety of proxy data and statistical methods, and is consistent with AR4. Continental-scale surface temperature reconstructions show, with *high confidence*, multidecadal intervals during the Medieval Climate Anomaly (950 to 1250) that were in some regions as warm as in the mid-20th century and in others as warm as in the late 20th century. With *high confidence*, these intervals were not as synchronous across seasons and regions as the warming since the mid-20th century. Based on the comparison between reconstructions and simulations, there is *high confidence* that not only external orbital, solar and volcanic forcing, but also internal variability, contributed substantially to the spatial pattern and timing of surface-temperature changes between the Medieval Climate Anomaly and the Little Ice Age (1450 to 1850). {5.3.5, 5.5.1}

TS.2.2.2 Troposphere and Stratosphere

Based upon multiple independent analyses of measurements from radiosondes and satellite sensors, it is *virtually certain* that globally the troposphere has warmed and the stratosphere has cooled since the mid-20th century (Figure TS.1). Despite unanimous agreement on the sign of the trends, substantial disagreement exists between available estimates as to the rate of temperature changes, particularly outside the Northern Hemisphere extra-tropical troposphere, which has been well sampled by radiosondes. Hence there is only *medium confidence* in the rate of change and its vertical structure in the Northern Hemisphere extra-tropical troposphere and *low confidence* elsewhere. {2.4.4}

TS.2.2.3 Ocean

It is *virtually certain* that the upper ocean (above 700 m) has warmed from 1971 to 2010, and *likely* that it has warmed from the 1870s to 1971 (Figure TS.1). There is less certainty in changes prior to 1971 because of relatively sparse sampling in earlier time periods. Instrumental biases in historical upper ocean temperature measurements have been identified and mitigated since AR4, reducing artificial decadal variation in temperature and upper ocean heat content, most prominent during the 1970s and 1980s. {3.2.1, 3.2.2, 3.2.3, 3.5.3}

It is *likely* that the ocean warmed between 700 and 2000 m from 1957 to 2010, based on five-year averages. It is *likely* that the ocean warmed from 3000 m to the bottom from 1992 to 2005, when sufficient observations became available for a global assessment. No significant trends in global average temperature

were observed between 2000 and 3000 m depth for either overlapping time period. The largest changes in deep ocean temperature have been observed close to the sources of deep and bottom water in the northern North Atlantic and especially in the Southern Ocean with anomaly amplitudes lessening along the routes through which these waters spread. {3.2.4, 3.5.1}

TS.2.3 Changes in Energy Budget and Heat Content

Earth has been in radiative imbalance, with more energy from the sun entering than exiting the top of the atmosphere, since at least circa 1970. It is *virtually certain* that Earth has gained substantial energy from 1971–2010. The estimated increase in energy inventory between 1971 and 2010 is 274 [196 to 351] x 10^{21} J), with a heating rate of 213 x 10^{12} W from a linear fit to the annual values over that time period (see also TFE.4).

Ocean warming dominates that total heating rate, with full ocean depth warming accounting for about 93% (and warming of the upper (0–700 m) ocean accounting for about 64%). Melting ice (including Arctic sea ice, ice sheets, and glaciers) and warming of the continents each account for 3 of the total. Warming of the atmosphere makes up the remaining 1%. The 1971–2010 estimated rate of ocean energy gain is 199×10^{12} W from a linear fit to data over that time period, equivalent to 0.42 W m^{-2} heating applied continuously over Earth's entire surface, and 0.55 W m^{-2} for the portion owing to ocean warming applied over the ocean's entire surface area. Earth's estimated energy increase from 1993–2010 is 163 [127 to 201] $\times 10^{21}$ J with a trend estimate of 275×10^{15} W. The ocean portion of the trend for 1993–2010 is 257×10^{12} W, equivalent to a mean heat flux into the ocean of 0.71 W m^{-2}. {3.2.3, 3.2.4; Box 3.1}

The rate of ocean warming in some of the 0–700 m estimates was lower from 2003 to 2010 than in the previous decade (Figure TS.1); however, warming in the subsurface layer between 700 and 2000 m *likely* continued unabated during this period. {3.2.3, 3.2.4; Box 9.2}

TS.2.4 Changes in Circulation and Modes of Variability

Large variability on interannual to decadal time scales hampers robust conclusions on long-term changes in atmospheric circulation in many instances. *Confidence* is *high* that the increase of the northern mid-latitude westerly winds and the NAO index from the 1950s to the 1990s, and the weakening of the Pacific Walker circulation from the late 19th century to the 1990s, have been largely offset by recent changes. With *high confidence*, decadal and multi-decadal changes in the winter North Atlantic Oscillation index (NAO) observed since the 20th century are not unprecedented in the context of the past 500 years. {2.7.2, 2.7.5, 2.7.8, 5.4; Box 2.5; Tables 2.12}

It is *likely* that circulation features have moved poleward since the 1970s, involving a widening of the tropical belt, a poleward shift of storm tracks and jet streams, and a contraction of the northern polar vortex. Evidence is more robust for the Northern Hemisphere. It is *likely* that the Southern Annular Mode has become more positive since the 1950s. The increase in the strength of the observed summer Southern Annular Mode since 1950 has been anomalous, with *medium confidence*, in the context of the past 400 years. {2.7.5, 2.7.6, 2.7.8, 5.4; Box 2.5; Tables 2.2–2.12}

New results from high-resolution coral records document with *high confidence* that the El Niño-Southern Oscillation (ENSO) system has remained highly variable throughout the past 7,000 years, showing no discernible evidence for an orbital modulation of ENSO. {5.4}

Recent observations have strengthened evidence for variability in major ocean circulation systems on time scales from years to decades. It is *very likely* that the subtropical gyres in the North Pacific and South Pacific have expanded and strengthened since 1993. Based on measurements of the full Atlantic Meridional Overturning Circulation (AMOC) and its individual components at various latitudes and different time periods, there is no evidence of a long-term trend. There is also no evidence for trends in the transports of the Indonesian Throughflow, the Antarctic Circumpolar Current (ACC), or in the transports between the Atlantic Ocean and Nordic Seas. However, a southward shift of the ACC by about 1° of latitude is observed in data spanning the time period 1950 to 2010 with *medium confidence*. {3.6}

TS.2.5 Changes in the Water Cycle and Cryosphere

TS.2.5.1 Atmosphere

Confidence in precipitation change averaged over global land areas *is low* prior to 1950 and *medium* afterwards because of insufficient data, particularly in the earlier part of the record (for an overview of observed and projected changes in the global water cycle see TFE.1). Available globally incomplete records show mixed and non-significant long-term trends in reported global mean changes. Further, when virtually all the land area is filled in using a reconstruction method, the resulting time series shows little change in land-based precipitation since 1900. Northern hemisphere mid-latitude land areas do show a *likely* overall increase in precipitation (*medium confidence* prior to 1950, but *high confidence* afterwards). {2.5.1}

It is *very likely* that global near surface and tropospheric air specific humidity have increased since the 1970s. However, during recent years the near-surface moistening trend over land has abated (*medium confidence*) (Figure TS.1). As a result, fairly widespread decreases in relative humidity near the surface are observed over the land in recent years. {2.4.4, 2.5.5, 2.5.6}

While trends of cloud cover are consistent between independent data sets in certain regions, substantial ambiguity and therefore *low confidence* remains in the observations of global-scale cloud variability and trends. {2.5.7}

TS.2.5.2 Ocean and Surface Fluxes

It is *very likely* that regional trends have enhanced the mean geographical contrasts in sea surface salinity since the 1950s: saline surface waters in the evaporation-dominated mid-latitudes have become more saline, while relatively fresh surface waters in rainfall-dominated tropical and polar regions have become fresher. The mean contrast between high and low salinity regions increased by 0.13 [0.08 to 0.17] from 1950 to 2008. It is *very likely* that the inter-basin contrast in freshwater content has increased: the Atlantic has become saltier and the Pacific and Southern Oceans have freshened. While similar conclusions were reached in AR4, recent studies based on expanded data sets and new analysis approaches provide *high confidence* in this assessment. {3.3.2, 3.3.3, 3.9; FAQ 3.3}

The spatial patterns of the salinity trends, mean salinity and the mean distribution of evaporation minus precipitation are all similar (see also TFE.1, Figure 1). These similarities provide indirect evidence that the pattern of evaporation minus precipitation over the oceans has been enhanced since the 1950s (*medium confidence*). Uncertainties in currently available surface fluxes prevent the flux products from being reliably used to identify trends in the regional or global distribution of evaporation or precipitation over the oceans on the timescale of the observed salinity changes since the 1950s. {3.3.2, 3.3.3, 3.3.4, 3.4.2, 3.4.3, 3.9; FAQ 3.3}

TS.2.5.3 Sea Ice

Continuing the trends reported in AR4, there is *very high confidence* that the Arctic sea ice extent (annual, multiyear and perennial) decreased over the period 1979–2012 (Figure TS.1). The rate of the annual decrease was *very likely* between 3.5 and 4.1% per decade. The average decrease in decadal extent of annual Arctic sea ice has been most rapid in summer and autumn (*high confidence*), but the extent has decreased in every season, and in every successive decade since 1979 (*high confidence*). The extent of Arctic perennial and multiyear ice decreased between 1979 and 2012 (*very high confidence}.* The rates are *very likely* 11.5 [9.4 to 13.6] % per decade for the perennial sea ice area at summer minimum and *very likely* 13.5 [11 to 16] % per decade for multiyear ice. There is *medium confidence* from reconstructions that the 1980–2012 summer sea-ice retreat and increase in sea-surface temperatures in the Arctic are anomalous in the last 2,000 years. {4.2.2, 5.5.2}

It is *likely* that the annual period of surface melt on Arctic perennial sea ice lengthened by 5.7 [4.8 to 6.6] days per decade over the period 1979–2012. Over this period, in the region between the East Siberian Sea and the western Beaufort Sea, the duration of ice-free conditions increased by nearly 2 months. {4.2.2}

There is *high confidence* that the average winter sea ice thickness within the Arctic Basin decreased between 1980 and 2008. The average decrease was *likely* between 1.3 m and 2.3 m. *High confidence* in this assessment is based on observations from multiple sources: submarine, electromagnetic probes, and satellite altimetry; and is consistent with the decline in multiyear and perennial ice extent. Satellite measurements made in the period 2010–2012 show a decrease in sea ice volume compared to those made over the period 2003–2008 (*medium confidence*). There is *high confidence* that in the Arctic, where the sea ice thickness has decreased, the sea ice drift speed has increased. {4.2.2}

It is *very likely* that the annual Antarctic sea ice extent increased at a rate of between 1.2 and 1.8% per decade between 1979 and 2012. There was a greater increase in sea ice area, due to a decrease in the percentage of open water within the ice pack. There is *high confidence* that there are strong regional differences in this annual rate, with some regions increasing in extent/area and some decreasing. {4.2.3}

TS.2.5.4 Glaciers and Ice Sheets

There is *very high confidence*—with a very few regional exceptions—that, since AR4, overall glaciers world-wide have continued to shrink as revealed by the time series of measured changes in glacier length, area, volume and mass (Figure TS.1, Figure TS.3). Measurements of glacier change have increased substantially in number since AR4. Most of the new datasets, along with a globally complete glacier inventory, have been derived from satellite remote sensing {4.3.1, 4.3.3}

There is *very high confidence* that, during the last decade, most ice was lost from glaciers in Alaska, the Canadian Arctic, the periphery of the Greenland ice sheet, the Southern Andes and the Asian mountains. Together these areas account for more than 80% of the total ice loss. Total mass loss from all glaciers in the world, excluding those on the periphery of the ice sheets, was *very likely* 226 [91 to 361] Gt yr^{-1} (sea-level equivalent, 0.62 [0.25 to 0.99] mm yr^{-1}) in the period 1971–2009, 275 [140 to 410] Gt yr^{-1} (0.76 [0.39 to 1.13] mm yr^{-1}) in the period 1993–2009, and 301 [166 to 436] Gt yr^{-1} (0.83 [0.46 to 1.20] mm yr^{-1}) between 2005 and 2009[7]. {4.3.3; Tables 4.4, 4.5}

There is *high confidence* that current glacier extents are out of balance with current climatic conditions, indicating that glaciers will continue to shrink in the future even without further temperature increase. {4.3.3}

There is *very high confidence* that the Greenland Ice Sheet has lost ice during the last two decades. Combinations of satellite and airborne remote sensing together with field data indicate with *high confidence* that the ice loss has occurred in several sectors and that large rates of mass loss have spread to wider regions than reported in AR4 (Figure TS.3). There is *high confidence* that the mass loss of the Greenland Ice Sheet has accelerated since 1992: the average rate has *very likely* increased from 34 [–6 to 74] Gt yr^{-1} over the period 1992–2001 (sea-level equivalent, 0.09 [–0.02 to 0.20] mm yr^{-1}), to 215 [157 to 274] Gt yr^{-1} over the period 2002–2011 (0.59 [0.43 to 0.76] mm yr^{-1}). There is *high confidence* that ice loss from Greenland resulted from increased surface melt and runoff, and increased outlet glacier discharge, and these occurred in similar amounts. There is *high confidence* that the area subject to summer melt has increased over the last two decades. {4.4.2, 4.4.3}

[INSERT FIGURE TS.3 HERE]

Figure TS.3: Upper panels: distribution of ice loss determined from GRACE time-variable gravity for (a) Antarctica and (b) Greenland, shown in centimetres of water per year (cm of water yr^{-1}) for the period 2003 to 2012. Lower panel: the assessment of the total loss of ice from glaciers and ice sheets in terms of sea level equivalent (in mm). The contribution from glaciers excludes those on the periphery of the ice sheets. {4.3.4; Figures 4.12, 4.13, 4.14, 4.16, 4.17}

There is *high confidence* that the Antarctic Ice Sheet has been losing ice during the last two decades (Figure TS.3). There is *very high confidence* that these losses are mainly from the northern Antarctic Peninsula and the Amundsen Sea sector of West Antarctica, and *high confidence* that they result from the acceleration of outlet glaciers. The average rate of ice loss from Antarctica *likely* increased from 30 [–37 to 97] Gt yr^{-1} (sea

[7] 100 Gt yr^{-1} of ice loss corresponds to about 0.28 mm yr^{-1} of sea level equivalent.

level equivalent, 0.08 [–0.10 to 0.27] mm yr^{-1}) over the period 1992–2001, to 147 [72 to 221] Gt yr^{-1} over the period 2002–2011 (0.40 [0.20 to 0.61] mm yr^{-1}). {4.4.2, 4.4.3}

There is *high confidence* that in parts of Antarctica floating ice shelves are undergoing substantial changes. There is *medium confidence* that ice shelves are thinning in the Amundsen Sea region of West Antarctica, and *low confidence* that this is due to high ocean heat flux. There is *high confidence* that ice shelves around the Antarctic Peninsula continue a long-term trend of retreat and partial collapse that began decades ago. {4.4.2, 4.4.5}

TS.2.5.5 Snow Cover, Freshwater Ice and Frozen Ground

There is *very high confidence* that snow cover extent has decreased in the Northern Hemisphere, especially in spring (Figure TS.1). Satellite records indicate that over the period 1967–2012, snow cover extent *very likely* decreased; the largest change, –53% [–40% to –66%], occurred in June. No month had statistically significant increases. Over the longer period, 1922–2012, data are only available for March and April, but these show *very likely* a 7% [4.5% to 9.5%] decline and a negative correlation (–0.76) with March to April 40°N–60°N land temperature. In the Southern Hemisphere, evidence is too limited to conclude whether changes have occurred. {4.5.2, 4.5.3}

Permafrost temperatures have increased in most regions around the world since the early 1980s (*high confidence*). These increases were in response to increased air temperature, and changes in the timing and thickness of snow cover (*high confidence*). The temperature increase for colder permafrost was generally greater than for warmer permafrost (*high confidence*). {4.7.2, Table 4.8}

TFE.1: Water Cycle Change

The water cycle describes the continuous movement of water through the climate system in its liquid, solid and vapour forms, and storage in the reservoirs of ocean, cryosphere, land surface and atmosphere. In the atmosphere, water occurs primarily as a gas, water vapour, but it also occurs as ice and liquid water in clouds. The ocean is primarily liquid water, but the ocean is partly covered by ice in Polar Regions. Terrestrial water in liquid form appears as surface water (lakes, rivers), soil moisture and groundwater. Solid terrestrial water occurs in ice sheets, glaciers, snow and ice on the surface and permafrost. The movement of water in the climate system is essential to life on land, since much of the water that falls on land as precipitation and supplies the soil moisture and river flow has been evaporated from the ocean and transported to land by the atmosphere. Water that falls as snow in winter can provide soil moisture in springtime and river flow in summer and is essential to both natural and human systems. The movement of fresh water between the atmosphere and the ocean can also influence oceanic salinity, which is an important driver of the density and circulation of the ocean. The latent heat contained in water vapour in the atmosphere is critical to driving the circulation of the atmosphere on scales ranging from individual thunderstorms to the global circulation of the atmosphere. {12.4.5; FAQ 3.3, FAQ 12.2}

Observations of Water Cycle Change

Because the saturation vapour pressure of air increases with temperature, it is expected that the amount of water vapour suspended in air will increase with a warming climate. Observations from surface stations, radiosondes, global positioning systems, and satellite measurements indicate increases in tropospheric water vapour at large spatial scales (TFE.1, Figure 1). It is *very likely* that tropospheric specific humidity has increased since the 1970s. The magnitude of the observed global change in water vapour of about 3.5% in the past 40 years is consistent with the observed temperature change of about 0.5°C during the same period, and the relative humidity has stayed approximately constant. The water vapour change can be attributed to human influence with *medium confidence*. {2.5.4, 10.3.2}

Changes in precipitation are harder to measure with the existing records, both because of the greater difficulty in sampling precipitation and also because it is expected that precipitation will have a smaller fractional change than the water vapour content of air as the climate warms. When virtually all the land area

is filled in using a reconstruction method, the resulting time series shows little change in land-based precipitation since 1900. At present there is *medium confidence* that there has been a significant human influence on global scale changes in precipitation patterns, including increases in northern hemisphere mid to high latitudes. Changes in the extremes of precipitation, and other climate extremes related to the water cycle are comprehensively discussed in TFE.9. {2.5.1, 10.3.2}

Although direct trends in precipitation and evaporation are difficult to measure with the available records, the observed oceanic surface salinity, which is strongly dependent on the difference between evaporation and precipitation, shows significant trends (TFE.1, Figure 1). The spatial patterns of the salinity trends since 1950, the mean salinity and the mean distribution of evaporation–precipitation are similar to each other: regions of high salinity where evaporation dominates have become more saline, while regions of low salinity where rainfall dominates have become fresher (TFE.1, Figure 1). This provides indirect evidence that the pattern of evaporation-precipitation over the oceans has been enhanced since the 1950s (*medium confidence*). The inferred changes in evaporation minus precipitation are consistent with the observed increased water vapour content of the warmer air. It is *very likely* that observed changes in surface and subsurface salinity are due in part to anthropogenic increases in forcings. {2.5, 3.3.2, 3.3.3, 3.3.4, 3.4, 3.9, 10.4.2; FAQ 3.3}

[INSERT TFE.1, FIGURE 1 HERE]

TFE.1, Figure 1: Changes in sea surface salinity are related to the atmospheric patterns of Evaporation minus Precipitation (E-P) and trends in total precipitable water: (a) Linear trend (1988 to 2010) in total precipitable water (water vapor integrated from Earth's surface up through the entire atmosphere) (kg m^{-2} per decade) from satellite observations. (b) The 1979–2005 climatological mean net evaporation minus precipitation (cm yr^{-1}) from meteorological reanalysis data. (c) Trend (1950 to 2000) in surface salinity (PSS78 per 50years). (d) The climatological-mean surface salinity (PSS78) (blues <35; yellows-reds >35). (e) Global difference between salinity averaged over regions where the sea surface salinity is greater than the global mean sea surface salinity ("High Salinity") and salinity averaged over regions values below the global mean ("Low Salinity"). Details of data sources: see Figure 3.21 and FAQ 3.3, Figure 1. {3.9}

In most regions analyzed, it is *likely* that decreasing numbers of snowfall events are occurring where increased winter temperatures have been observed. Both satellite and in-situ observations show significant reductions in the Northern Hemisphere snow cover extent over the past 90 years, with most of the reduction occurring in the 1980s. Snow cover decreased most in spring when the average extent decreased by around 8% (7 million km^2) over the period 1970–2010 compared with the period 1922–1970. Because of earlier spring snowmelt, the duration of the Northern Hemisphere snow season has declined by 5.3 days per decade since the 1972/1973 winter. It is *likely* that there has been an anthropogenic component to these observed reductions in snow cover since the 1970s. {4.5.2, 10.5.1, 10.5.3}

The most recent and most comprehensive analyses of river runoff do not support the AR4 conclusion that global runoff has increased during the 20th century. New results also indicate that the AR4 conclusions regarding global increasing trends in droughts since the 1970s are no longer supported. {2.5.2, 2.6.2}

Projections of Future Changes

Changes in the water cycle are projected to occur in a warming climate (TFE.1, Figure 2, see also TS 4.6, TS 5.6, Annex I). Global-scale precipitation is projected to gradually increase in the 21st century. It is *virtually certain*, that precipitation increase will be much smaller, approximately 2% K^{-1}, than the rate of lower tropospheric water vapour increase (~7% K^{-1}), due to global energetic constraints. It is *virtually certain* that changes of average precipitation in a much warmer world will not be uniform, with some regions experiencing increases, and others with decreases or not much change at all. The high latitudes are *likely* to experience greater amounts of precipitation due to the additional water carrying capacity of the warmer troposphere. Many mid-latitude arid and semi-arid regions will *likely* experience less precipitation. The largest precipitation changes over northern Eurasia and North America are projected to occur during the winter. {12.4.5, Annex I}

[INSERT TFE.1, FIGURE 2 HERE]

TFE.1, Figure 2: Annual mean changes in precipitation (P), evaporation (E), relative humidity, E-P, runoff and soil moisture, for 2081–2100 relative to 1986–2005 under the RCP8.5 scenario (see Box TS.6). The number of CMIP5

models to calculate the multi-model mean is indicated in the upper right corner of each panel. Hatching indicates regions where the multi model mean is less than one standard deviation of internal variability. Stippling indicates regions where the multi model mean is greater than two standard deviations of internal variability and where 90% of models agree on the sign of change (see Box 12.1). {Figures 12.25–12.27}

Regional to global-scale projections of soil moisture and drought remain relatively uncertain compared to other aspects of the water cycle. Nonetheless, drying in the Mediterranean, southwestern U.S. and south African regions are consistent with projected changes in Hadley circulation, so drying in these regions as global temperatures increase is *likely* for several degrees of warming under the RCP8.5 scenario. Decreases in runoff are *likely* in southern Europe and the Middle East. The high northern latitude runoff increases are likely and consistent with the projected precipitation increases. {12.4.5}

TS.2.6 Changes in Sea Level

The primary contributions to changes in the volume of water in the ocean are the expansion of the ocean water as it warms and the transfer to the ocean of water currently stored on land, particularly from glaciers and ice sheets. Water impoundment in reservoirs and ground water depletion (and its subsequent run-off to the ocean) also affects sea level. Change in sea level relative to the land (relative sea level) can be significantly different from the global mean sea level (GMSL) change because of changes in the distribution of water in the ocean and vertical movement of the land. For an overview on the scientific understanding and uncertainties associated with recent (and projected) sea level change see TFE.2. {3.7.3, 13.1}

During the warm intervals of the middle Pliocene (3.3 to 3.0 million years ago), when there is *medium confidence* that global mean surface temperatures were 2°C to 3.5°C warmer than for pre-industrial climate and CO_2 levels were between 250 and 450 ppm, sedimentary records suggest periodic deglaciation of West Antarctica and parts of the East Antarctica. Ice-sheet models suggest near-complete deglaciation of the Greenland, West Antarctica and partial deglaciation of East Antarctica. Together, the evidence suggests that GMSL was above present levels at that time, but did not exceed 20 m above present (*high confidence*). {5.6.1, 13.2}

During the Last Interglacial Period (about 129,000 to 116,000 years ago) when peak global warmth was not more than 2°C above pre-industrial temperatures, and peak global annual sea surface temperatures were 0.7 [0.1 to 1.3] °C warmer (*medium confidence*), maximum GMSL was at least 5 m higher than at present (very *high confidence*), but did not exceed 10 m (*high confidence*). Based on ice-sheet model simulations consistent with elevation changes derived from a new Greenland ice core, the Greenland ice sheet *very likely* contributed between 1.4 m and 4.3 m sea level equivalent, implying with *medium confidence* a contribution from the Antarctic ice sheet to the global mean sea level during the last interglacial period. {5.6.2, 13.2}

Based on proxy data, the magnitude of centennial-scale global mean sea level variations did not exceed 0.25 m over the past few millennia (*medium confidence*). The current rate of global mean sea level change, starting in the late 19th-early 20th century, is, with *medium confidence*, unusually high in the context of centennial-scale variations of the last two millennia. Tide gauge data also indicate a *likely* acceleration during the last two centuries. Based on proxy and instrumental data, it is *virtually certain* that the rate of global mean sea level rise has accelerated during the last two centuries, marking the transition from relatively low rates of change during the late Holocene (order tenths of mm yr^{-1}) to modern rates (order mm yr^{-1}). {3.7, 5.6.3, 13.2}

Global mean sea level has risen by 0.19 [0.17 to 0.21] m, estimated from a linear trend over the period 1901–2010, based on tide gauge records and additionally on satellite data since 1993. It is *very likely* that the mean rate of sea level rise was 1.7 [1.5 to 1.9] mm yr^{-1} between 1901 and 2010. Between 1993 and 2010, the rate was *very likely* higher at 3.2 [2.8 to 3.6] mm yr^{-1}; similarly high rates *likely* occurred between 1930 and 1950. The rate of global mean sea level rise has *likely* increased since the early 1900 with estimates ranging from 0.000 to 0.013 [–0.002 to 0.019] mm yr^{-2}. {3.7, 5.6.3, 13.2}

TFE.2: Sea Level Change: Scientific Understanding and Uncertainties

After the Last Glacial Maximum, global mean sea levels reached close to present-day values several thousand years ago. Since then, it is *virtually certain* that the rate of global mean sea level rise has increased from low rates of sea level change during the late Holocene (order tenths of mm yr^{-1}) to 20th century rates (order mm yr^{-1}, Figure TS1). {3.7, 5.6, 13.2}

Ocean thermal expansion and glacier mass loss are *very likely* the dominant contributors to global mean sea level rise during the 20th century. It is *very likely* that warming of the ocean has contributed 0.8 [0.5 to 1.1] mm yr^{-1} of sea level change during 1971–2010, with the majority of the contribution coming from the upper 700 m. The model-mean rate of ocean thermal expansion for 1971–2010 is close to observations. {3.7, 13.3}

Observations, combined with improved methods of analysis, indicate that the global glacier contribution (excluding the peripheral glaciers around Greenland and Antarctica) to sea level was 0.25 to 1.00 mm yr^{-1} sea level equivalent during 1971–2010. *Medium confidence* in global glacier mass balance models used for projections of global changes arises from the ability of the models of the well-observed glaciers to reproduce time series of historical changes of those glaciers using observed climate input. A simulation using observed climate data shows a larger rate of glacier mass loss during the 1930s than the simulations using AOGCM input, possibly a result of an episode of warming in Greenland associated with unforced regional climate variability. {4.3, 13.3}

Observations indicate that the Greenland Ice Sheet has *very likely* experienced a net loss of mass due to both increased surface melting and run off, and increased ice discharge over the last two decades (Figure TS.3). Regional climate models indicate that Greenland ice-sheet surface mass balance showed no significant trend from the 1960s to the 1980s, but melting and consequent runoff has increased since the early 1990s. This tendency is related to pronounced regional warming, which may be attributed to a combination of anomalous regional variability in recent years and anthropogenic climate change. *High confidence* in projections of future warming in Greenland and increased surface melting is based on the qualitative agreements of models in projecting amplified warming at high northern latitudes for well-understood physical reasons. {4.4, 13.3}

There is *high confidence* that the Antarctic Ice Sheet is in a state of net mass loss and its contribution to sea level is also *likely* to have increased in the last two decades. Acceleration in ice outflow has been observed since the 1990s, especially in the Amundsen Sea sector of West Antarctica. Interannual variability in accumulation is large and as a result no significant trend is present in accumulation since 1979 in either models or observations. Surface melting is currently negligible in Antarctica. {4.4, 13.3}

Model-based estimates of climate-related changes in water storage on land (as snow cover, surface water, soil moisture and ground water) do not show significant long-term contributions to sea level change for recent decades. However, human-induced changes (reservoir impoundment and groundwater depletion) have each contributed at least several tenths of mm yr^{-1} to sea level change. Reservoir impoundment exceeded groundwater depletion for the majority of the 20th century but the rate of groundwater depletion has increased and now exceeds the rate of impoundment. Their combined net contribution for the 20th century is estimated to be small. {13.3}

[INSERT TFE.2, FIGURE 1 HERE]

TFE.2, Figure 1: Comparison of the observed global mean sea level rise from the sum of the modelled contributions from ocean thermal expansion, glaciers (excluding glaciers peripheral to the Antarctic ice sheet, PGs) and changes in land-water storage. In panels (a)-(d): the grey lines are results for individual CMIP5 AOGCMs; the black line is the model mean plus a correction for the omission of volcanic forcing in the AOGCM control experiments; the adjusted model mean (dashed black line) is the sum of the corrected model mean thermal expansion, the change in land-water storage, the glacier estimate using observed (rather than modelled) climate, and an illustrative long-term ice-sheet contribution (of 0.1 mm yr^{-1}); the adjusted model mean including the observed ice sheet contribution (dotted black line) begins in 1993 and includes the ice-sheet contributions, but excludes the glaciers peripheral to both the Greenland Ice Sheet and the Antarctic Ice Sheet, to avoid double counting because the observational ice-sheet estimates include the peripheral glaciers; three estimates of global mean sea level, with the shading indicating the uncertainty estimates (two standard deviations) are shown; the satellite altimeter data since 1993 are shown in red. The modelled sea level is given (a) for the period 1900 to 2010, (b) the rates of sea level change for the same period, with the satellite altimeter data shown as a red dot for the rate, (c) for 1961 to 2010 and (d) for 1990 to 2010. Panel (e) compares the sum of the observed contributions (orange) and the observed sea level from the satellite altimeter data (red). {13.3; Figure 13.7}

The observed global mean sea level (GMSL) rise for 1993–2010 is consistent with the sum of the observationally estimated contributions (TFE.2, Figure 1e). The closure of the observational budget for recent periods within uncertainties represents a significant advance since the AR4 in physical understanding of the causes of past GMSL change, and provides an improved basis for critical evaluation of models of these contributions in order to assess their reliability for making projections. {13.3}

The sum of modelled ocean thermal expansion and glacier contributions and the estimated change in land water storage (which is relatively small) accounts for about 65% of the observed GMSL rise for 1901–1990, and 90% for 1971–2010 and 1993–2010 (TFE.2, Figure 1). After inclusion of small long-term contributions from ice sheets and the possible greater mass loss from glaciers during the 1930s due to unforced climate variability, the sum of the modelled contribution is close to the observed rise. The addition of the observed ice sheet contribution since 1993 improves the agreement further between the observed and modelled sea level rise (TFE.2, Figure 1). The evidence now available gives a clearer account than in previous IPCC assessments of 20th century sea level change. {13.3}

When calibrated appropriately, recently improved dynamical ice-sheet models can reproduce the observed rapid changes in ice-sheet outflow for individual glacier systems (e.g., Pine Island Glacier in Antarctica; *medium confidence*). However, models of ice sheet response to global warming and particularly ice sheet-ocean interactions are incomplete and the omission of ice-sheet models, especially of dynamics, from the model budget of the past means that they have not been as critically evaluated as other contributions. {13.3, 13.4}

Global mean sea level rise for 2081–2100 (relative to 1986–2005) for the RCPs will *likely* be in the 5–95% ranges derived from CMIP5 climate projections in combination with process-based models (*medium confidence*), i.e., 0.26–0.54 m (RCP2.6), 0.32–0.62 m (RCP4.5), 0.33–0.62 m (RCP6.0), 0.45–0.81 (RCP8.5) m (see Table TS.1 and Figure TS.15 for RCP forcing). For RCP8.5 the range at 2100 is 0.53–0.97 m. Confidence in the projected *likely* ranges comes from the consistency of process-based models with observations and physical understanding. It is assessed that there is currently insufficient evidence to evaluate the probability of specific levels above the *likely* range. Based on current understanding, only the collapse of marine-based sectors of the Antarctic ice sheet, if initiated, could cause GMSL to rise substantially above the *likely* range during the 21st century. There is a lack of consensus on the probability for such a collapse, and the potential additional contribution to GMSL rise cannot be precisely quantified, but there is *medium confidence* that it would not exceed several tenths of a meter of sea level rise during the 21st century. It is *virtually certain* that global mean sea level rise will continue beyond 2100. {13.5.1, 13.5.3}

Many semi-empirical models projections of global mean sea level rise are higher than process-based model projections, but there is low agreement in semi-empirical model projections, and no consensus about their reliability. {13.5.2, 13.5.3}

TFE.2, Figure 2 combines the paleo, tide-gauge, and altimeter observations of sea level rise from 1700 with the projected global mean sea level change to 2100. {13.5, 13.7, 13.8}

[INSERT TFE.2, FIGURE 2 HERE]

TFE.2, Figure 2: Compilation of paleo sea level data (purple), tide gauge data (blue, red and green), altimeter data (light blue), and central estimates and likely ranges for projections of global-mean sea level rise from the combination of CMIP5 and process-based models for RCP2.6 (blue) and RCP8.5 (red) scenarios, all relative to pre-industrial values. {Figures 13.3, 13.11, 13.27}

TS.2.7 Changes in Extremes

TS.2.7.1 Atmosphere

Recent analyses of extreme events generally support the AR4 and SREX conclusions (see TFE.9 and in particular TFE.9, Table 1, for a synthesis). It is *very likely* that the number of cold days and nights has decreased and the number of warm days and nights has increased on the global scale between 1951 and

2010. Globally, there is *medium confidence* that the length and frequency of warm spells, including heat waves, has increased since the middle of the 20th century mostly due to lack of data or studies in Africa and South America. However it is *likely* that heat wave frequency has increased over this period in large parts of Europe, Asia, and Australia. {2.6.1; Table 2.12, 2.13}

It is *likely* that since 1950 the number of heavy precipitation events over land has increased in more regions than it has decreased. Regional trends vary but confidence is *high* for North America with *very likely* trends towards heavier precipitation events. {2.6.2; Table 2.13}

There is *low confidence* in a global-scale observed trend in drought or dryness (lack of rainfall), due to lack of direct observations, dependencies of inferred trends on the index choice and geographical inconsistencies in the trends. However this masks important regional changes and, for example, the frequency and intensity of drought has *likely* increased in the Mediterranean and West Africa and *likely* decreased in Central North America and North-West Australia since 1950. {2.6.2; Table 2.13}

During the last millennium, there is *high confidence* for the occurrence of droughts of greater magnitude and longer duration than observed since 1900 in many regions. There is *medium confidence* that more megadroughts occurred in monsoon Asia and wetter conditions prevailed in arid Central Asia and the South American monsoon region during the Little Ice Age (1450–1850) compared to the Medieval Climate Anomaly (950–1250). {5.5.4, 5.5.5}

Confidence remains *low* for long-term (centennial) changes in tropical cyclone activity, after accounting for past changes in observing capabilities. However since the 1970s, it is *virtually certain* that the frequency and intensity of storms in the North Atlantic has increased although the reasons for this increase are debated (see TFE.9). There is *low confidence* of large-scale trends in storminess over the last century and there is still insufficient evidence to determine whether robust trends exist in small-scale severe weather events such as hail or thunder storms. {2.6.2, 2.6.3, 2.6.4}

With *high confidence*, past floods larger than recorded since the 20th century occurred during the past five centuries in northern and central Europe, the western Mediterranean region, and eastern Asia. There is *medium confidence* that in the Near East, India, central North America, modern large floods are comparable or surpass historical floods in magnitude and/or frequency. {5.5.5}

TS.2.7.2 Oceans

It is *likely* that the magnitude of extreme high sea level events has increased since 1970 (see TFE.9, Table 1). Most of the increase in extreme sea level can be explained by the mean sea level rise: changes in extreme high sea levels are reduced to less than 5 mm yr^{-1} at 94% of tide gauges once the rise in mean sea level is accounted for. There is *medium confidence* based on reanalysis forced model hindcasts and ship observations that mean significant wave height has increased since the 1950s over much of the North Atlantic north of 45°N, with typical winter season trends of up to 20 cm per decade. {3.4.5, 3.7.5}

TS.2.8 Changes in Carbon and Other Biogeochemical Cycles

Concentrations of the atmospheric greenhouse gases carbon dioxide (CO_2), methane (CH_4), and nitrous oxide (N_2O) in 2011, exceed the range of concentrations recorded in ice cores during the past 800,000 years. Past changes in atmospheric greenhouse-gas concentrations are determined with *very high confidence* from polar ice cores. Since AR4 these records have been extended from 650,000 years to 800,000 years ago. {5.2.2}

With *very high confidence*, the current rates of CO_2, CH_4 and N_2O rise in atmospheric concentrations and the associated increases in radiative forcing are unprecedented with respect to the "highest resolution" ice core records of the last 22,000 years. There is *medium confidence* that the rate of change of the observed greenhouse gas rise is also unprecedented compared with the lower resolution records of the past 800,000 years. {2.2.1, 5.2.2}

In several periods characterized by high atmospheric CO_2 concentrations, there is *medium confidence* that global mean temperature was significantly above pre-industrial level. During the mid-Pliocene (3.3 to 3.0 million years ago), atmospheric CO_2 concentration between 350 ppm and 450 ppm (*medium confidence*) occurred when global mean surface temperature was approximately 2°C to 3.5°C warmer (*medium confidence*) than for pre-industrial climate. During the Early Eocene (52 to 48 million years ago), atmospheric CO_2 concentration exceeded ~1000 ppm when global mean surface temperature was 9°C to 14°C higher (*medium confidence*) than for pre-industrial conditions. {5.3.1}

TS.2.8.1 CO_2

Between 1750 and 2011, CO_2 emissions from fossil fuel combustion and cement production are estimated from energy and fuel use statistics to have released 365 [335 to 395] PgC[8]. In 2000–2009, average fossil fuel and cement manufacturing emissions were 7.8 [7.2 to 8.4] PgC yr^{-1}, with an average growth rate of 3.2% yr^{-1} (Figure TS.4). This rate of increase of fossil fuel emissions is higher than during the 1990's (1.0% yr^{-1}). In 2011, fossil fuel emissions were 9.5 [8.7 to 10.3] PgC. {2.2.1, 6.3.1; Table 6.1}

[INSERT FIGURE TS.4 HERE]

Figure TS.4: Annual anthropogenic CO_2 emissions and their partitioning among the atmosphere, land and ocean (PgC yr^{-1}) from 1750 to 2011. (Top) Fossil fuel and cement CO_2 emissions by category, estimated by the Carbon Dioxide Information Analysis Center (CDIAC). (Bottom) Fossil fuel and cement CO_2 emissions as above. CO_2 emissions from net land use change, mainly deforestation, are based on land cover change data (see Table 6.2). The atmospheric CO_2 growth rate prior to 1959 is based on a spline fit to ice core observations and a synthesis of atmospheric measurements from 1959. The fit to ice core observations does not capture the large interannual variability in atmospheric CO_2 and is represented with a dashed line. The ocean CO_2 sink is from a combination of models and observations. The residual terrestrial sink (term in green in the figure) is computed from the residual of the other terms. The emissions and their partitioning only include the fluxes that have changed since 1750, and not the natural CO_2 fluxes (e.g., atmospheric CO_2 uptake from weathering, outgassing of CO_2 from lakes and rivers, and outgassing of CO_2 by the ocean from carbon delivered by rivers; see Figure 6.1) between the atmosphere, land and ocean reservoirs that existed before that time and still exist today. The uncertainties in the various terms are discussed in chapter 6 and reported in Table 6.1 for decadal mean values. {Figure 6.8}

Between 1750 and 2011, land use change (mainly deforestation), derived from land cover data and modelling, is estimated to have released 180 [100 to 260] PgC. Land use change emissions between 2000 and 2009 are dominated by tropical deforestation, and are estimated at 1.1 [0.3 to 1.9] PgC yr^{-1}, with possibly a small decrease from the 1990s due to lower reported forest loss during this decade. This estimate includes gross deforestation emissions of around 3 PgC yr^{-1} compensated by around 2 PgC yr^{-1} of forest regrowth in some regions, mainly abandoned agricultural land. {6.3.2; Table 6.2}

Of the 545 [460 to 630] PgC released to the atmosphere from fossil fuel and land use emissions from 1750 to 2011, 240 [230 to 250] PgC accumulated in the atmosphere, as estimated with very high accuracy from the observed increase of atmospheric CO_2 concentration from 278 [275 to 281] ppm[9] in 1750 to 390.5 ppm in 2011. The amount CO_2 in the atmosphere grew by 4.0 [3.8 to 4.2] PgC yr^{-1} in the first decade of the 21st century. The distribution of observed atmospheric CO_2 increases with latitude clearly shows that the increases are driven by anthropogenic emissions which primarily occur in the industrialized countries north of the equator. Based on annual average concentrations, stations in the Northern Hemisphere show slightly higher concentrations than stations in the Southern Hemisphere. An independent line of evidence for the anthropogenic origin of the observed atmospheric CO_2 increase comes from the observed consistent decrease in atmospheric O_2 content and a decrease in the stable isotopic ratio of CO_2 ($^{13}C/^{12}C$) in the atmosphere (Figure TS.5). {2.2.1, 6.1.3}

The remaining amount of carbon released by fossil fuel and land-use emissions has been re-absorbed by the ocean and terrestrial ecosystems. Based on high agreement between independent estimates using different methods and data sets (e.g., oceanic carbon, oxygen, and transient tracer data), it is *very likely* that the global

[8] 1 Petagram of carbon = 1 PgC = 10^{15} grams of carbon = 1 Gigatonne of carbon = 1 GtC. This corresponds to 3.67 $GtCO_2$.

[9] ppm (parts per million) or ppb (parts per billion, 1 billion = 1,000 million) is the ratio of the number of greenhouse gas molecules to the total number of molecules of dry air. For example, 300 ppm means 300 molecules of a greenhouse gas per million molecules of dry air.

ocean inventory of anthropogenic carbon increased from 1994 to 2010. In 2011, it is estimated to be 155 [125 to 185] PgC. The annual global oceanic uptake rates calculated from independent data sets (from oceanic C_{ant} inventory changes, from atmospheric O_2/N_2 measurements or from pCO_2 data) and for different time periods agree with each other within their uncertainties, and *very likely* are in the range of 1.0–3.2 PgC yr^{-1}. Regional observations of the storage rate of anthropogenic carbon in the ocean are in broad agreement with the expected rate resulting from the increase in atmospheric CO_2 concentrations, but with significant spatial and temporal variations. {3.8.1, 6.3}

[INSERT FIGURE TS.5 HERE]

Figure TS.5: Atmospheric concentration of CO_2, oxygen, $^{13}C/^{12}C$ stable isotope ratio in CO_2, as well as CH_4 and N_2O atmospheric concentrations and oceanic surface observations of pCO_2 and pH, recorded at representative time series stations in the Northern and the Southern Hemispheres. MLO: Mauna Loa Observatory, Hawaii; SPO: South Pole; HOT: Hawaii Ocean Time-Series station; MHD: Mace Head, Ireland; CGO: Cape Grim, Tasmania; ALT: Alert, Northwest Territories, Canada. {Figure 6.3, FAQ 3.2, Figure 1}

Natural terrestrial ecosystems (those not affected by land use change) are estimated by difference from changes in other reservoirs to have accumulated 150 [60 to 240] PgC between 1750 and 2010. The gain of carbon by natural terrestrial ecosystems is estimated to take place mainly through the uptake of CO_2 by enhanced photosynthesis at higher CO_2 levels and nitrogen deposition, longer growing seasons in mid and high latitudes. Natural carbon sinks vary regionally due to physical, biological and chemical processes acting on different time scales. An excess of atmospheric CO_2 absorbed by land ecosystems gets stored as organic matter in diverse carbon pools, from short lived (leaves, fine roots) to long-lived (stems, soil carbon). {6.3; Table 6.1}

TS.2.8.2 Carbon and Ocean Acidification

It is *very likely* that oceanic uptake of anthropogenic CO_2 results in gradual acidification of the ocean. The pH[10] of seawater has decreased by 0.1 since the beginning of the industrial era, corresponding to a 26% increase in hydrogen ion concentration. The observed pH trends range between –0.0014 and –0.0024 per year in surface waters. In the ocean interior, natural physical and biological processes, as well as uptake of anthropogenic CO_2 can cause changes in pH over decadal and longer time scales. {3.8.2; Box 3.2; Table 3.2; FAQ 3.2}

TS.2.8.3 CH_4

The concentration of CH_4 has increased by a factor of 2.5 since preindustrial times, from 720 [695 to 745] ppb in 1750 to 1803 [1799 to 1807] ppb in 2011 (Figure TS.5). There is *very high confidence* that the atmospheric CH_4 increase during the Industrial Era is caused by anthropogenic activities. The massive increase in the number of ruminants, the emissions from fossil fuel extraction and use, the expansion of rice paddy agriculture and the emissions from landfills and waste, are the dominant anthropogenic CH_4 sources. Anthropogenic emissions account for 50% to 65% of total emissions. By including natural geological CH_4 emissions that were not accounted for in previous budgets, the fossil component of the total CH_4 emissions (i.e., anthropogenic emissions related to leaks in the fossil fuel industry and natural geological leaks) is now estimated to amount to about 30% of the total CH_4 emissions (*medium confidence*). {2.2.1, 6.1, 6.3.3}

In recent decades, CH_4 growth in the atmosphere has been variable. CH_4 concentrations were relatively stable for about a decade in the 1990s, but then started growing again starting in 2007. The exact drivers of this renewed growth are still debated. Climate driven fluctuations of CH_4 emissions from natural wetlands (177 to 284 $\times 10^{12}$ g (CH_4) yr^{-1} for 2000–2009 based on bottom-up estimates) are the main drivers of the global inter-annual variability of CH_4 emissions (*high confidence*), with a smaller contribution from biomass burning emissions during high fire years {2.2.1, 6.3.3; Table 6.8}.

TS.2.8.4 Nitrogen

[10] pH is a measure of acidity : a decrease in pH value means an increase in acidity, i.e., acidification.

Since preindustrial times, the concentration of N_2O in the atmosphere has increased by a factor of 1.2 (Figure TS.5). Changes in the nitrogen cycle, in addition to interactions with CO_2 sources and sinks, affect emissions of N_2O both on land and from the ocean. {2.2.1, 6.4.6}

TS.2.8.5 Oceanic Oxygen

High agreement among analyses provides *medium confidence* that oxygen concentrations have decreased in the open ocean thermocline in many ocean regions since the 1960s. The general decline is consistent with the expectation that warming-induced stratification leads to a decrease in the supply of oxygen to the thermocline from near surface waters, that warmer waters can hold less oxygen, and that changes in wind-driven circulation affect oxygen concentrations. It is *likely* that the tropical oxygen minimum zones have expanded in recent decades. {3.8.3}

TS.3 Drivers of Climate Change

TS.3.1 Introduction

Human activities have changed and continue to change the Earth's surface and atmospheric composition. Some of these changes have a direct or indirect impact on the energy balance of the Earth and are thus drivers of climate change. Radiative forcing (RF) is a measure of the net change in the energy balance of the Earth system in response to some external perturbation (see Box TS.2), with positive RF leading to a warming and negative RF to a cooling. The RF concept is valuable for comparing the influence on global mean temperature of most individual agents affecting Earth's radiation balance. The quantitative values provided in AR5 are consistent with those in previous IPCC reports, though there have been some important revisions (Figure TS.6). Effective radiative forcing (ERF) is now used to quantify the impact of some forcing agents that involve rapid adjustments of components of the atmosphere and surface that are assumed constant in the RF concept (see Box TS.2). RF and ERF are estimated from the change between 1750 and 2011, referred to as "industrial era", if other time periods are not explicitly stated. Uncertainties are given associated with the best estimates of RF and ERF, with values representing the 5–95% (90%) confidence range. {8.1, 7.1}

In addition to the global mean RF or ERF, the spatial distribution and temporal evolution of forcing, as well as climate feedbacks, play a role in determining the eventual impact of various drivers on climate. Land surface changes may also impact the local and regional climate through processes that are not radiative in nature {8.1, 8.3.5, 8.6}.

[START BOX TS.2 HERE]

Box TS.2: Radiative Forcing and Effective Radiative Forcing

Radiative Forcing (RF) and Effective Radiative Forcing (ERF) are used to quantify the change in Earth's energy balance that occurs as a result of an externally imposed change. They are expressed in Watts per square meter ($W\ m^{-2}$). RF is defined in AR5, as in previous IPCC assessments, as the change in net downward flux (shortwave + longwave) at the tropopause after allowing for stratospheric temperatures to readjust to radiative equilibrium, while holding other state variables such as tropospheric temperatures, water vapor and cloud cover fixed at the unperturbed values (see Glossary). {8.1.1}

Although the RF concept has proved very valuable, improved understanding has shown that including rapid adjustments of the Earth's surface and troposphere can provide a better metric of climate response. These rapid adjustments occur over a variety of timescales, but are relatively distinct from responses to global mean surface temperature change. Aerosols in particular impact the atmosphere temperature profile and cloud properties on a time scale much shorter than adjustments of the ocean (even the upper layer) to forcings. The ERF concept defined in AR5 allows rapid adjustments to perturbations, for all variables except for global mean surface temperature or ocean temperature and sea ice cover. The ERF and RF values are significantly different for the anthropogenic aerosols, due to their influence on clouds and on snow or ice cover. For other components that drive the Earth energy balance, such as greenhouse gases, ERF and RF are fairly similar, and RF may have comparable utility given that it requires fewer computational resources to

calculate and is not affected by meteorological variability and hence can better isolate small forcings. In cases where RF and ERF differ substantially, ERF has been shown to be a better indicator of the global mean temperature response and is therefore emphasized in AR5. {7.1.3, 8.1; Box 8.1}

[END BOX TS.2 HERE]

TS.3.2 Radiative Forcing from Greenhouse Gases

Human activity leads to change in the atmospheric composition either directly (via emissions of gases or particles) or indirectly (via atmospheric chemistry). Anthropogenic emissions have driven the changes in well-mixed greenhouse gas (WMGHG) concentrations during the industrial era (see Section TS.2.8 and TFE.7). As historical WMGHG concentrations since the preindustrial are well known based on direct measurements and ice core records, and WMGHG radiative properties are also well known, the computation of RF due to concentration changes provides tightly constrained values (Figure TS.6). There has not been significant change in our understanding of WMGHG radiative impact, so that the changes in RF estimates relative to AR4 are due essentially to concentration increases. The best estimate for WMGHG ERF is the same as RF, but the uncertainty range is twice as large due to the poorly constrained cloud responses. Due to high-quality observations, it is certain that increasing atmospheric burdens of most WMGHGs, especially CO_2, resulted in a further increase in their radiative forcing from 2005 to 2011. Based on concentration changes, the RF of all WMGHG in 2011 is 2.83 [2.54 to 3.12] W m^{-2} (*very high confidence*). This is an increase since AR4 of 0.20 [0.18 to 0.22] W m^{-2}, with nearly all of the increase due to the increase in the abundance of CO_2 since 2005. The industrial era RF for CO_2 alone is 1.82 [1.63 to 2.01] W m^{-2}. Over the last 15 years, CO_2 has been the dominant contributor to the increase in RF from the WMGHGs, with RF of CO_2 having an average growth rate slightly less than 0.3 W m^{-2} per decade. The uncertainty in the WMGHG RF is due in part to its radiative properties but mostly to the full accounting of atmospheric radiative transfer including clouds. {2.2.1, 5.2, 6.3, 8.3, 8.3.2; Table 6.1}

[INSERT FIGURE TS.6 HERE]

Figure TS.6: Radiative Forcing (RF) and Effective Radiative Forcing (ERF) of climate change during the industrial era. Top: Forcing by concentration change between 1750 and 2011 with associated uncertainty range (solid bars are ERF, hatched bars are RF, green diamonds and associated uncertainties are for RF assessed in AR4). Bottom: Probability Density Functions for the ERF, for the aerosol, well-mixed greenhouse gas (WMGHG) and total. The green lines show the AR4 RF 90% confidence intervals and can be compared with the red, blue and black lines which show the AR5 ERF 90% confidence intervals (although RF and ERF differ, especially for aerosols). The ERF from surface albedo changes and combined contrails and contrail induced cirrus is included in the total anthropogenic forcing, but not shown as a separate probability density function. For some forcing mechanisms (ozone, land use, solar) the RF is assumed to be representative of the ERF but an additional uncertainty of 17% is added in quadrature to the RF uncertainty. {Figures 8.15, 8.16}

After a decade of near stability, the recent increase of CH_4 concentration led to an enhanced RF compared to AR4 by 2% to 0.48 [0.43 to 0.53] W m^{-2}. It is *very likely* that the RF from methane is now larger than that of all halocarbons combined. {2.2.1, 8.3}

Atmospheric N_2O has increased by 6% since AR4 causing a RF of 0.17 [0.15 to 0.19] W m^{-2}. N_2O concentrations continue to rise while those of CFC-12, the third largest WMGHG contributor to RF for several decades, are decreasing due to phase-out of emissions of this chemical under the Montreal Protocol. N_2O is now *likely* the third largest WMGHG contributor to RF. The RF from halocarbons is very similar to the value in AR4, with a reduced RF from CFCs but increases in many of their replacements. Four of the halocarbons (CFC-11, CFC-12, CFC-113, and HCFC-22) account for 85% of the total halocarbon RF. The former three compounds have declining RF over the last five years but are more than compensated for by the increased RF from HCFC-22. There is *high confidence* that the growth rate in RF from all WMGHG is weaker over the last decade than in the 1970s and 1980s owing to a slower increase in the non-CO_2 RF. {2.2.1, 8.3}

The short-lived GHGs ozone (O_3) and stratospheric water vapour also contribute to anthropogenic forcing. Observations indicate that O_3 *likely* increased at many undisturbed (background) locations through the 1990s. These increases have continued mainly over Asia (though observations cover a limited area) and flattened over Europe during the last decade. The total RF due to changes in ozone is 0.35 [0.15 to 0.55] W

m^{-2} (*high confidence*) (Figure TS.6), with RF due to tropospheric ozone of 0.40 [0.20 to 0.60] W m^{-2} (*high confidence*) and due to stratospheric ozone of –0.05 [–0.15 to +0.05] W m^{-2} (*high confidence*). Ozone is not emitted directly into the atmosphere; instead it is formed by photochemical reactions. In the troposphere these reactions involve precursor compounds that are emitted into the atmosphere from a variety of natural and anthropogenic sources. Tropospheric ozone RF is largely attributed to increases in emissions of methane, carbon monoxide, volatile organics and nitrogen oxides, while stratospheric RF results primarily from ozone depletion by anthropogenic halocarbons. However, there is now strong evidence for substantial links between the changes in tropospheric and stratospheric ozone and a total ozone RF of 0.50 [0.30 to 0.70] W m^{-2} is attributed to tropospheric ozone precursor emissions and –0.15 [–0.30 to 0.00] W m^{-2} to ozone-depletion by halocarbons. There is strong evidence that tropospheric ozone also has a detrimental impact on vegetation physiology, and therefore on its CO_2 uptake. This reduced uptake leads to an indirect increase in the atmospheric CO_2 concentration. Thus a fraction of the CO_2 RF should be attributed to ozone or its precursors rather than direct emission of CO_2, but there is a *low confidence* on the quantitative estimates. RF for stratospheric water vapour produced from CH_4 oxidation is 0.07 [0.02 to 0.12] W m^{-2}. Other changes in stratospheric water vapour, and all changes in water vapour in the troposphere, are regarded as a feedback rather than a forcing. {2.2.2, 8.1, 8.2, 8.3; FAQ 8.1}

TS.3.3 Radiative Forcing from Anthropogenic Aerosols

Anthropogenic aerosols are responsible for a radiative forcing of climate through multiple processes which can be loosely grouped into two types: aerosol-radiation interactions (ari) and aerosol-cloud interactions (aci) (Figure TS.6). There has been progress since AR4 on observing and modeling climate-relevant aerosol properties (including their size distribution, hygroscopicity, chemical composition, mixing state, optical and cloud nucleation properties) and their atmospheric distribution. Nevertheless, substantial uncertainties remain in assessments of long-term trends of global aerosol optical depth and other global properties of aerosols due to difficulties in measurement and lack of observations of some relevant parameters, high spatial and temporal variability and the relatively short observational records that exist. The anthropogenic RFari is given a best estimate of –0.35 [–0.85 to +0.15] W m^{-2} (*high confidence*) using evidence from aerosol models and some constraints from observations. The RFari is caused by multiple aerosol types (see Section TS3.6). The rapid adjustment to RFari leads to further negative forcing, in particular through cloud adjustments. As a consequence, the ERFari is more negative than the RFari (*low confidence*) and given a best estimate of –0.45 [–0.95 to +0.05] W m^{-2}. The assessment for RFari is less negative than reported in AR4 because of a re-evaluation of aerosol absorption. The uncertainty estimate is wider but more robust. {2.2.3, 7.3, 7.5.2}

Improved understanding of aerosol-cloud interactions has led to a reduction in the estimated magnitude of many global aerosol-cloud forcings estimates. The total effective radiative forcing due to aerosols (ERFari+aci, excluding the effect of absorbing aerosol on snow and ice) is assessed to be –0.9 [–1.9 to –0.1] W m^{-2} (*medium confidence*). This estimate encompasses all rapid adjustments, including changes to the cloud lifetime and aerosol microphysical effects on mixed-phase, ice and convective clouds. This range was obtained by giving equal weight to satellite-based studies and estimates from climate models and inverse studies grouped together. It is consistent with multiple lines of evidence suggesting less negative estimates for aerosol-cloud interactions than those discussed in AR4. {7.4, 7.5}

The RF from black carbon (BC) on snow and ice is assessed to be 0.04 [0.02 to 0.09] W m^{-2} (*low confidence*). Unlike in the previous IPCC assessment, this estimate includes the effects on sea-ice, accounts for more physical processes, and incorporates evidence from both models and observations. This RF causes a 2–4 times larger global mean surface temperature change per unit forcing than CO_2 primarily because all of the forcing energy is deposited directly into the cryosphere, whose evolution drives a positive albedo feedback on climate. This effect thus can represent a significant forcing mechanism in the Arctic and other snow or ice covered regions. {7.3, 7.5}

Despite the large uncertainty ranges on aerosol forcing, there is a *high confidence* that aerosols have offset a substantial portion of GHG forcing. Aerosol-cloud interactions can influence the character of individual storms, but evidence for a systematic aerosol effect on storm or precipitation intensity is more limited and ambiguous. {7.4, 7.6}

TS.3.4 Radiative Forcing from Land Surface Changes and Contrails

There is robust evidence that anthropogenic land use changes such as deforestation have increased the land surface albedo, which leads to a RF of –0.15 [–0.25 to –0.05] W m^{-2} (Figure TS.6). There is still a large spread of quantitative estimates due to different assumptions for the albedo of natural and managed surfaces (e.g., croplands, pastures). In addition, the time evolution of the land use change, and in particular how much was already completed in the reference year 1750, are still debated. Furthermore, land use change causes other modifications that are not radiative but impact the surface temperature, including modifications in the surface roughness, latent heat flux, river runoff, and irrigation. These are more uncertain and they are difficult to quantify, but they tend to offset the impact of albedo changes at the global scale. As a consequence, there is low agreement on the sign of the net change in global mean temperature as a result of land use change. Land use change, and in particular deforestation, also has significant impacts on WMGHG concentrations. It contributes to the corresponding RF associated with CO_2 emissions or concentration changes. {8.3}

Persistent contrails from aviation contribute a positive RF of 0.01 [0.005 to 0.03] W m^{-2} (*medium confidence*) for year 2011, and the combined contrail and contrail-cirrus ERF from aviation is assessed to be 0.05 [0.02 to 0.15] W m^{-2} (*low confidence*). This forcing can be much larger regionally but there is now *medium confidence* that it does not produce observable regional effects on either the mean or diurnal range of surface temperature. {7.2.7}

TS.3.5 Radiative Forcing from Natural Drivers of Climate Change

Solar and volcanic forcings are the two dominant natural contributors to global climate change during the industrial era. Satellite observations of total solar irradiance (TSI) changes since 1978 show quasi-periodic cyclical variation with a period of roughly 11 years. Longer-term forcing is typically estimated by comparison of solar minima (during which variability is least). This gives a RF change of –0.04 [–0.08 to 0.00] W m^{-2} between the most recent (2008) minimum and the 1986 minimum. There is some diversity in the estimated trends of the composites of various satellite data, however. Secular trends of TSI before the start of satellite observations rely on a number of indirect proxies. The best estimate of RF from TSI changes over the industrial era is 0.05 [0.00 to 0.10] W m^{-2} (*medium confidence*), which includes greater RF up to around 1980 and then a small downward trend. This RF estimate is substantially smaller than the AR4 estimate due to the addition of the latest solar cycle and inconsistencies in how solar RF was estimated in earlier IPCC assessments. The recent solar minimum appears to have been unusually low and long-lasting and several projections indicate lower TSI for the forthcoming decades. However, current abilities to project solar irradiance are extremely limited so that there is *very low confidence* concerning future solar forcing. Nonetheless, there is a *high confidence* that 21st century solar forcing will be much smaller than the projected increased forcing due to GHGs. {5.2.1, 8.4; FAQ 5.1}

Changes in solar activity affect the cosmic ray flux impinging upon the Earth's atmosphere, which has been hypothesized to affect climate through changes in cloudiness. Cosmic rays enhance aerosol nucleation and thus may affect cloud condensation nuclei production in the free troposphere, but the effect is too weak to have any climatic influence during a solar cycle or over the last century (*medium evidence, high agreement)* . No robust association between changes in cosmic rays and cloudiness has been identified. In the event that such an association exists, it is *very unlikely* to be due to cosmic ray-induced nucleation of new aerosol particles. {7.3, 7.4.6}

The RF of stratospheric volcanic aerosols is now well understood and there is a large RF for a few years after major volcanic eruptions (Box TS.5, Figure 1). While volcanic eruptions inject both mineral particles and sulphate aerosol precursors into the atmosphere, it is the latter, because of their small size and long lifetimes, which are responsible for radiative forcing important for climate. The emissions of CO_2 from volcanic eruptions are at least 100 times smaller than anthropogenic emissions, and inconsequential for climate on century time scales. Large tropical volcanic eruptions have played an important role in driving annual to decadal scale climate change during the industrial era due to their sometimes very large negative RF. There has not been any major volcanic eruption since Mt. Pinatubo in 1991, which caused a one-year RF of about –3.7 W m^{-2}, but several smaller eruptions have caused a RF for the years 2008–2011 of –0.10 [–0.13 to –0.07] W m^{-2} (*high confidence*), twice as strong in magnitude compared to 1999–2002. The smaller

eruptions have led to better understanding of the dependence of radiative forcing on the amount of material from and time of the year of high-latitude injections. {5.2.1, 5.3.5, 8.4; Annex II}

TS.3.6 Synthesis of Forcings; Spatial and Temporal Evolution

A synthesis of the industrial era forcing finds that among the forcing agents, there is a *very high confidence* only for the WMGHG RF. Relative to AR4, the confidence level has been elevated for seven forcing agents due to improved evidence and understanding. {8.5; Figure 8.14}

The time evolution of the total anthropogenic RF shows a nearly continuous increase from 1750, primarily since about 1860. There is *very high confidence* that the total anthropogenic RF increase rate since 1960 has been much greater than during earlier industrial-era periods, driven primarily by the continuous increase in most WMGHG concentrations. There is still low agreement on the time evolution of the total aerosol ERF, which is the primary factor for the uncertainty in the total anthropogenic forcing. The fractional uncertainty in the total anthropogenic forcing decreases gradually after 1950 due to the smaller offset of positive WMGHG forcing by negative aerosol forcing. There is robust evidence and high agreement that natural forcing is a small fraction of the WMGHG forcing. Natural forcing changes over the last 15 years have *likely* offset a substantial fraction (10–95%) of the anthropogenic forcing increase during this period (Box TS.3). Forcing by CO_2 is the largest single contributor to the total forcing during the industrial era and during 1980 to 2011. Compared to the entire industrial era the dominance of CO_2 forcing is larger for 1980 to 2011 with respect to other WMGHG, and there is *high confidence* that the offset from aerosol forcing to WMGHG forcing during this period was much smaller than over the 1950–1980 period. {8.5.2}

Forcing can also be attributed to emissions rather than to the resulting concentration changes (Figure TS.7). Carbon dioxide is the largest single contributor to historical RF from either the perspective of changes in the atmospheric concentration of CO_2 or the impact of changes in net emissions of CO_2. The relative importance of other forcing agents can vary markedly with the perspective chosen, however. In particular, methane emissions have a much larger forcing (~1.0 W m^{-2} over the industrial era) than methane concentration increases (~0.5 W m^{-2}) due to several indirect effects through atmospheric chemistry. In addition, carbon monoxide emissions have a clear positive forcing, while emissions of reactive nitrogen oxides *likely* cause a net negative forcing but uncertainties are large. Emissions of ozone-depleting halocarbons *very likely* cause a net positive forcing as their direct radiative effect is larger than the impact of the stratospheric ozone depletion that they induce. Emissions of SO_2, organic carbon and ammonia cause a negative forcing, while emissions of black carbon lead to positive forcing via aerosol-radiation interactions. Note that mineral dust forcing may include a natural component or a climate feedback effect. {7.3, 7.5.2, 8.5.1}

[INSERT FIGURE TS.7 HERE]

Figure TS.7: Radiative forcing of climate change during the industrial era shown by emitted components from 1750 to 2011. The horizontal bars indicate the overall uncertainty, while the vertical bars are for the individual components (vertical bar lengths proportional to the relative uncertainty, with a total length equal to the bar width for a ±50% uncertainty). Best estimates for the totals and individual components (from left to right) of the response are given in the right column. Values are RF except for the ERF of aerosol-cloud interactions (ERFaci). An additional rapid adjustment to aerosol-radiation interactions of –0.1 [–0.3 to +0.1] W m^{-2} is attributable primarily to black carbon (ERFari-RFari in Figure TS.6). CFCs= Chlorofluorocarbons, HCFCs= Hydrochlorofluorocarbons, HFCs=Hydrofluorocarbons, PFCs= Perfluorocarbons, NMVOC= Non-Methane Volatile Organic Compounds, BC= Black Carbon. {Figure 8.17}

Although the WMGHG show a spatially fairly homogeneous forcing, other agents such as aerosols, ozone and land-use changes are highly heterogeneous spatially. RFari showed maximum negative values over eastern North America and Europe during the early 20th century, with large negative values extending to East and Southeast Asia, South America and central Africa by 1980. Since then, however, the magnitude has decreased over eastern North America and Europe due to pollution control and the peak negative forcing has shifted to South and East Asia primarily as a result of economic growth and the resulting increase in emissions in those areas. Total aerosol ERF shows similar behaviour for locations with maximum negative forcing, but also shows substantial positive forcing over some deserts and the Arctic. In contrast, the global mean whole atmosphere ozone forcing increased throughout the 20th century, and has peak positive amplitudes around 15°N–30°N but negative values over Antarctica. Negative land-use forcing by albedo changes has been strongest in industrialized and biomass burning regions. The inhomogeneous nature of

these forcings can cause them to have a substantially larger influence on the hydrologic cycle than an equivalent global mean homogeneous forcing. {8.3, 8.6}

Over the 21st century, there is *very high confidence* that the anthropogenic radiative forcing will increase. Simple model estimates of the RF resulting from the Representative Concentration Pathways (RCPs, see Box TS.6), which include WMGHG emissions spanning a broad range of possible futures, show anthropogenic RF relative to 1750 increasing to 3.0–4.8 W m^{-2} in 2050, and 2.7–8.4 W m^{-2} at 2100. In the near-term, the RCPs are quite similar to one another (and emissions of near-term climate forcers do not span the literature range of possible futures), with RF at 2030 ranging only from 2.9 to 3.3 W m^{-2} (additional 2010 to 2030 RF of 0.7–1.1 W m^{-2}), but they show highly diverging values for the second half of the 21st century driven largely by CO_2. Results based on the RCP scenarios suggest only small changes in aerosol ERF between 2000 and 2030, followed by a strong reduction in the aerosols and a substantial weakening of the negative total aerosol ERF. Nitrate aerosols are an exception to this reduction with a substantially increased negative forcing which is a robust feature among the few available models. The divergence across the RCPs indicates that, although a certain amount of future climate change is already 'in the system' due to the current radiative imbalance caused by historical emissions and the long lifetime of some atmospheric forcing agents, societal choices can still have a very large effect on future radiative forcing, and hence on climate change. {8.2, 8.5, 8.6, 12.3}

TS.3.7 Climate Feedbacks

Feedbacks will also play an important role in determining future climate change. Indeed, climate change may induce modification in the carbon, water and geochemical cycles which may reinforce (positive feedback) or dampen (negative feedback) the expected temperature increase. Snow and ice albedo feedbacks are known to be positive. The combined water vapor and lapse rate feedback is *extremely likely* and now fairly well quantified, while cloud feedbacks have larger uncertainties (see TFE.6). In addition, the new Coupled Model Intercomparison Project Phase 5 (CMIP5) models consistently estimate a positive carbon-cycle feedback, i.e. reduced natural sinks or increased natural CO_2 sources in response to future climate change. In particular, carbon-cycle feedbacks in the oceans are positive in the models. Carbon sinks in tropical land ecosystems are less consistent, and may be susceptible to climate change via processes such as drought and fire that are sometimes not yet fully represented. A key update since AR4 is the introduction of nutrient dynamics in some of the CMIP5 land carbon models, in particular the limitations on plant growth imposed by nitrogen availability. The net effect of accounting for the nitrogen cycle is a smaller projected land sink for a given trajectory of anthropogenic CO_2 emissions (see TFE.7). {6.3, 6.4; Box 6.1, 7.2}

Models and ecosystem warming experiments show high agreement that wetland CH_4 emissions will increase per unit area in a warmer climate, but wetland areal extent may increase or decrease depending on regional changes in temperature and precipitation affecting wetland hydrology, so that there is low confidence in quantitative projections of wetland CH_4 emissions. Reservoirs of carbon in hydrates and permafrost are very large, and thus could potentially act as very powerful feedbacks. Although poorly constrained, the 21st century global release of CH_4 from hydrates to the atmosphere is *likely* to be low due to the under-saturated state of the ocean, long-ventilation time of the ocean, and slow propagation of warming through the seafloor. Release of carbon from thawing permafrost is *very likely* to provide a positive feedback, but there is limited confidence in quantitative projections of its strength. {6.4}

Aerosol-climate feedbacks occur mainly through changes in the source strength of natural aerosols or changes in the sink efficiency of natural and anthropogenic aerosols; a limited number of modeling studies have assessed the magnitude of this feedback to be small with a *low confidence*. There is *medium confidence* for a weak feedback (of uncertain sign) involving dimethyl sulphide, cloud condensation nuclei, and cloud albedo due to a weak sensitivity of cloud condensation nuclei population to changes in dimethyl sulphide emissions. {7.3.5}

TS.3.8 Emission Metrics

Different metrics can be used to quantify and communicate the relative and absolute contributions to climate change of emissions of different substances, and of emissions from regions/countries or sources/sectors. Up to AR4, the most common metric has been the Global Warming Potential (GWP) that integrates RF out to a

particular time horizon. This metric thus accounts for the radiative efficiencies of the various substances, and their lifetimes in the atmosphere, and gives values relative to those for the references gas CO_2. There is now increasing focus on the Global Temperature change Potential (GTP), which is based on the change in global mean surface temperature at a chosen point in time, again relative to that caused by the references gas CO_2, and thus accounts for climate response along with radiative efficiencies and atmospheric lifetimes. Both the GWP and the GTP use a time horizon (Figure TS.8 top), the choice of which is subjective and context-dependent. In general, GWPs for near-term climate forcers are higher than GTPs due to the equal time-weighting in the integrated forcing used in the GWP. Hence the choice of metric can greatly affect the relative importance of near-term climate forcers and WMGHGs, as can the choice of time horizon. Analysis of the impact of current emissions (one-year pulse of emissions) shows that near-term climate forcers, such as black carbon, sulfur dioxide or methane, can have contributions comparable to CO_2's for short time horizons (of either the same or opposite sign), but their impacts become progressively less for longer time horizons over which emissions of CO_2 dominate (Figure TS.8 top). {8.7}

[INSERT FIGURE TS.8 HERE]

Figure TS.8: (Upper Panel) Global anthropogenic present-day emissions weighted by the Global Warming Potential (GWP) and the Global Temperature change Potential (GTP) for the chosen time horizons. Year 2008 (single-year pulse) emissions weighted by GWP, which is the global mean radiative forcing per unit mass emitted integrated over the indicated number of years relative to the forcing from CO_2 emissions, and GTP which estimates the impact on global mean temperature based on the temporal evolution of both radiative forcing and climate response per unit mass emitted relative to the impact of CO_2 emissions. The units are "CO_2 equivalents" which reflects equivalence only in the impact parameter of the chosen metric (integrated RF over the chosen time horizon for GWP; temperature change at the chosen point in time for GTP), given as Pg(CO_2)eq (left axis) and PgCeq (right axis) (see footnote 5). . (Bottom Panel) The Absolute GTP (AGTP) as a function of time multiplied by the present-day emissions of all compounds from the indicated sectors is used to estimate global mean temperature response (AGTP is the same as GTP, except is not normalized by the impact of CO_2 emissions). There is little change in the relative values for the sectors over the 60–100 year time horizon. The effects of aerosol-cloud interactions and aviation-induced cirrus are not included in the upper panel. {Figures 8.32, 8.33}

A large number of other metrics may be defined down the driver-response-impact chain. No single metric can accurately compare all consequences (i.e., responses in climate parameters over time) of different emissions, and a metric that establishes equivalence with regard to one effect will not give equivalence with regard to other effects. The choice of metric therefore depends strongly on the particular consequence one wants to evaluate. It is important to note that the metrics do not define policies or goals, but facilitate analysis and implementation of multi-component policies to meet particular goals. All choices of metric contain implicit value-related judgments such as type of effect considered and weighting of effects over time. While GWP integrates the effects up to a chosen time horizon (i.e. giving equal weight to all times up to the horizon and zero weight thereafter), the GTP gives the temperature just for one chosen year with no weight on years before or after. {8.7}

The GWP and GTP have limitations and suffer from inconsistencies related to the treatment of indirect effects and feedbacks, for instance if climate-carbon feedbacks are included for the reference gas CO_2 but not for the non-CO_2 gases. The uncertainty in the GWP increases with time horizon and for the 100-year GWP of WMGHGs the uncertainty can be as large as ±40%. Several studies also point out that this metric is not well suited for policies with a maximum temperature target. Uncertainties in GTP also increase with time as they arise from the same factors contributing to GWP uncertainties along with additional contributions from it being further down the driver-response-impact chain and including climate response. The GTP metric is better suited to target-based policies, but is again not appropriate for every goal. Updated metric values accounting for changes in knowledge of lifetimes and radiative efficiencies and for climate-carbon feedbacks are now available. {8.7}

With these emission metrics, the climate impact of past or current emissions attributable to various activities can be assessed. Such activity-based accounting can provide additional policy-relevant information since these activities are more directly affected by particular societal choices than overall emissions. A single-year's worth of emissions (a pulse) is often used to quantify the impact on future climate. From this perspective and with the absolute GTP metric used to illustrate the results, energy and industry have the largest contributions to warming over the next 50–100 years (Figure TS.8 bottom). Household fossil and biofuel, biomass burning and on-road transportation are also relatively large contributors to warming over

these timescales, while current emissions from sectors that emit large amounts of methane (animal husbandry, waste/landfills and agriculture) are also important over shorter time horizons (up to ~20 years). Another useful perspective is to examine the effect of sustained current emissions. Since emitted substances are removed according to their residence time, short-lived species remain at nearly constant values while long-lived gases accumulate in this analysis. In both cases, the sectors that have the greatest long-term warming impacts (energy and industry) lead to cooling in the near-term (primarily due to SO_2 emissions), and thus emissions from those sectors can lead to opposite global mean temperature responses at short and long timescales. The relative importance of the other sectors depends upon the time and perspective chosen. As with RF or ERF, uncertainties in aerosol impacts are large, and in particular attribution of aerosol-cloud interactions to individual components is poorly constrained. {8.7}

TS.4 Understanding the Climate System and its Recent Changes

TS.4.1 Introduction

Understanding of the climate system results from combining observations, theoretical studies of feedback processes, and model simulations. Compared to AR4, more detailed observations and improved climate models (see Box TS.4) now enable the attribution of detected changes to human influences in more climate system components. The consistency of observed and modeled changes across the climate system, including regional temperatures, the water cycle, global energy budget, cryosphere and oceans (including ocean acidification), point to global climate change resulting primarily from anthropogenic increases in greenhouse gas concentrations. {10}

TS.4.2 Surface Temperature

Several advances since the AR4 have allowed a more robust quantification of human influence on surface temperature changes. Observational uncertainty has been explored much more thoroughly than previously and the assessment now considers observations from the first decade of the 21st century and simulations from a new generation of climate models whose ability to simulate historical climate has improved in many respects relative to the previous generation of models considered in AR4. Observed global mean surface temperature anomalies relative to 1880-1919 in recent years lie well outside the range of temperature anomalies in CMIP5 simulations with natural forcing only, but are consistent with the ensemble of CMIP5 simulations including both anthropogenic and natural forcing (Figure TS.9) even though some individual models overestimate the warming trend, while others underestimate it. Simulations with greenhouse gas changes only, and no aerosol changes, generally exhibit stronger warming than has been observed (Figure TS.9). Observed temperature trends over the period 1951–2010, which are characterized by warming over most of the globe with the most intense warming over the Northern Hemisphere continents, are, at most observed locations, consistent with the temperature trends in CMIP5 simulations including anthropogenic and natural forcings and inconsistent with the temperature trends in CMIP5 simulations including natural forcings only. A number of studies have investigated the effects of the Atlantic Multidecadal Oscillation (AMO) on global mean surface temperature. While some studies find a significant role for the AMO in driving multi-decadal variability in GMST, the AMO exhibited little trend over the period 1951-2010 on which these assessments are based, and the AMO is assessed with *high confidence* to have made little contribution to the GMST trend between 1951 and 2010 (considerably less than 0.1°C). {2.4, 9.8.1, 10.3; FAQ 9.1}.

[INSERT FIGURE TS.9 HERE]

Figure TS.9: Three observational estimates of global mean surface temperature (black lines) from HadCRUT4, GISTEMP, and MLOST, compared to model simulations (CMIP3 models – thin blue lines and CMIP5 models – thin yellow lines) with anthropogenic and natural forcings (a), natural forcings only (b) and greenhouse gas forcing only (c). Thick red and blue lines are averages across all available CMIP5 and CMIP3 simulations respectively. All simulated and observed data were masked using the HadCRUT4 coverage (since this dataset has the most restricted spatial coverage), and global average anomalies are shown with respect to 1880–1919, where all data are first calculated as anomalies relative to 1961–1990 in each grid box. Inset to (b) shows the three observational datasets distinguished by different colours. {Figure 10.1}

It is *extremely likely* that human activities caused more than half of the observed increase in global average surface temperature from 1951 to 2010. This assessment is supported by robust evidence from multiple

Figures

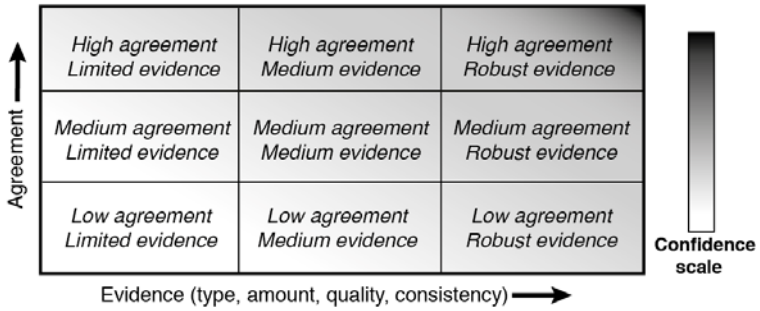

Box TS.1, Figure 1: A depiction of evidence and agreement statements and their relationship to confidence. Confidence increases toward the top-right corner as suggested by the increasing strength of shading. Generally, evidence is most robust when there are multiple, consistent independent lines of high-quality. {Figure 1.11}

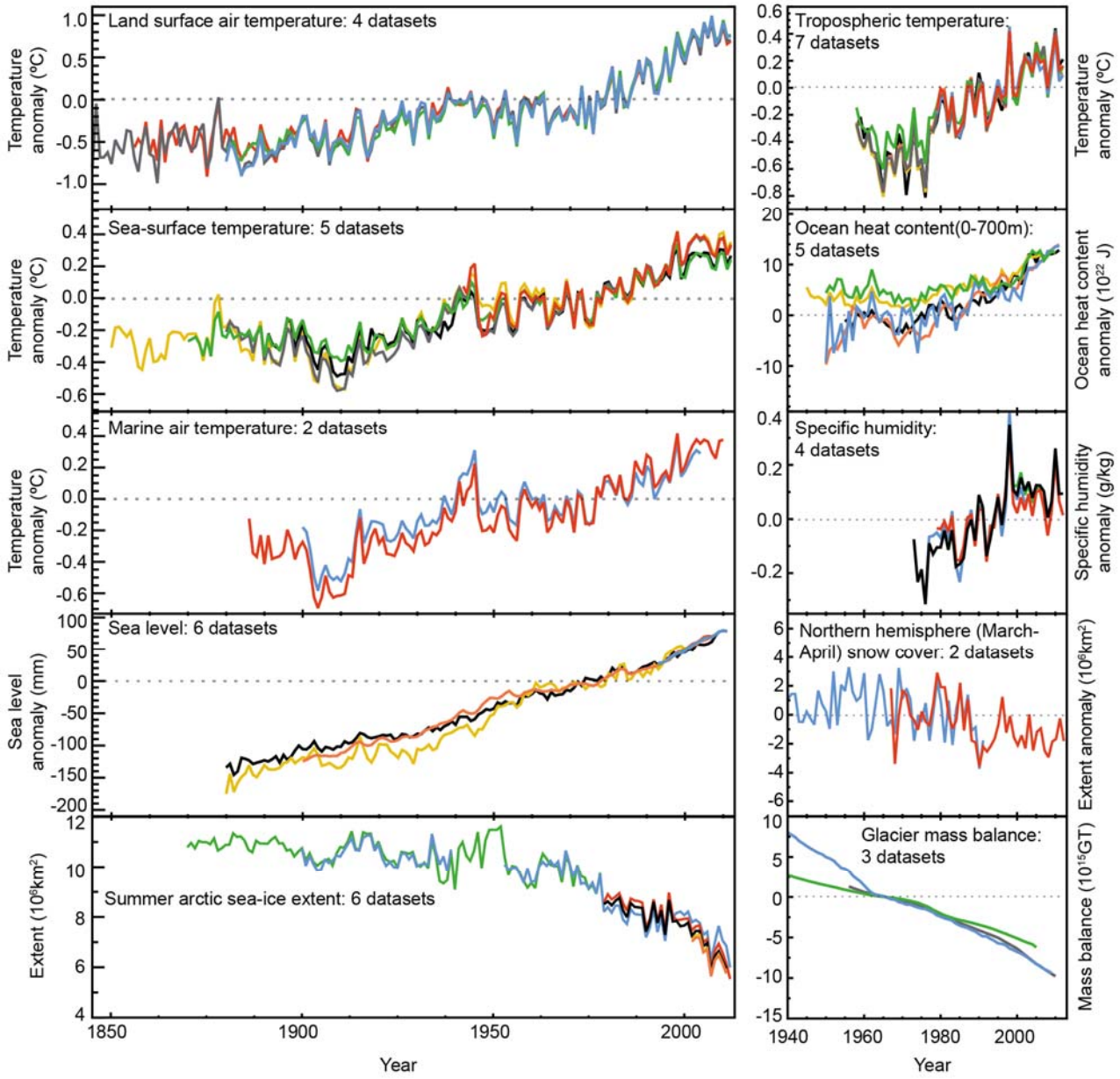

Figure TS.1: Multiple complementary indicators of a changing global climate. Each line represents an independently-derived estimate of change in the climate element. The times series presented are assessed in chapters 2, 3, and 4. In each panel all datasets have been normalized to a common period of record. A full detailing of which source datasets go into which panel is given in Chapter 2, Supplementary Material 2.SM.5 and in the respective chapters (See also FAQ 2.1, Figure 1). {2.4, 2.5, 3.2, 3.7, 4.5.2, 4.5.3}

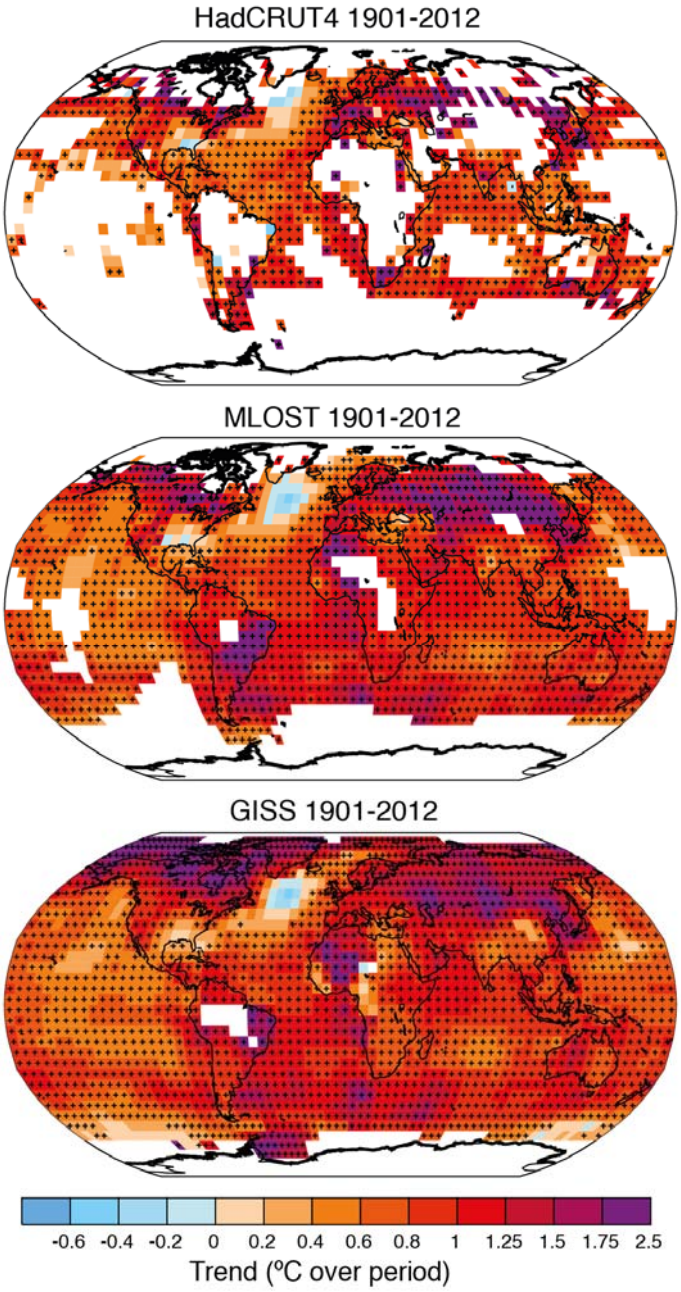

Figure TS.2: Change in surface temperature over 1901-2012 as determined by linear trend for three data sets. White areas indicate incomplete or missing data. Trends have been calculated only for those grid boxes with greater than 70% complete records and more than 20% data availability in the first and last 10% of the time period. Black plus signs (+) indicate grid boxes where trends are significant (i.e., a trend of zero lies outside the 90% confidence interval). Differences in coverage primarily reflect the degree of interpolation to account for data void regions undertaken by the dataset providers ranging from none beyond grid box averaging (HadCRUT4) to substantial (GISS). {Figure 2.21}

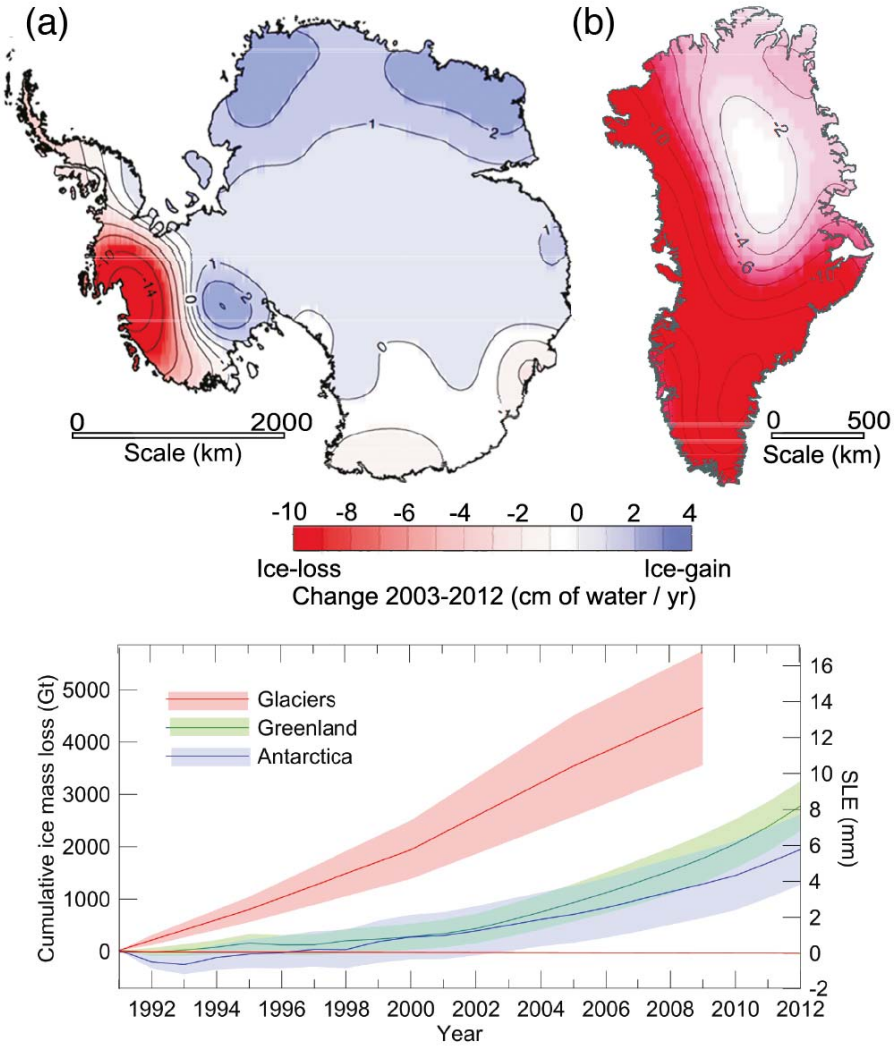

Figure TS.3: Upper panels: distribution of ice loss determined from GRACE time-variable gravity for (a) Antarctica and (b) Greenland, shown in centimetres of water per year (cm of water yr^{-1}) for the period 2003 to 2012. Lower panel: the assessment of the total loss of ice from glaciers and ice sheets in terms of sea level equivalent (in mm). The contribution from glaciers excludes those on the periphery of the ice sheets. {4.3.4; Figures 4.12, 4.13, 4.14, 4.16, 4.17}

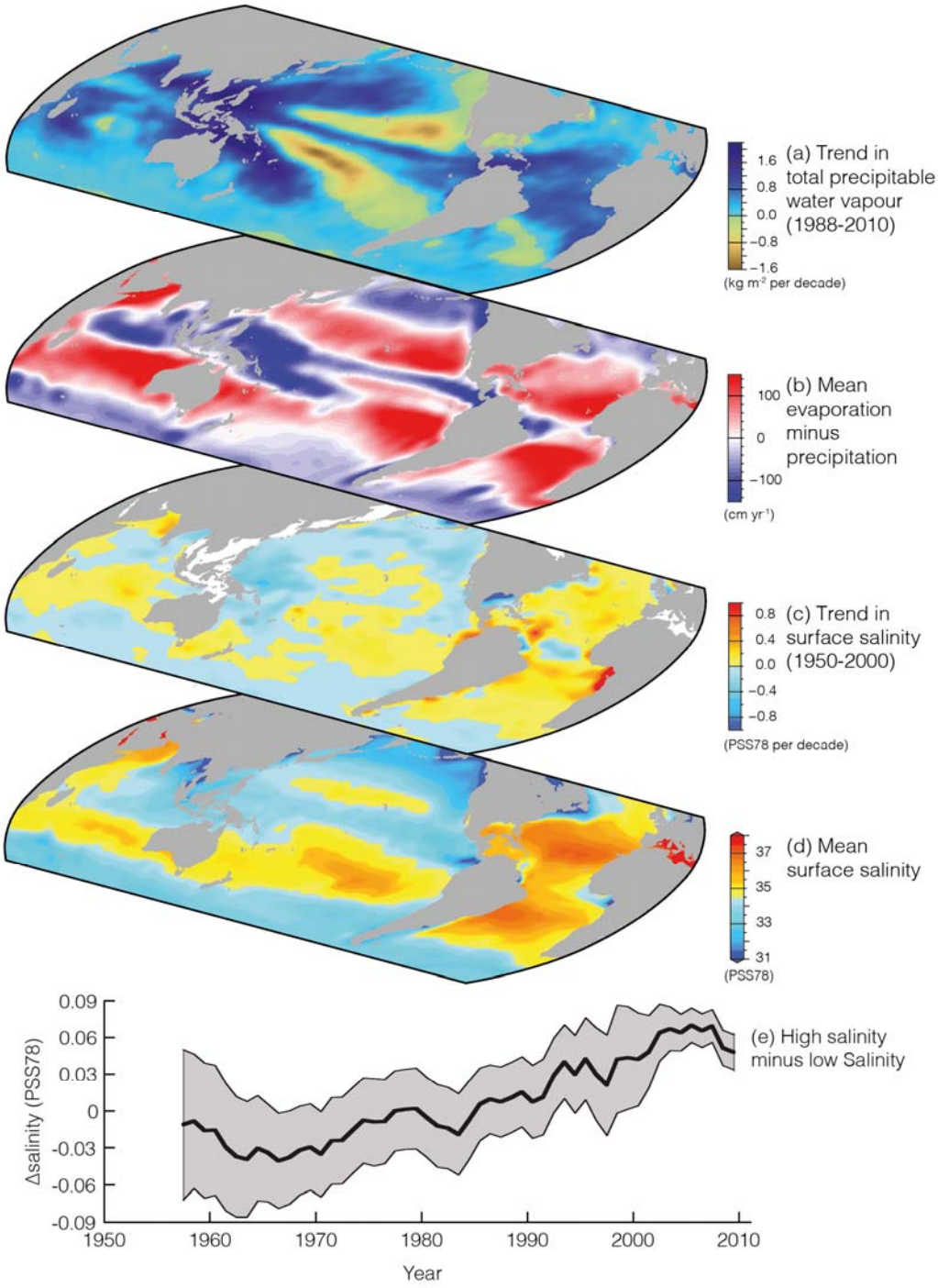

TFE.1, Figure 1: Changes in sea surface salinity are related to the atmospheric patterns of Evaporation minus Precipitation (E-P) and trends in total precipitable water: (a) Linear trend (1988 to 2010) in total precipitable water (water vapor integrated from Earth's surface up through the entire atmosphere) (kg m^{-2} per decade) from satellite observations. (b) The 1979–2005 climatological mean net evaporation minus precipitation (cm yr^{-1}) from meteorological reanalysis data. (c) Trend (1950 to 2000) in surface salinity (PSS78 per 50years). (d) The climatological-mean surface salinity (PSS78) (blues <35; yellows-reds >35). (e) Global difference between salinity averaged over regions where the sea surface salinity is greater than the global mean sea surface salinity ("High Salinity") and salinity averaged over regions values below the global mean ("Low Salinity"). Details of data sources: see Figure 3.21 and FAQ 3.3, Figure 1. {3.9}

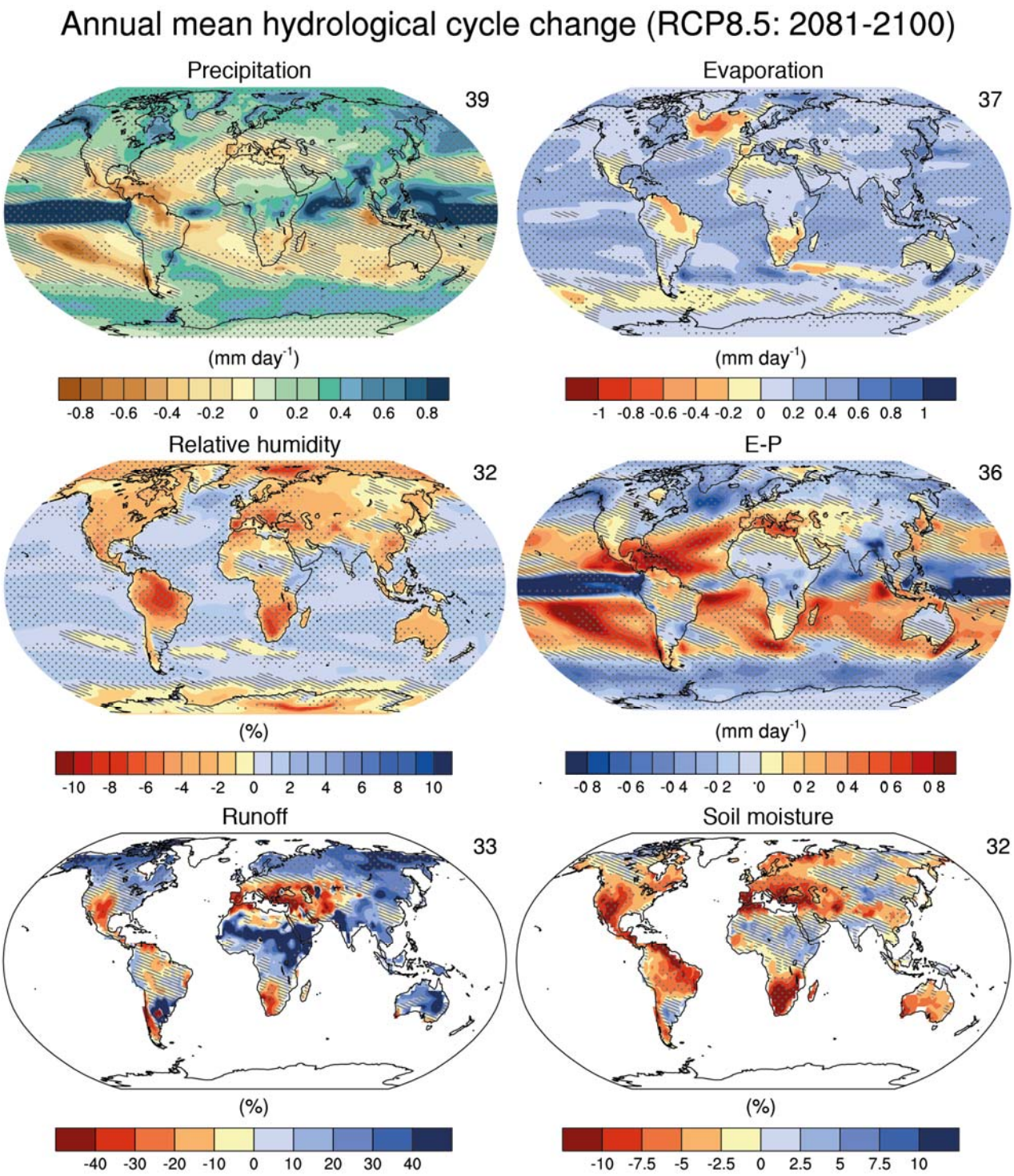

TFE.1, Figure 2: Annual mean changes in precipitation (P), evaporation (E), relative humidity, E-P, runoff and soil moisture, for 2081–2100 relative to 1986–2005 under the RCP8.5 scenario (see Box TS.6). The number of CMIP5 models to calculate the multi-model mean is indicated in the upper right corner of each panel. Hatching indicates regions where the multi model mean is less than one standard deviation of internal variability. Stippling indicates regions where the multi model mean is greater than two standard deviations of internal variability and where 90% of models agree on the sign of change (see Box 12.1). {Figures 12.25–12.27}

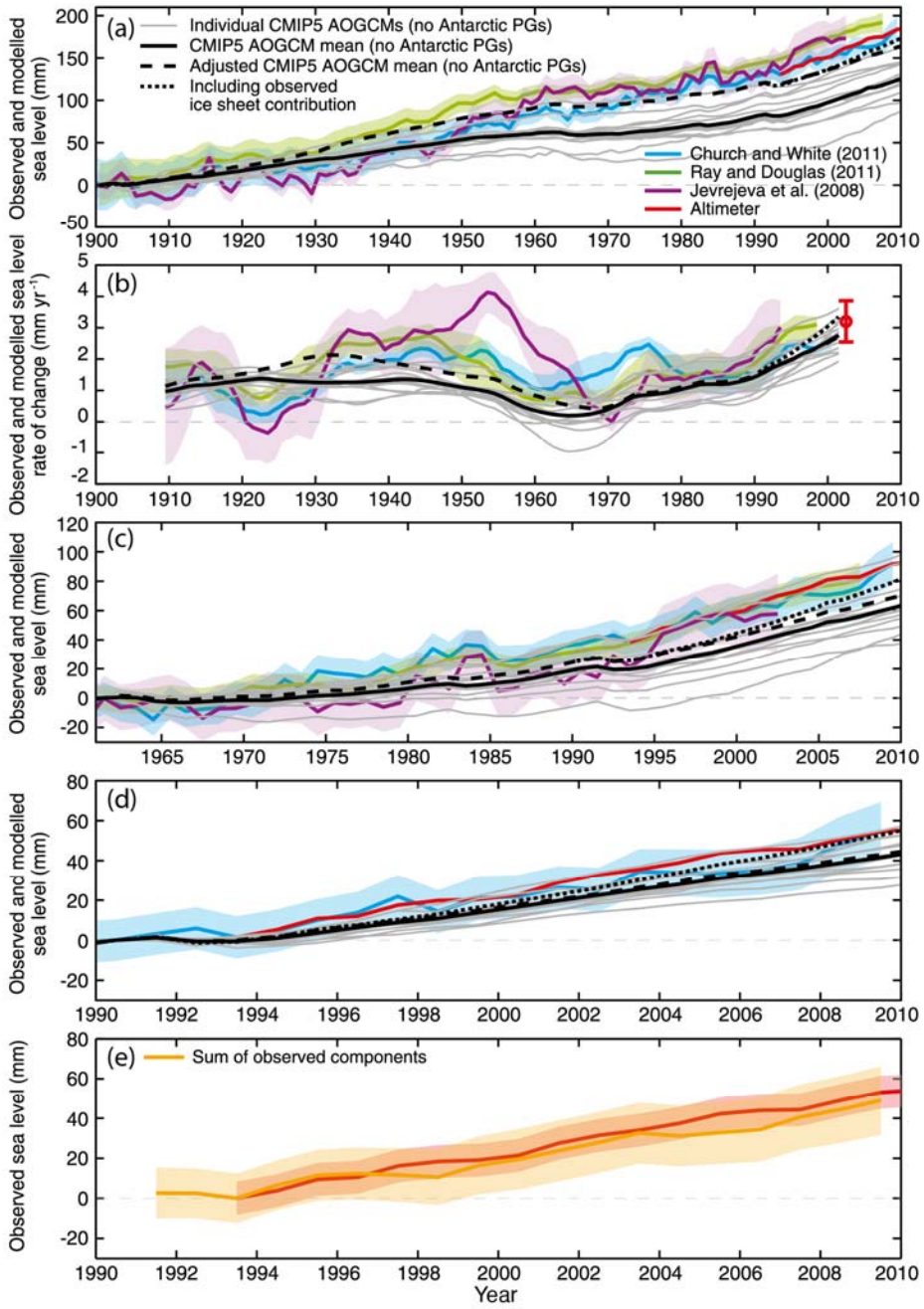

TFE.2, Figure 1: Comparison of the observed global mean sea level rise from the sum of the modelled contributions from ocean thermal expansion, glaciers (excluding glaciers peripheral to the Antarctic ice sheet, PGs) and changes in land-water storage. In panels (a)-(d): the grey lines are results for individual CMIP5 AOGCMs; the black line is the model mean plus a correction for the omission of volcanic forcing in the AOGCM control experiments; the adjusted model mean (dashed black line) is the sum of the corrected model mean thermal expansion, the change in land-water storage, the glacier estimate using observed (rather than modelled) climate, and an illustrative long-term ice-sheet contribution (of 0.1 mm yr^{-1}); the adjusted model mean including the observed ice sheet contribution (dotted black line) begins in 1993 and includes the ice-sheet contributions, but excludes the glaciers peripheral to both the Greenland Ice Sheet and the Antarctic Ice Sheet, to avoid double counting because the observational ice-sheet estimates include the peripheral glaciers; three estimates of global mean sea level, with the shading indicating the uncertainty estimates (two standard deviations) are shown; the satellite altimeter data since 1993 are shown in red. The modelled sea level is given (a) for the period 1900 to 2010, (b) the rates of sea level change for the same period, with the satellite altimeter data shown as a red dot for the rate, (c) for 1961 to 2010 and (d) for 1990 to 2010. Panel (e) compares the sum of the observed contributions (orange) and the observed sea level from the satellite altimeter data (red). {13.3; Figure 13.7}

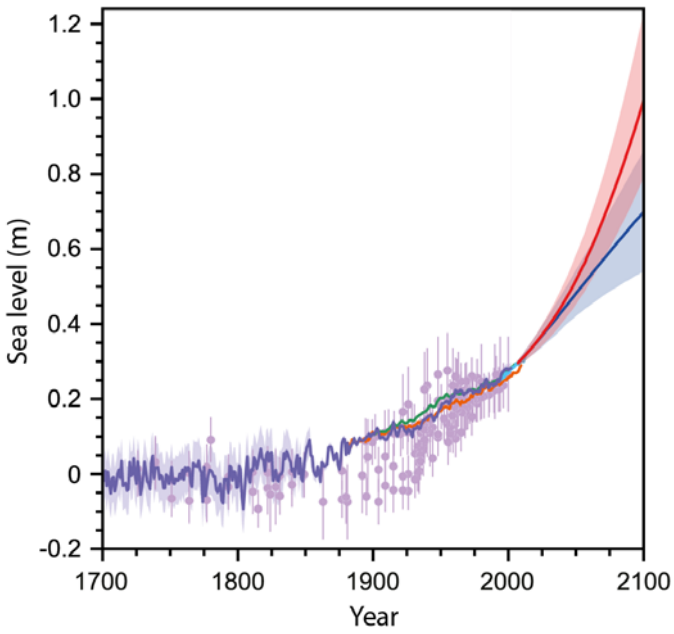

TFE.2, Figure 2: Compilation of paleo sea level data (purple), tide gauge data (blue, red and green), altimeter data (light blue), and central estimates and likely ranges for projections of global-mean sea level rise from the combination of CMIP5 and process-based models for RCP2.6 (blue) and RCP8.5 (red) scenarios, all relative to pre-industrial values. {Figures 13.3, 13.11, 13.27}

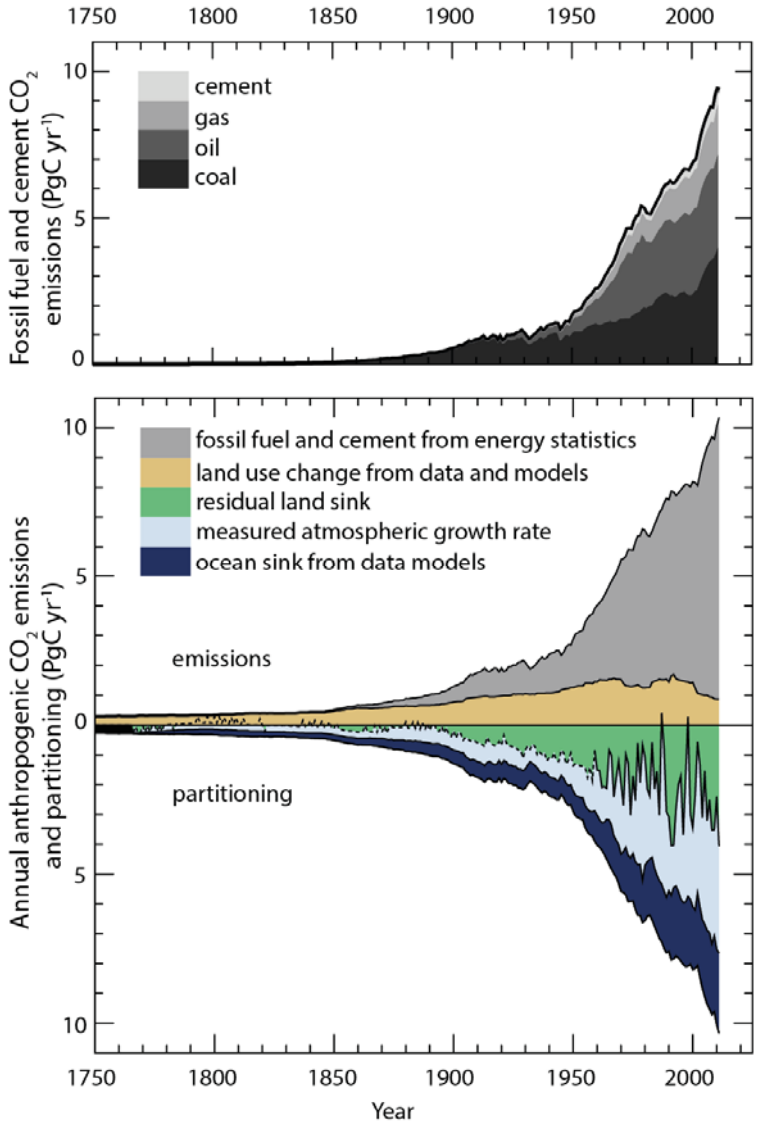

Figure TS.4: Annual anthropogenic CO_2 emissions and their partitioning among the atmosphere, land and ocean (PgC yr^{-1}) from 1750 to 2011. (Top) Fossil fuel and cement CO_2 emissions by category, estimated by the Carbon Dioxide Information Analysis Center (CDIAC). (Bottom) Fossil fuel and cement CO_2 emissions as above. CO_2 emissions from net land use change, mainly deforestation, are based on land cover change data (see Table 6.2). The atmospheric CO_2 growth rate prior to 1959 is based on a spline fit to ice core observations and a synthesis of atmospheric measurements from 1959. The fit to ice core observations does not capture the large interannual variability in atmospheric CO_2 and is represented with a dashed line. The ocean CO_2 sink is from a combination of models and observations. The residual terrestrial sink (term in green in the figure) is computed from the residual of the other terms. The emissions and their partitioning only include the fluxes that have changed since 1750, and not the natural CO_2 fluxes (e.g., atmospheric CO_2 uptake from weathering, outgassing of CO_2 from lakes and rivers, and outgassing of CO_2 by the ocean from carbon delivered by rivers; see Figure 6.1) between the atmosphere, land and ocean reservoirs that existed before that time and still exist today. The uncertainties in the various terms are discussed in chapter 6 and reported in Table 6.1 for decadal mean values. {Figure 6.8}

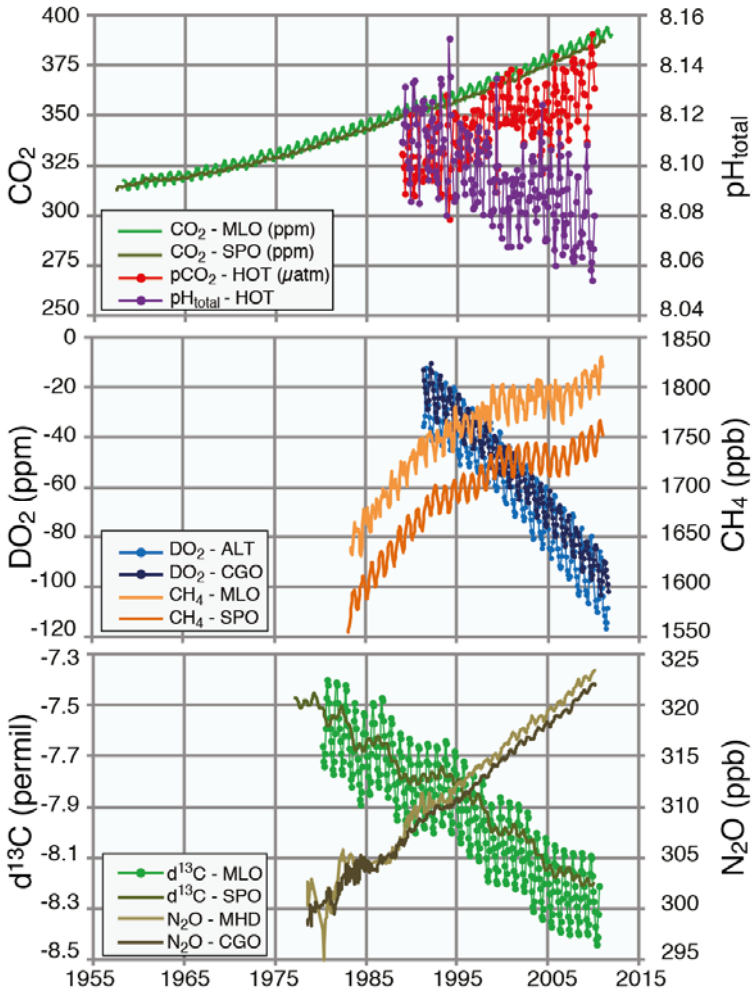

Figure TS.5: Atmospheric concentration of CO_2, oxygen, $^{13}C/^{12}C$ stable isotope ratio in CO_2, as well as CH_4 and N_2O atmospheric concentrations and oceanic surface observations of pCO_2 and pH, recorded at representative time series stations in the Northern and the Southern Hemispheres. MLO: Mauna Loa Observatory, Hawaii; SPO: South Pole; HOT: Hawaii Ocean Time-Series station; MHD: Mace Head, Ireland; CGO: Cape Grim, Tasmania; ALT: Alert, Northwest Territories, Canada. {Figure 6.3, FAQ 3.2, Figure 1}

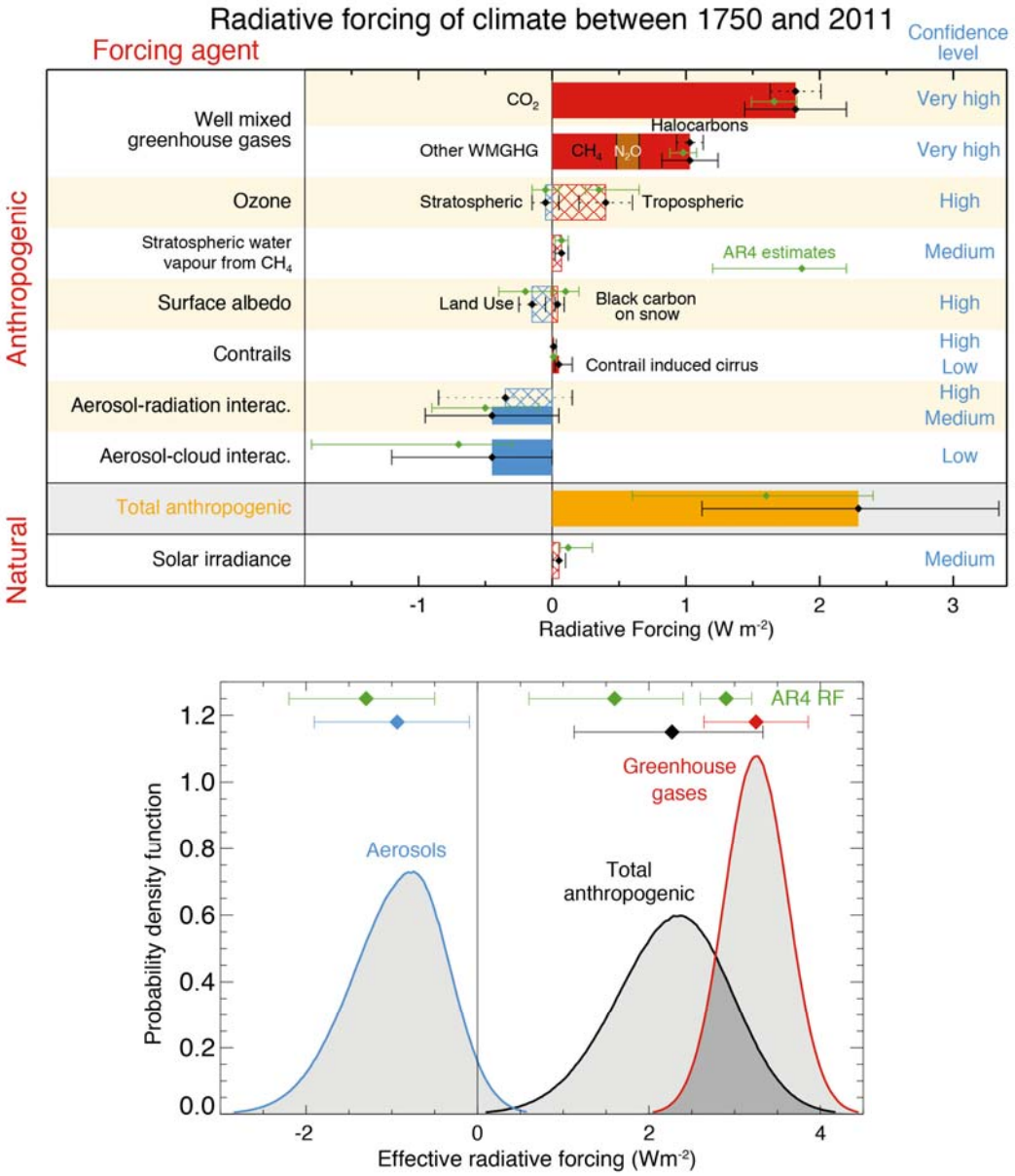

Figure TS.6: Radiative Forcing (RF) and Effective Radiative Forcing (ERF) of climate change during the industrial era. Top: Forcing by concentration change between 1750 and 2011 with associated uncertainty range (solid bars are ERF, hatched bars are RF, green diamonds and associated uncertainties are for RF assessed in AR4). Bottom: Probability Density Functions for the ERF, for the aerosol, well-mixed greenhouse gas (WMGHG) and total. The green lines show the AR4 RF 90% confidence intervals and can be compared with the red, blue and black lines which show the AR5 ERF 90% confidence intervals (although RF and ERF differ, especially for aerosols). The ERF from surface albedo changes and combined contrails and contrail induced cirrus is included in the total anthropogenic forcing, but not shown as a separate probability density function. For some forcing mechanisms (ozone, land use, solar) the RF is assumed to be representative of the ERF but an additional uncertainty of 17% is added in quadrature to the RF uncertainty. {Figures 8.15, 8.16}

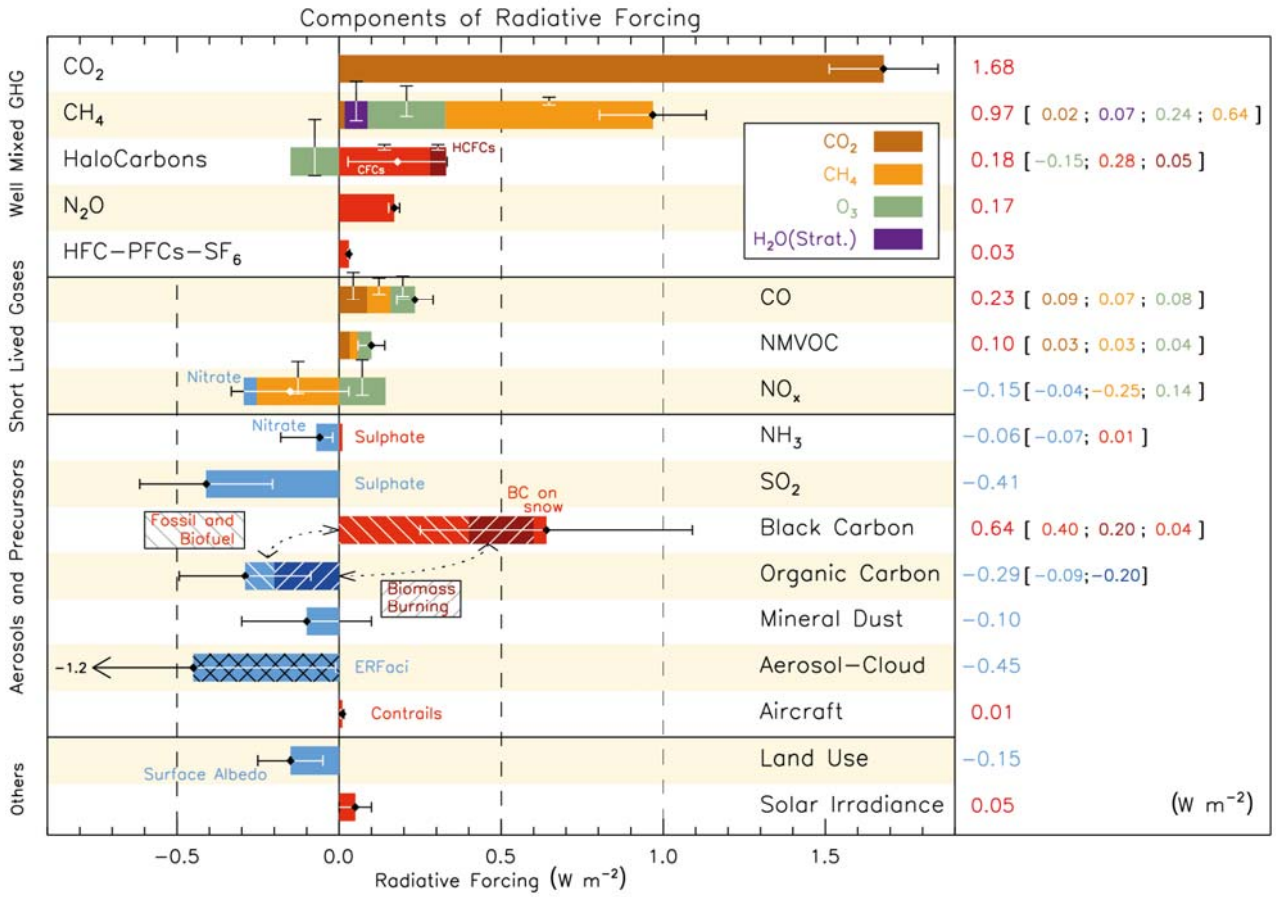

Figure TS.7: Radiative forcing of climate change during the industrial era shown by emitted components from 1750 to 2011. The horizontal bars indicate the overall uncertainty, while the vertical bars are for the individual components (vertical bar lengths proportional to the relative uncertainty, with a total length equal to the bar width for a ±50% uncertainty). Best estimates for the totals and individual components (from left to right) of the response are given in the right column. Values are RF except for the ERF of aerosol-cloud interactions (ERFaci). An additional rapid adjustment to aerosol-radiation interactions of –0.1 [–0.3 to +0.1] W m^{-2} is attributable primarily to black carbon (ERFari-RFari in Figure TS.6). CFCs= Chlorofluorocarbons, HCFCs= Hydrochlorofluorocarbons, HFCs=Hydrofluorocarbons, PFCs= Perfluorocarbons, NMVOC= Non-Methane Volatile Organic Compounds, BC= Black Carbon. {Figure 8.17}

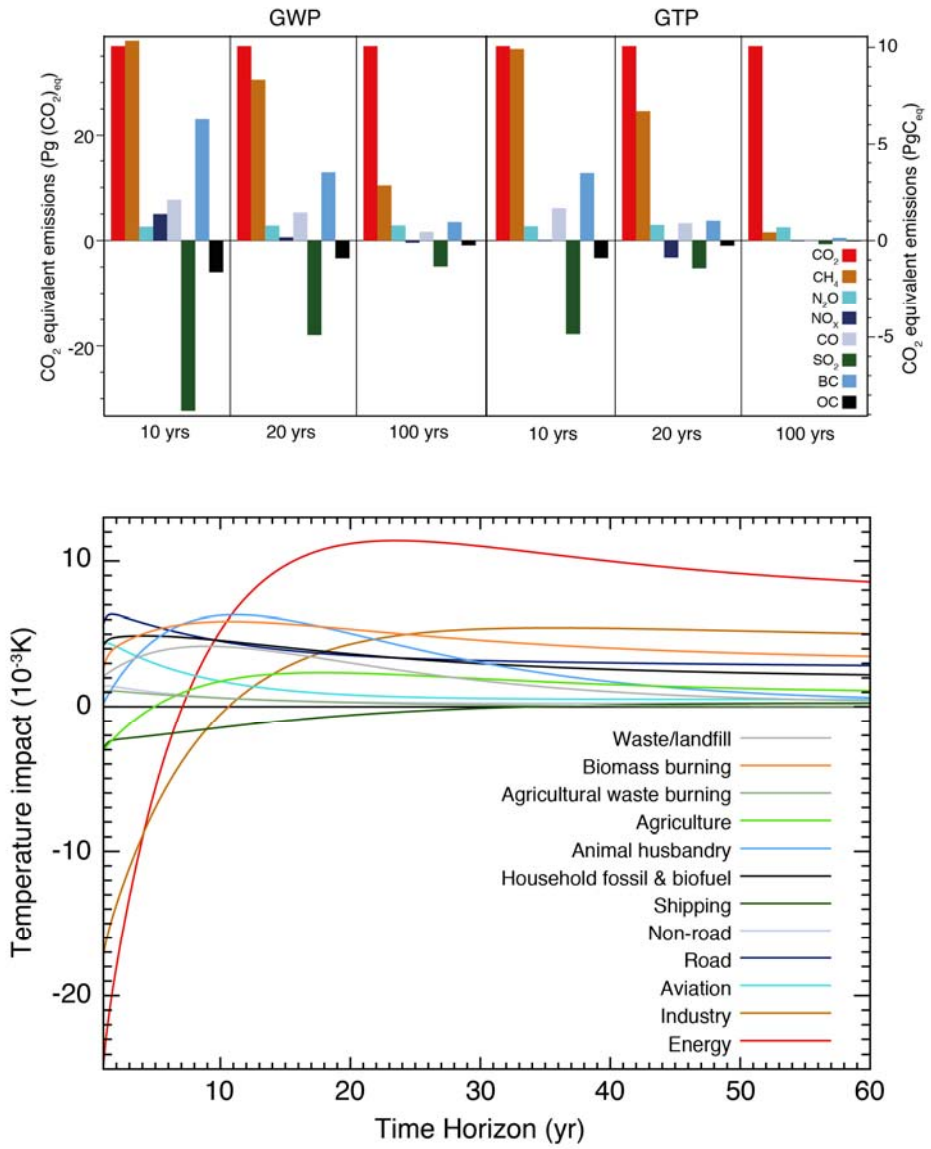

Figure TS.8: (Upper Panel) Global anthropogenic present-day emissions weighted by the Global Warming Potential (GWP) and the Global Temperature change Potential (GTP) for the chosen time horizons. Year 2008 (single-year pulse) emissions weighted by GWP, which is the global mean radiative forcing per unit mass emitted integrated over the indicated number of years relative to the forcing from CO_2 emissions, and GTP which estimates the impact on global mean temperature based on the temporal evolution of both radiative forcing and climate response per unit mass emitted relative to the impact of CO_2 emissions. The units are "CO_2 equivalents" which reflects equivalence only in the impact parameter of the chosen metric (integrated RF over the chosen time horizon for GWP; temperature change at the chosen point in time for GTP), given as Pg(CO_2)eq (left axis) and PgCeq (right axis) (see footnote 5). (Bottom Panel) The Absolute GTP (AGTP) as a function of time multiplied by the present-day emissions of all compounds from the indicated sectors is used to estimate global mean temperature response (AGTP is the same as GTP, except is not normalized by the impact of CO_2 emissions). There is little change in the relative values for the sectors over the 60–100 year time horizon. The effects of aerosol-cloud interactions and aviation-induced cirrus are not included in the upper panel. {Figures 8.32, 8.33}

Executive Summary

Atmospheric Temperatures

More than half of the observed increase in global mean surface temperature (GMST) from 1951 to 2010 is *very likely*[1] due to the observed anthropogenic increase in greenhouse gas concentrations. The consistency of observed and modeled changes across the climate system, including warming of the atmosphere and ocean, sea level rise, ocean acidification, and changes in the water cycle, the cryosphere and climate extremes points to a large-scale warming resulting primarily from anthropogenic increases in greenhouse gas concentrations. Solar forcing is the only known natural forcing acting to warm the climate over this period but it has increased much less than greenhouse gas forcing, and the observed pattern of long term tropospheric warming and stratospheric cooling is not consistent with the expected response to solar irradiance variations. The Atlantic Multi-decadal Oscillation (AMO) could be a confounding influence but studies that find a significant role for the AMO show that this does not project strongly onto 1951–2010 temperature trends. [10.3.1, Table 10.1]

It is *extremely likely* that human activities caused more than half of the observed increase in global mean surface temperature from 1951–2010. This assessment is supported by robust evidence from multiple studies using different methods. Observational uncertainty has been explored much more thoroughly than previously and the assessment now considers observations from the first decade of the 21st century and simulations from a new generation of climate models whose ability to simulate historical climate has improved in many respects relative to the previous generation of models considered in AR4. Uncertainties in forcings and in climate models' temperature responses to individual forcings, and difficulty in distinguishing the patterns of temperature response due to greenhouse gases and other anthropogenic forcings prevent a more precise quantification of the temperature changes attributable to greenhouse gases. [9.4.1, 9.5.3, 10.3.1, Figure 10.5, Table 10.1]

Greenhouse gases contributed a global mean surface warming *likely* to be between 0.5°C and 1.3°C over the period 1951–2010, with the contributions from other anthropogenic forcings *likely* to be between –0.6°C and 0.1°C, from natural forcings *likely* to be between –0.1°C and 0.1°C, and from internal variability *likely* to be between –0.1°C and 0.1°C. Together these assessed contributions are consistent with the observed warming of approximately 0.6°C over this period. [10.31, Figure 10.5]

It is *virtually certain* that internal variability alone cannot account for the observed global warming since 1951. The observed global-scale warming since 1951 is large compared to climate model estimates of internal variability on 60 year time scales. The Northern Hemispheric warming over the same period is far outside the range of any similar length trends in residuals from reconstructions of the past millennium. The spatial pattern of observed warming differs from those associated with internal variability. The model-based simulations of internal variability are assessed to be adequate to make this assessment. [9.5.3, 10.3.1, 10.7.5, Table 10.1]

It is *likely* that anthropogenic forcings, dominated by greenhouse gases, have contributed to the warming of the troposphere since 1961 and *very likely* that anthropogenic forcings, dominated by the depletion of the ozone layer due to ozone depleting substances, have contributed to the cooling of the lower stratosphere since 1979. Observational uncertainties in estimates of tropospheric temperatures have now been assessed more thoroughly than at the time of AR4. The structure of stratospheric temperature trends and multi-year to decadal variations are well represented by models and physical understanding is consistent with the observed and modelled evolution of stratospheric temperatures. Uncertainties in radiosonde and satellite records makes assessment of causes of observed trends in the upper troposphere less confident than an assessment of the overall atmospheric temperature changes. [2.4.4, 9.4.1, 10.3.1, Table 10.1]

[1] In this Report, the following terms have been used to indicate the assessed likelihood of an outcome or a result: Virtually certain 99–100% probability, Very likely 90-100%, Likely 66-100%, About as likely as not 33–66%, Unlikely 0–33%, Very unlikely 0–10%, Exceptionally unlikely 0-1%. Additional terms (Extremely likely: 95–100%, More likely than not >50–100%, and Extremely unlikely 0–5%) may also be used when appropriate. Assessed likelihood is typeset in italics, e.g., *very likely* (see Section 1.4 and Box TS.1 for more details).

Further evidence has accumulated of the detection and attribution of anthropogenic influence on temperature change in different parts of the world. Over every continental region, except Antarctica, it is *likely* that anthropogenic influence has made a substantial contribution to surface temperature increases since the mid-20th century. The robust detection of human influence on continental scales is consistent with the global attribution of widespread warming over land to human influence. It is *likely* that there has been an anthropogenic contribution to the very substantial Arctic warming over the past 50 years. For Antarctica large observational uncertainties result in *low confidence*[2] that anthropogenic influence has contributed to the observed warming averaged over available stations. Anthropogenic influence has *likely* contributed to temperature change in many sub-continental regions. [2.4.1, 10.3.1, Table 10.1]

Robustness of detection and attribution of global-scale warming is subject to models correctly simulating internal variability. Although, estimates of multi-decadal internal variability of GMST need to be obtained indirectly from the observational record since the observed record contains the effects of external forcings (meaning the combination of natural and anthropogenic forcings), the standard deviation of internal variability would have to be under-estimated in climate models by a factor of at least three to account for the observed warming in the absence of anthropogenic influence. Comparison with observations provides no indication of such a large difference between climate models and observations. [9.5.3, Figures 9.33, 10.2, 10.3.1, Table 10.1]

The observed recent warming hiatus, defined as the reduction in GMST trend during 1998–2012 as compared to the trend during 1951–2012, is attributable in roughly equal measure to a cooling contribution from internal variability and a reduced trend in external forcing (expert judgment, *medium confidence*). The forcing trend reduction is primarily due to a negative forcing trend from both volcanic eruptions and the downward phase of the solar cycle. However, there is *low confidence* in quantifying the role of forcing trend in causing the hiatus, because of uncertainty in the magnitude of the volcanic forcing trends and *low confidence* in the aerosol forcing trend. Many factors, in addition to greenhouse gases, including changes in tropospheric and stratospheric aerosols, stratospheric water vapour, and solar output, as well as internal modes of variability, contribute to the year to year and decade to decade variability of GMST. [Box 9.2, 10.3.1, Figure 10.6]

Ocean Temperatures and Sea Level Rise

It is *very likely* that anthropogenic forcings have made a substantial contribution to upper ocean warming (above 700 m) observed since the 1970s. This anthropogenic ocean warming has contributed to global sea level rise over this period through thermal expansion. New understanding since AR4 of measurement errors and their correction in the temperature data sets have increased the agreement in estimates of ocean warming. Observations of ocean warming are consistent with climate model simulations that include anthropogenic and volcanic forcings but are inconsistent with simulations that exclude anthropogenic forcings. Simulations which include both anthropogenic and natural forcings have decadal variability that is consistent with observations. These results are a major advance on AR4. [3.2.3, 10.4.1, Table 10.1].

It is *very likely* that there is a substantial contribution from anthropogenic forcings to the global mean sea level rise since the 1970s. It is *likely* that sea level rise has an anthropogenic contribution from Greenland melt since 1990 and from glacier mass loss since 1960's. Observations since 1971 indicate with *high confidence* that thermal expansion and glaciers (excluding the glaciers in Antarctica) explain 75% of the observed rise. [10.4.1, 10.4.3, 10.5.2, Table 10.1, 13.3.6]

Ocean Acidification and Oxygen Change

[2] In this Report, the following summary terms are used to describe the available evidence: limited, medium, or robust; and for the degree of agreement: low, medium, or high. A level of confidence is expressed using five qualifiers: very low, low, medium, high, and very high, and typeset in italics, e.g., *medium confidence*. For a given evidence and agreement statement, different confidence levels can be assigned, but increasing levels of evidence and degrees of agreement are correlated with increasing confidence (see Section 1.4 and Box TS.1 for more details).

It is *very likely* that oceanic uptake of anthropogenic carbon dioxide has resulted in acidification of surface waters which is observed to be between –0.0014 and –0.0024 pH units per year. There is *medium confidence* that the observed global pattern of decrease in oxygen dissolved in the oceans can be attributed in part to human influences. [3.8.2, Box 3.2, 10.4.4, Table 10.1]

The Water Cycle

New evidence is emerging for an anthropogenic influence on global land precipitation changes, on precipitation increases in high northern latitudes, and on increases in atmospheric humidity. There is *medium confidence* that there is an anthropogenic contribution to observed increases in atmospheric specific humidity since 1973 and to global scale changes in precipitation patterns over land since 1950, including increases in northern hemisphere mid to high latitudes. Remaining observational and modelling uncertainties, and the large internal variability in precipitation preclude a more confident assessment at this stage. [2.5.1, 2.5.4, 10.3.2, Table 10.1]

It is *very likely* that anthropogenic forcings have made a discernable contribution to surface and subsurface oceanic salinity changes since 1960's. More than 40 studies of regional and global surface and subsurface salinity show patterns consistent with understanding of anthropogenic changes in the water cycle and ocean circulation. The expected pattern of anthropogenic amplification of climatological salinity patterns derived from climate models is detected in the observations although there remains incomplete understanding of the observed internal variability of the surface and sub-surface salinity fields. [3.3.2, 10.4.2, Table 10.1].

It is *likely* that human influence has affected the global water cycle since 1960. This assessment is based on the combined evidence from the atmosphere and oceans of observed systematic changes that are attributed to human influence in terrestrial precipitation, atmospheric humidity and oceanic surface salinity through its connection to precipitation and evaporation. This is a major advance since AR4. [3.3.2, 10.3.2, 10.4.2, Table 10.1].

The Cryosphere

Anthropogenic forcings are *very likely* to have contributed to Arctic sea ice loss since 1979. There is a robust set of results from simulations that show the observed decline in sea-ice extent is simulated only when models include anthropogenic forcings. There is *low confidence* in the scientific understanding of the observed increase in Antarctic sea ice extent since 1979, due to the incomplete and competing scientific explanations for the causes of change and *low confidence* in estimates of internal variability. [10.5.1, Table 10.1]

Ice sheets and glaciers are melting, and anthropogenic influences are *likely* to have contributed to the surface melting of Greenland since 1990 and to the retreat of glaciers since the 1960s. Since 2007, internal variability is likely to have further enhanced the melt over Greenland. For glaciers there is a high level of scientific understanding from robust estimates of observed mass loss, internal variability and glacier response to climatic drivers. Due to a low level of scientific understanding there is *low confidence* in attributing the causes of the observed loss of mass from the Antarctic ice sheet since 1993. [4.3.3, 10.5.2, Table 10.1]

It is *likely* that there has been an anthropogenic component to observed reductions in northern hemisphere snow cover since 1970. There is high agreement across observations studies and attribution studies find a human influence at both continental and regional scales. [10.5.3, Table 10.1]

Climate Extremes

There has been a strengthening of the evidence for human influence on temperature extremes since the AR4 and SREX reports. It is *very likely* that anthropogenic forcing has contributed to the observed changes in the frequency and intensity of daily temperature extremes on the global scale since the mid-20th century. Attribution of changes in temperature extremes to anthropogenic influence is robustly seen in independent analyses using different methods and different datasets. It is *likely* that human influence has

substantially increased the probability of occurrence of heatwaves in some locations. [10.6.1, 10.6.2, Table 10.1]

In land regions where observational coverage is sufficient for assessment, there is *medium confidence* that anthropogenic forcing has contributed to a global-scale intensification of heavy precipitation over the second half of the 20th century. There is *low confidence* in attributing changes in drought over global land areas since the mid-20th century to human influence due to observational uncertainties and difficulties in distinguishing decadal scale variability in drought from long term trends. [10.6.1, Table 10.1]

There is *low confidence* in attribution of changes in tropical cyclone activity to human influence due to insufficient observational evidence, lack of physical understanding of the links between anthropogenic drivers of climate and tropical cyclone activity and the low level of agreement between studies as to the relative importance of internal variability, and anthropogenic and natural forcings. This assessment is consistent with that of SREX. [10.6.1, Table 10.1]

Atmospheric Circulation

It is *likely* that human influence has altered sea level pressure patterns globally. Detectable anthropogenic influence on changes in sea level pressure patterns is found in several studies. Changes in atmospheric circulation are important for local climate change since they could lead to greater or smaller changes in climate in a particular region than elsewhere. There is *medium confidence* that stratospheric ozone depletion has contributed to the observed poleward shift of the southern Hadley Cell border during austral summer. There are large uncertainties in the magnitude of this poleward shift. It is *likely* that stratospheric ozone depletion has contributed to the positive trend in the Southern Annular Mode seen in austral summer since the mid-0th century which corresponds to sea level pressure reductions over the high latitudes and an increase in the subtropics. There is *medium confidence* that greenhouse gases have also played a role in these trends of the southern Hadley Cell border and the Southern Annular Mode in Austral summer. [10.3.3, Table 10.1]

A Millennia to Multi-Century Perspective

Taking a longer term perspective shows the substantial role played by anthropogenic and natural forcings in driving climate variability on hemispheric scales prior to the twentieth century. It is *very unlikely* that northern hemisphere temperature variations from 1400 to 1850 can be explained by internal variability alone. There is *medium confidence* that external forcing contributed to Northern Hemispheric temperature variability from 850 to 1400 and that external forcing contributed to European temperature variations over the last 5 centuries. [10.7.2, 10.7.5, Table 10.1]

Climate System Properties

The extended record of observed climate change has allowed a better characterisation of the basic properties of the climate system that have implications for future warming. New evidence from 21st century observations and stronger evidence from a wider range of studies have strengthened the constraint on the transient climate response (TCR) which is estimated with *high confidence* to be *likely* between 1°C and 2.5°C and extremely unlikely to be greater than 3°C. The Transient Climate Response to Cumulative CO_2 Emissions (TCRE) is estimated with *high confidence* to be *likely* between 0.8°C and 2.5°C per 1000 PgC for cumulative CO_2 emissions less than about 2000 PgC until the time at which temperatures peak. Estimates of the Equilibrium Climate Sensitivity (ECS) based on multiple and partly independent lines of evidence from observed climate change indicate that there is *high confidence* that ECS is extremely unlikely to be less than 1°C and *medium confidence* that the ECS is *likely* to be between 1.5°C and 4.5°C and *very unlikely* greater than 6°C. These assessments are consistent with the overall assessment in Chapter 12, where the inclusion of additional lines of evidence increases confidence in the assessed likely range for ECS. [10.8.1, 10.8.2, 10.8.4, Box 12.2]

Combination of Evidence

Human influence has been detected in the major assessed components of the climate system. Taken together, the combined evidence increases the level of confidence in the attribution of observed climate change, and reduces the uncertainties associated with assessment based on a single climate variable. From this combined evidence it is *virtually certain* that human influence has warmed the global climate system. Anthropogenic influence has been identified in changes in temperature near the surface of the earth, in the atmosphere and in the oceans, as well as changes in the cryosphere, the water cycle and some extremes. There is strong evidence that excludes solar forcing, volcanoes, and internal variability as the strongest drivers of warming since 1950. [10.9.2, Table 10.1]

10.1 Introduction

This chapter assesses the causes of observed changes assessed in Chapters 2 to 5 and uses understanding of physical processes, climate models and statistical approaches. The chapter adopts the terminology for detection and attribution proposed by the IPCC good practice guidance paper on detection and attribution (Hegerl et al., 2010) and for uncertainty Mastrandrea et al. (2011). Detection and attribution of impacts of climate changes are assessed by Working Group II where Chapter 18 assesses the extent to which atmospheric and oceanic changes influence ecosystems, infrastructure, human health and activities in economic sectors.

Evidence of a human influence on climate has grown stronger over the period of the four previous assessment reports of the IPCC. There was little observational evidence for a detectable human influence on climate at the time of the first IPCC Assessment Report. By the time of the second report there was sufficient additional evidence for it to conclude that "the balance of evidence suggests a discernible human influence on global climate". The third Assessment Report found that a distinct greenhouse gas signal was robustly detected in the observed temperature record and that "most of the observed warming over the last fifty years is *likely* to have been due to the increase in greenhouse gas concentrations."

With the additional evidence available by the time of the Fourth Assessment Report, the conclusions were further strengthened. This evidence included a wider range of observational data, a greater variety of more sophisticated climate models including improved representations of forcings and processes, and a wider variety of analysis techniques. This enabled the AR4 report to conclude that "most of the observed increase in global average temperatures since the mid-20th century is *very likely* due to the observed increase in anthropogenic greenhouse gas concentrations". The AR4 also concluded that "discernible human influences now extend to other aspects of climate, including ocean warming, continental-average temperatures, temperature extremes and wind patterns."

A number of uncertainties remained at the time of AR4. For example, the observed variability of ocean temperatures appeared inconsistent with climate models, thereby reducing the confidence with which observed ocean warming could be attributed to human influence. Also, while observed changes in global rainfall patterns and increases in heavy precipitation were assessed to be qualitatively consistent with expectations of the response to anthropogenic forcings, detection and attribution studies had not been carried out. Since the AR4, improvements have been made to observational datasets, taking more complete account of systematic biases and inhomogeneities in observational systems, further developing uncertainty estimates, and correcting detected data problems (Chapters 2, 3). A new set of simulations from a greater number of AOGCMs have been performed as part of the Fifth Coupled Model Intercomparison Project (CMIP5). These new simulations have several advantages over the CMIP3 simulations assessed in the AR4 (Hegerl et al., 2007b). They incorporate some moderate increases in resolution, improved parameterisations, and better representation of aerosols (Chapter 9). Importantly for attribution, in which it is necessary to partition the response of the climate system to different forcings, most CMIP5 models include simulations of the response to natural forcings only, and the response to increases in well mixed greenhouse gases only (Taylor et al., 2012).

The advances enabled by this greater wealth of observational and model data are assessed in this chapter. In this assessment, there is increased focus on the extent to which the climate system as a whole is responding in a coherent way across a suite of climate variables such as surface mean temperature, temperature extremes, ocean heat content, ocean salinity and precipitation change. There is also a global to regional perspective, assessing the extent to which not just global mean changes but also spatial patterns of change across the globe can be attributed to anthropogenic and natural forcings.

10.2 Evaluation of Detection and Attribution Methodologies

Detection and attribution methods have been discussed in previous assessment reports (Hegerl et al., 2007b) and the IPCC Good Practice Guidance Paper (Hegerl et al., 2010), to which we refer. This section reiterates key points and discusses new developments and challenges.

10.2.1 The Context of Detection and Attribution

In IPCC Assessments, detection and attribution involve quantifying the evidence for a causal link between external drivers of climate change and observed changes in climatic variables. It provides the central, although not the only (see Section 1.2.3) line of evidence that has supported statements such as "the balance of evidence suggests a discernible human influence on global climate" or "most of the observed increase in global average temperatures since the mid-20th century is very likely due to the observed increase in anthropogenic greenhouse gas concentrations."

The definition of detection and attribution used here follows the terminology in the IPCC guidance paper (Hegerl et al., 2010). '*Detection* of change is defined as the process of demonstrating that climate or a system affected by climate has changed in some defined statistical sense without providing a reason for that change. An identified change is detected in observations if its likelihood of occurrence by chance due to internal variability alone is determined to be small' (Hegerl et al., 2010). *Attribution* is defined as 'the process of evaluating the relative contributions of multiple causal factors to a change or event with an assignment of statistical confidence'. As this wording implies, attribution is more complex than detection, combining statistical analysis with physical understanding (Allen et al., 2006; Hegerl and Zwiers, 2011). In general, a component of an observed change is attributed to a specific causal factor if the observations can be shown to be consistent with results from a process-based model that includes the causal factor in question, and inconsistent with an alternate, otherwise identical, model that excludes this factor. The evaluation of consistency in both of these cases takes into account both internal chaotic variability and known uncertainties in the observations and responses to external causal factors.

Attribution does not require, and nor does it imply, that every aspect of the response to the causal factor in question is simulated correctly. Suppose, for example, the global cooling following a large volcano matches the cooling simulated by a model, but the model underestimates the magnitude of this cooling: the observed global cooling can still be attributed to that volcano, although the error in magnitude would suggest that details of the model response may be unreliable. Physical understanding is required to assess what constitutes a plausible discrepancy above that expected from internal variability. Even with complete consistency between models and data, attribution statements can never be made with 100% certainty because of the presence of internal variability.

This definition of attribution can be extended to include antecedent conditions and internal variability among the multiple causal factors contributing to an observed change or event. Understanding the relative importance of internal versus external factors is important in the analysis of individual weather events (Section 10.6.2), but the primary focus of this chapter will be on attribution to factors external to the climate system, like rising greenhouse gas levels, solar variability and volcanic activity.

There are four core elements to any detection and attribution study:

1. Observations of one or more climate variables, such as surface temperature, that are understood, on physical grounds, to be relevant to the process in question;
2. An estimate of how external drivers of climate change have evolved before and during the period under investigation, including both the driver whose influence is being investigated (such as rising greenhouse gas levels) and potential confounding influences (such as solar activity);
3. A quantitative physically-based understanding, normally encapsulated in a model, of how these external drivers are thought to have affected these observed climate variables;
4. An estimate, often but not always derived from a physically-based model, of the characteristics of variability expected in these observed climate variables due to random, quasi-periodic and chaotic fluctuations generated in the climate system that are not due to externally-driven climate change.

A climate model driven with external forcing alone is not expected to replicate the observed evolution of internal variability, because of the chaotic nature of the climate system, but it should be able to capture the statistics of this variability (often referred to as "noise"). The reliability of forecasts of short-term variability is also a useful test of the representation of relevant processes in the models used for attribution, but forecast skill is not necessary for attribution: attribution focuses on changes in the underlying moments of the 'weather attractor', meaning the expected weather and its variability, while prediction focuses on the actual trajectory of the weather around this attractor.